Metal-mediated Adsorption of DNA Oligonucleotides onto Polymeric Materials

by

Mohamad (MoMo) Zandieh

A thesis

presented to the University of Waterloo

in fulfillment of the

thesis requirement for the degree of

Doctor of Philosophy

in

Chemistry

Waterloo, Ontario, Canada, 2022

Examining Committee Membership

The following served on the Examining Committee for this thesis. The decision of the Examining Committee is by majority vote.

External Examiner

Dr. Hua-Zhong Yu
Professor, Department of Chemistry,
Simon Fraser University, Burnaby, Canada

Supervisor

Dr. Juewen Liu
Professor, Department of Chemistry,
University of Waterloo, Waterloo, Canada

Internal Member

Dr. Dan Thomas
Professor, Department of Chemistry,
University of Guelph, Guelph, Canada

Internal Member

Dr. Vivek Maheshwari
Associate Professor, Department of Chemistry,
University of Waterloo, Waterloo, Canada

Internal/External Examiner

Dr. Michael Tam
Professor, Department of Chemical Engineering,
University of Waterloo, Waterloo, Canada

Author's Declaration

This thesis consists of material all of which I authored or co-authored: see Statement of Contributions included in the thesis. This is a true copy of the thesis, including any required final revisions, as accepted by my examiners. I understand that my thesis may be made electronically available to the public.

Statement of Contributions

The work presented in this thesis in the result of work performed by the author and several scientific collaborations. Contributions from each scientist and the resulting publications are listed in detail below.

Some sections in Chapter 1 (Introduction) have been published as: Mohamad Zandieh, Blake M. Hagar, and Juewen Liu. "Interfacing DNA and Polydopamine Nanoparticles and Its Applications" *Particle & Particle Systems Characterization* **2020**, 37, 11, 2000208. Blake wrote the "covalent DNA attachment" section. The rest of the manuscript was written by Mohamad Zandieh and Juewen Liu.

The work in Chapter 2 has been published as: Mohamad Zandieh and Juewen Liu. "Metal-Doped Polydopamine Nanoparticles for Highly Robust and Efficient DNA Adsorption and Sensing". *Langmuir* **2021**, 37, 30, 8953−8960. All experiments were performed by Mohamad Zandieh. The manuscript was written by Mohamad Zandieh and Juewen Liu.

The work in Chapter 3 has been published as: Mohamad Zandieh and Juewen Liu. "Cooperative Metal Ion-Mediated Adsorption of Spherical Nucleic Acids with a Large Hysteresis". *Langmuir* **2020**, 36, 47, 14324–14332, and Mohamad Zandieh and Juewen Liu. "Spherical Nucleic Acid Mediated Functionalization of Polydopamine-Coated Nanoparticles for Selective DNA Extraction and Detection". *Bioconjugate Chem.* **2021**, 32, 4, 801-809. All experiments were performed by Mohamad Zandieh. Both manuscripts were written by Mohamad Zandieh and Juewen Liu.

The work in Chapter 4 has been published as: Mohamad Zandieh, Kshiti Patel, and Juewen Liu. "Adsorption of Linear and Spherical DNA Oligonucleotides onto Microplastics". *Langmuir* **2022**, 38, 5, 1915-1922. Kshiti performed the ζ-potentials measurements. All other experiments were performed by Mohamad Zandieh. The manuscript was written by Mohamad Zandieh and Juewen Liu.

Abstract

In recent decades, DNA oligonucleotides have been extensively researched due to their applications for catalysis (DNAzymes), biosensing (DNA aptamers/Watson-Crick hybridization), and nanomaterials assembly (DNA origami). An important aspect is to form DNA/nano hybrids, where nanomaterials can serve as DNA carriers, fluorophores and fluorescence quenchers, magnetic separation and enrichment, and other purposes. Most previous work focused on inorganic nanomaterials, especially gold, carbon-based nanomaterials and metal oxides, whereas work on polymeric nanomaterials was less explored. In this thesis, we interface DNA oligonucleotides with two important polymeric materials: polydopamine (PDA) and microplastics. We investigate the metal-mediated adsorption of DNA on these materials to understand the nature of interactions. These two polymers are important from different aspects. On one hand, PDA is a biocompatible, versatile, and universal coating material. Therefore, by coating any surface with a thin layer of PDA and comprehending PDA interactions with DNA, we can provide DNA functionality on various nanomaterials. A wide range of biomedical applications can benefit from this. On the other hand, in recent years, microplastics pollution has been highlighted as a serious threat to ecosystem. Investigation of DNA adsorption on microplastics provides insights to comprehend the nature of interactions between environmental DNA and microplastics. Moreover, it paves the way towards selection of DNA aptamers for microplastics.

In Chapter 1, background information about DNA, PDA, and microplastics is presented, the current literature about PDA-DNA and microplastics-DNA interactions is reviewed, and the outline and goals of this thesis are introduced.

In Chapter 2, polyvalent metal ions are used during PDA synthesis to prepare metal-doped PDA nanoparticles (NPs), and we use these NPs for DNA adsorption for the first time. It is found that the metal-doped PDA NPs adsorb DNA with higher capacity and tighter binding compared to metal-adsorbed PDA NPs. The metal-doped PDA-DNA conjugate has a remarkable stability in biological media such as serum and PBS. Considering the improved selectivity and robustness, the metal-doped PDA NPs are found to be the better candidate for designing fluorescent-based DNA sensors compared to metal-adsorbed PDA NPs.

In Chapter 3, the adsorption of SNA and linear DNA on PDA NPs is compared and the cooperative effect of metal ions for promoting SNA adsorption is illustrated. Then based on the extraordinary

stability of PDA-SNA conjugate, a hybrid material is designed for DNA extraction and detection. The hybrid materials consist of a Fe_3O_4 core (to provide magnetic separation), a PDA shell (to achieve specific DNA extraction) and a SNA decoration (to achieve efficient hybridization of target DNA). Therefore, selective and highly robust extraction and detection of DNA is achieved.

In Chapter 4, the adsorption of linear DNA and SNA onto the most common microplastics is systematically studied for the first time. Metal-mediated interactions are found to be vital for DNA adsorption onto microplastics. Among the environmentally abundant metal ions, Ca^{2+} and Mg^{2+} show a higher efficiency than Na^+ for promoting the adsorption. Among the microplastics, PET and PS show higher DNA adsorption efficiency than PE, PP, and PVC. It is likely that the aromatic groups of PET and PS provide extra interactions for a more stable adsorption. Hydrogen bonding also is found to be important for such adsorption.

In Chapter 5, the strong SNA adsorption is applied to reveal the difference between fresh and water-stored microplastics. SNA adsorption is enhanced on the water-stored microplastics. However, the spectroscopic data suggest that these microplastics are the same in terms of surface chemistry. Therefore, the difference is because of the change of wettability of microplastics which is observable in the floating behavior of microplastics as well. Likely, due to microplastics storage in water, the surface the surface roughness features become wet allowing a more efficient SNA adsorption. Therefore, SNA adsorption is proposed as a simple technique to probe the degree of wettability of microplastics.

The main original contributions of this thesis include the use of surface science approaches to study the adsorption of DNA; the focus on the effect of metal ions for DNA adsorption; and the understanding of DNA adsorption forces on these polymeric materials.

Acknowledgements

Five years ago, when I was looking for a university to pursue my studies, I looked into over 100 research groups. And you know! The harder you work, the luckier you get! I have always felt lucky to be a part of Liu group since day one. Now, I would like to extend my special thanks to my supervisor, Dr. Juewen Liu for his approachable manner, the invaluable advice, and the constant encouragement. My friends outside work are surprised when they see my passion and positive attitude about research, and I think my attitude is just a reflection of what I learned in Dr. Liu's research group.

I would like to greatly thank Dr. Dan Thomas, and Dr. Vivek Maheshwari for agreeing to be on my advisory committee, for their helpful advice evaluating my research, and for serving as my examining committee. I would also like to extend my thanks to Dr. Micheal Tam and Dr. Hua-Zhong Yu for agreeing to be on my examining committee for my dissertation.

I would like to thank all the current and former students and scholars of the Liu lab for creating a positive and productive working environment. Special thanks to my friends and colleagues for all the support, productive discussions, and friendly uplifting chats: Dr. Po-Jung Jimmy Huang, Dr. Biwu Liu, Dr. Lingzi Ma, Dr. Anand Lopez, Dr. Zhicheng Huang, Dr. Yuqing Li, Dr. Fang Zhang, Dr. Fan He, Dr. Jinyi Zhang, Dr. Chang Lu, Dr. Yibo Liu, Dr. Kaya Wong, Yuzhe Ding, Yichen Zhao, and Jennifer Moon.

Although I did my PhD far away from home, I had the privilege of having some good old friends here by my side. My friends whom I have known for 12 years now. With you, here also feels like home: Hosein Abdoli, Behrooz Jadidi, Alireza Sobhani, and Mahshid Jannati. I also have been lucky to have the support of many other friends I made here: Niloo, Negin, Ali, Sam, Mina, Ghazaal, Andrew, Santo, Marzie, Mohsen, Nilz, Miguel, Mishell, Amir, Hossein, and Hamid.

I cannot find proper words to express my appreciation to my parents: maman (Zoleikha) and baba (Ali). I remember once a high school refused to enroll me, since I was not "as good" for them. My parents did not settle for worse and made every effort to enroll me to an even better school. They believed in me whenever no one else did. I also sincerely thank my sisters (Somi and Marzi) and my brother (Sam) for their never-ending love and encouragement.

Dedication

I would like to dedicate this thesis to my family members: Zoleikha, Ali, Somi, Marzi, and Sam.

Table of Contents

List of Figures

xiv

xv

List of Tables

Chapter 1
Introduction

1.1 Introduction to DNA

Deoxyribonucleic acid (DNA) is an important biomolecule well-known for containing the genetic information of living organisms. Alongside with the biological function, DNA has gained popularity in the past a few decades in the field of nanotechnology thanks to its high stability, low cost, ease of synthesis, and its unique and extremely simple base-pairing rule.[1-6] In addition, single-stranded DNA of certain sequences have catalytic and molecular recognition functions. In biotechnology, bioanalytical chemistry and nanotechnology, DNA is used for molecular recognition,[7] catalysis,[8] and nanomaterials assembly and patterning.[9-10]

1.1.1 Chemistry of DNA

A single-stranded DNA (ssDNA) is a polymer made up of multiple units called nucleotides. A nucleotide consists of three moieties: a nucleobase, a pentose sugar, and a phosphate residue (Figure 1.1). The nucleobase can be any of the 4 different molecules named adenine (A), thymine (T), cytosine (C), and guanine (G). The phosphate is covalently bonded to the carbon at 5' and 3' positions of the sugar to form the sugar phosphate backbone. At physiological pH, the nucleobases are charge-neutral, while each phosphate has a negative charge (pK_a lower than 2), thereby DNA is highly negatively charged.

A double-stranded DNA (dsDNA) forms when two anti-parallel strands of DNA bind via hydrogen bonding between A and T and between C and G nucleobases (Figure 1.1). This is called Watson-Crick base-pairing or hybridization which creates the typical right-handed double-helix structure of dsDNA. Alongside with hydrogen bonding, π–π stacking of the adjacent nucleobases also takes part in forming the highly stable dsDNA.[11]

In this thesis, we use ssDNA of shorter than 25 bases or base pairs, and such short ssDNAs are also called DNA oligonucleotides. Throughout the thesis, we simply used the term DNA to refer to the short ssDNA oligonucleotides unless otherwise mentioned.

1
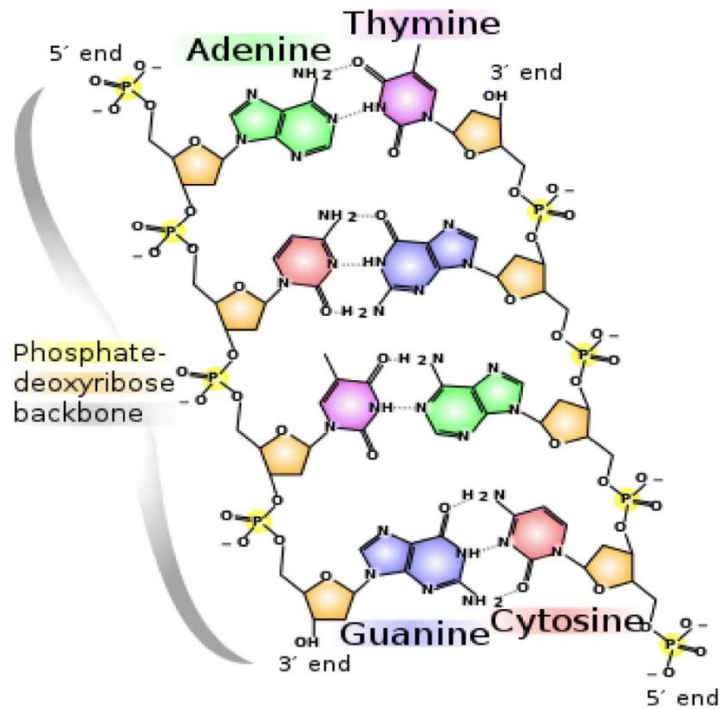
Figure 1.1 Chemical structure of DNA. Figure adapted with permission.[12] Copyright ©2019 Springer Nature.

1.1.2 DNA as Functional Polymer

Since a few decades ago, DNA has been used for its versatile chemical functions in the fields of molecular recognition, catalysis, and nanomaterials assembly. The following are some of the important roles of DNA as a functional polymer.

1.1.2.1 DNA Aptamers

Aptamers are single stranded oligonucleotides (DNA or RNA) which bind to a target molecule with remarkable affinity and specificity. As demonstrated in Figure 1.2A, aptamers interact with their target via structural recognition.[13] The first DNA aptamer was reported in 1992 for detection of thrombin,[14] and since then many DNA aptamers have been selected to detect metal ions, small molecules, protein and even cells.[15-17] As compared to antibodies, aptamers have shown advantages such as improved specificity, cost-effectiveness, and higher stability.[18]

1.1.2.2 DNAzymes

Nucleic acids can also act as enzymes. In the early 1980s, it was discovered that natural RNA has catalytic activity for a wide range of chemical reactions.[19] Unlike RNA enzymes (ribozymes), DNAzymes are not found in nature. In 1994, the first DNAzyme was isolated by *in vitro* selection that could cleave RNA.[20] DNAzymes can catalyze a wide range of reactions such as RNA/DNA cleavage, and RNA/DNA ligation. Figure 1.2B illustrates a Pb^{2+}-specific DNAzyme which catalyzes DNA cleavage.[21] The chemical stability for extracellular applications and the cost of DNAzymes has made them attractive as compared to ribozymes.
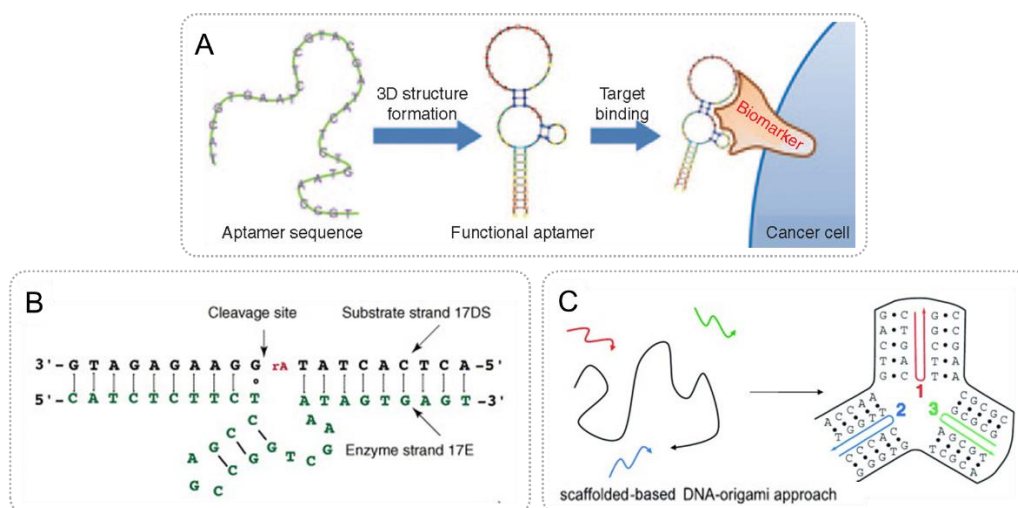
Figure 1.2. Different functionalities of DNA. (A) A scheme demonstrating the structural recognition of a target cell with a DNA aptamer. Figure adapted under the terms of the Creative Commons CC BY license.[13] Copyright © 2014, Elsevier B.V. (B) An example of DNAzyme: Pb^{2+}- specific DNAzyme for catalytic cleavage of a ssDNA. Figure adapted with permission.[21] Copyright © 2006 , Elsevier B.V. (C) A scheme demonstrating a DNA origami constructed via hybridization of a long scaffold DNA (the black strand) with multiple staple strands (red, green and blue strands). Figure adapted with permission.[22] Copyright © 2012 , Wiley-VCH.

1.1.2.3 DNA for Nanomaterials Assembly

The Watson-Crick base pairing rule can be used to fabricate micro- and nanostructures and patterns with nanoscale precisions. Many simple periodic patterns and sophisticated structures have been reported. One of the most impressive achievements were made using the DNA origami technology.[9] In a DNA origami, typically a long ssDNA (scaffold strand) is designed to hybridize with multiple short ssDNAs (staple strands) to form complexed nanostructures (Figure 1.2C).[22] More recently,

DNA-based nanomaterials were synthesized simply through coordination-driven self-assembly of metal ions and DNA molecules.[23] Such nanostructures improve the delivery of functional DNA into cells.

1.1.3 DNA Binding to Metal Ions

Oligonucleotides have been researched as metal ligands since decades ago.[24-27] Since DNA is highly negatively charged at physiological pH, binding with cations is expected via electrostatic interactions. Moreover, hydrated cations and DNA can bind via hydrogen bonding of water molecules.[28] The DNA metal binding sites are mainly the O atoms of phosphate and the O and N atoms of nucleobases (Figure 1.3).[2]

	AMP	phosphate	adenine N7	guanine N7 + O6	cytosine N3 + O2
Pb^{2+}	-	1.5	0.9	1.75	1.65
Cd^{2+}	-	1.4	1.1	2.05	1.35
Zn^{2+}	-	1.3	0.6	1.65	0.6
Cu^{2+}	3.18	1.6	1.35	2.65	2.05
Mn^{2+}	2.40	1.3	0.5	1.05	0.6
Mg^{2+}	1.97	1.05	0.35	0.75	0.5
Ca^{2+}	1.85	1.0	0.3	0.75	0.6
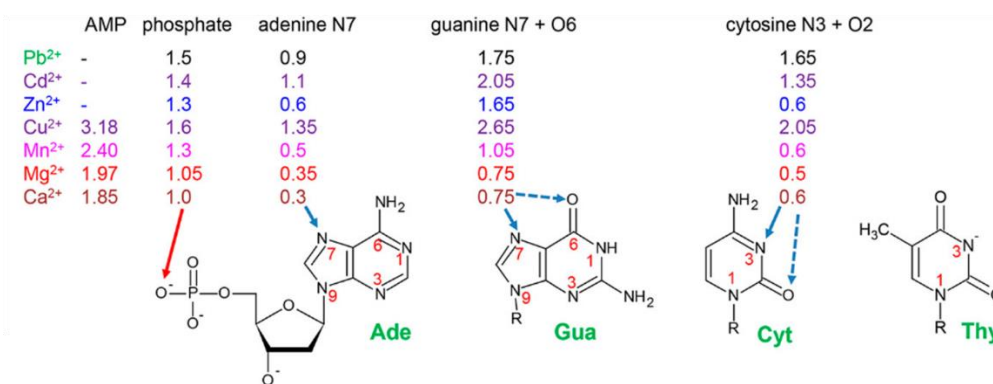
Figure 1.3 Affinity of various binding sites of nucleotides to various divalent metal ions. The values are log of K_a. Figure adapted with permission.[26] Copyright ©2010 American Chemical Society.

Based on the DNA-metal interactions, many DNA aptamers have been selected for specific detection of metal ions. Moreover, metal specific DNAzymes are used to detect metal ions.[29] More recently, it has been reported that metal ions can protect DNA at high temperatures upon coordination-driven self-assembly.[30]

Since most of the commonly used nanomaterials are negatively charged at neutral pH and inspired by the DNA-metal interactions, metal ions have been used to promote DNA adsorption on nanomaterials.[31-33] Adding Na^+ is an established method to screen the charge repulsion between DNA and nanomaterials; however, polyvalent metal ions (specifically transition metals) are reported to provide additional attractive forces to bridge the adsorption of DNA.[34]

1.1.4 Spherical Nucleic Acids

Spherical DNA or spherical nucleic acid (SNA) is a structure consisting of a high density of DNA oligonucleotides conjugated to a nanoparticle core typically via covalent binding. Such a structure has shown many interesting properties such as improved colloidal stability,[35-36] better cellular uptake,[37-38] sharper melting transitions,[39] and hybridization with complementary DNA with higher affinity.[40-41]

  Gold nanoparticles (AuNPs) are the most common particles to construct SNAs due to their stability, biocompatibility, and excellent optical properties such as high extinction coefficient, surface plasmon resonance, and distance-dependent colorimetry. DNA oligonucleotides are typically modified a thiol group to achieve covalent binding on AuNPs. As shown in Figure 1.4, to construct stable SNAs, various methods have been reported such as salt aging,[42] low-pH method,[43] freezing-assisted,[44] and different dehydration methods.[45-47]
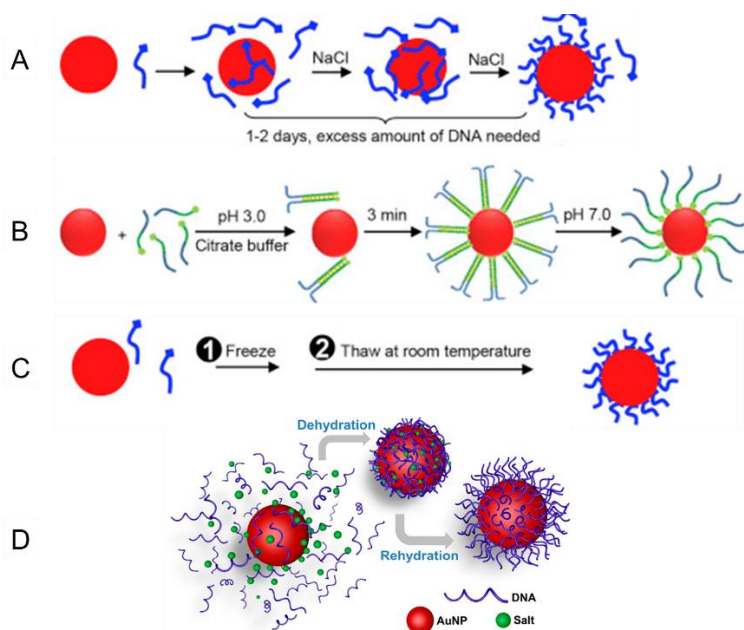
Figure 1.4 Methods for SNA preparation. (A) Salt aging: initial adsorption of thiolated DNA and gradual adding of salt to achieve stable covalent binding. (B) Low-pH: using poly-A blocks to assemble parallel duplex. (C) Freezing-directed: without use of additional reagents. Figures A-C adapted with permission.[48] Copyright ©2019, Elsevier B.V. (D) Dehydration: increase of local DNA concentration by evaporating using different methods such as butanol dehydration and microwave-assisted dehydration. Figure adapted with permission.[45] Copyright ©2021 American Chemical Society.

In a typical mechanism, it is believed that the DNA oligonucleotides are first adsorbed onto the AuNPs via both the thiol ending and the DNA bases. Then, upon adsorption of more DNA strands and steric confinement, thiol groups of additional strands gradually displace the bases of initially adsorbed strands. Eventually, all DNAs strands would attach to AuNPs via the thiol group holding an upright conformation.[49]

Recently, it was reported by our group that SNA can adsorb onto a wide group of nanomaterials. SNAs simultaneously use multiple DNA strands to anchor onto a surface.[50] Therefore, a weaker binding affinity of a ssDNA can amplify by means of polyvalent interactions resulting an ultrahigh adsorption stability comparable to covalent binding. Such strong adsorption affinity would also provide more insights about DNA interactions with nanomaterials.

1.2 Interfacing DNA and Nanomaterials

Nanomaterials have been extensively used in scientific fields such as chemistry, physics, pharmacy, and materials science.[51-53] They exhibit different properties from their bulk counterpart. For instance, they own superior optical and mechanical properties, and higher surface-to-volume ratio.

Many biomedical applications of nanomaterials such as in biosensing and drug delivery have been realized when nanomaterials were interfaced with biomolecules such as DNA. To conjugate nanomaterial and DNA, covalent or non-covalent interaction may be involved. In this thesis, the focus is on non-covalent interactions of DNA with a few polymeric nanomaterials. The non-covalent interactions are typically hydrogen bonding, electrostatic interaction, hydrophobic interactions and π-π stacking which result in adsorption of DNA on the nanomaterials.

The most extensively used nanomaterials for DNA adsorption are AuNPs, graphene oxide (GO), and metal oxides. Adsorption of DNA on AuNPs is based on the coordination bonds between DNA nucleobases and Au as a soft Lewis acid.[54] Based on the different affinity of ssDNA and dsDNA for AuNPs, many colorimetric biosensors have been designed with high sensitivity.[55]

GO adsorbs DNA mainly via hydrogen bonding and π-π stacking. The hydrogen bonding forms between hydroxyl and carboxyl groups of GO and phosphate and nucleobases of DNA, and π-π stacking occurs between aromatic rings of GO and nucleobases of DNA.[56] Bare metal oxides nanoparticles mainly adsorb DNA via the electrostatic interactions with DNA phosphate backbone.[57] GO- or metal oxides-DNA

conjugates can be applied for fluorescent and electrochemical biosensors, drug delivery and photocatalysis.

Following, I will respectively elaborate polydopamine (PDA) and microplastics as two important polymeric materials and will delineate the necessity of the study of DNA adsorption onto these materials.

1.3 Introduction to Polydopamine

The extraordinary wet adhesion of some marine creatures, such as mussels, is caused by their secreted proteins that are rich in catecholamine groups. This has inspired scientists to develop a universal coating material that can mimic the natural wet adhesion.[58] Although dopamine is a catecholamine, PDA is not yet found naturally. PDA is a synthetic analog of melanin, and natural melanin exists in the color pigments of the skin, hair, and eyes of the human body. Melanin is produced by the aggregation and polymerization of catecholamines such as DOPA or tyrosine (Figure 1.5A).[59-60]

To date, the polymerization pathways of dopamine are still unknown, but a few likely pathways have been proposed.[61-65] In a model explained by Klosterman and Bettinger,[65] PDA is formed after multiple stages of oxidation, cyclization, cleavage, and polymerization reactions. As shown in Figure 1.5B, dopamine–semiquinone and O_2^- are the products of the oxidation of deprotonated dopamine. After the next oxidation step, dopamine–quinone is produced which undergoes an intramolecular cyclization to produce leucodopaminechrome. Further oxidation and rearrangement steps produce different heterocyclic species shown in Figure 1.5B. Species from all stages of the oxidation pathway attach together through covalent interactions, and noncovalent π–π stacking and hydrogen bonding to form PDA aggregates (Figure 1.5C).[66-67]
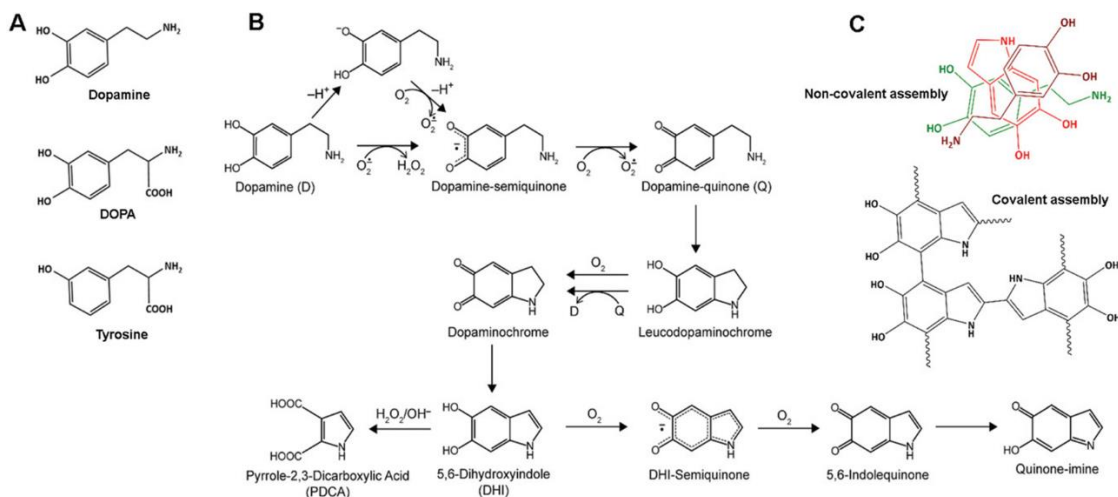
Figure 1.5 (A) Chemical structure of dopamine, DOPA, and tyrosine. (B) Different oxidation products of dopamine in an alkaline solution in the presence of dissolved oxygen. The final PDA NPs consist of covalent and noncovalent assemblies of these species. C) Some covalent and noncovalent assemblies in PDA NPs. Figure adapted under the terms of the Creative Commons CC-BY 4.0 License.[65] Copyright ©2017, The Authors, published by MDPI.

1.3.1 Synthesis of Polydopamine

PDA typically has two forms: films and NPs. Due to its extraordinary adhesive strength, PDA films can be coated on various types of surfaces via the oxidative polymerization of dopamine.[58] In the case that no surfaces are available to host or intermediate PDA aggregation, PDA oligomers get together and form PDA NPs, typically in the shape of nanospheres. Below, we discuss some conditions affecting the synthesis of PDA.

1.3.1.1 Effect of pH

PDA synthesis is generally performed with dissolved oxygen under alkaline conditions to facilitate the deprotonation of dopamine. It is common to use Tris buffer at pH 8.5,[68] or to directly add NaOH to an aqueous solution of dopamine.[69] Interestingly, some works claimed to have synthesized PDA at lower pH, but extra oxidizing agents were needed.[70] This could be a helpful strategy to coat PDA on alkaline-sensitive materials. It is also claimed that at lower pH PDA is formed in a more controlled manner, as the autoxidation of dopamine by dissolved oxygen is prevented.[71]

1.3.1.2 Control of PDA NPs Size

Typically, the diameter of PDA NPs is in the range of 150–300 nm. At fixed pH and temperature, the main factor regulating the size of PDA NPs is the initial dopamine concentration, with higher dopamine concentrations producing larger NPs.[69] On the other hand, the size of PDA NPs or the thickness of PDA films is inversely related with pH.[69, 72] Increasing temperature is another strategy of decreasing PDA NPs size.[69] Moreover, addition of surfactants such as SDS can also decrease the size of PDA NPs, with this limited to the size of surfactant micelles.[73]

1.3.1.3 Intermediating Agents

Due to their strong interaction with dopamine oligomers, metal ions can accelerate PDA formation. To date, Fe^{3+}, Gd^{3+}, Mn^{3+}, Co^{2+}, Ni^{2+}, Cu^{2+}, Zn^{2+}, and Ga^{3+} have been used in the process of PDA polymerization,[74-78] and the synthesis time was shortened down to 2 h from the 72 h typically needed. Polycations like poly(vinyl alcohol)[79] and poly (allyl amine hydrochloride)[80] or polyanions like poly(acrylic acid) and poly(4-styrene sulfonate)[80] have also been used during the synthesis. These materials can electrostatically or covalently interact with PDA. Folic acid (FA) is also found to interact with dopamine through hydrogen bonding and π–π stacking, affecting the self-assembly of PDA.[81-82]

1.3.1.4 Core–Shell Structures

Due to the mild conditions of PDA synthesis and its metal chelating property, a high level of interest was devoted to the fabrication of core–shell hybrid materials with PDA on metal oxide[83-88] and noble metal NPs.[89-91] The shell thickness can vary from a few nm up to 100 nm and is tunable via the duration of the polymerization.[92] The PDA shell not only provides functional groups for additional surface modifications, but it can also protect the core (e.g., Fe_3O_4) from direct exposure to biological systems.

1.3.2 Applications of PDA

PDA is a biocompatible material with many interesting applications from water treatment,[93] oil absorption,[94-95] membranes,[96] to Li-ion batteries,[97-98] supercapacitors,[99] and solar cells[100] due to its metal binding, coating and light absorption properties.[92] In materials science, the abundance of catechol functional groups in PDA provides a reducing property.[58] A variety of metal nanoparticles (NPs), such as Au,[101-102]Ag,[103] and Pt,[104-105] as well as reduced graphene oxide (rGO),[106-107] have been

9

produced when PDA is used as reductant. Additionally, a shell of PDA can be coated on various NPs as discussed earlier. In biomedical science, PDA can adhere to cell walls,[108-109] encapsulate cells[109] and drugs,[110-111] and decrease the toxicity of biomaterials.[112] Finally, PDA can be used for sensing. PDA-containing biosensors have been used to detect various organic molecules,[113-114] biomolecules,[115-116] and metal ions.[117]

1.4 Interfacing DNA and Polydopamine

1.4.1 Covalent DNA attachment

Covalent conjugation of DNA onto PDA is accomplished by using DNA modified with a thiol or amine group (Figure 1.6). The catechol group of dopamine is known to undergo a reversible two-electron oxidation to form dopamine–quinone. The quinone form is susceptible to nucleophilic attack at the 3 or 5 positions from Michael acceptors such as primary amines and thiol residues, known as a Michael addition reaction (Figure 1.6). This type of covalent crosslinking has also been observed between dopamine and large biomolecules with cysteine in its primary structure.[118] To act as a Michael acceptor, amine and thiol groups must be protonated, meaning maintaining pH at or below the pK_a of the acceptor can greatly increase the rate of reaction. However, since quinone is favored at higher pH, pH needs to be carefully controlled.

   Amines generally have a pK_a of 10–11, and thus this range is suitable for covalent binding to PDA. In a solution of pH between 10 and 11, the rate-limiting step in the reaction between dopamine and primary amines is the oxidation of dopamine to the quinone form.[119] Under the same reaction conditions a Schiff-base reaction is also possible, coupling the donor to the 1 or 2 positions on the quinone, with amine, forming an imine species (Figure 1.6). The ability for PDA to react with amines and thiols is thought to be due to residual unreacted quinone moieties, which exist at the PDA NP surface after polymerization, as well as electrophilic moieties within the polymer backbone.[120]
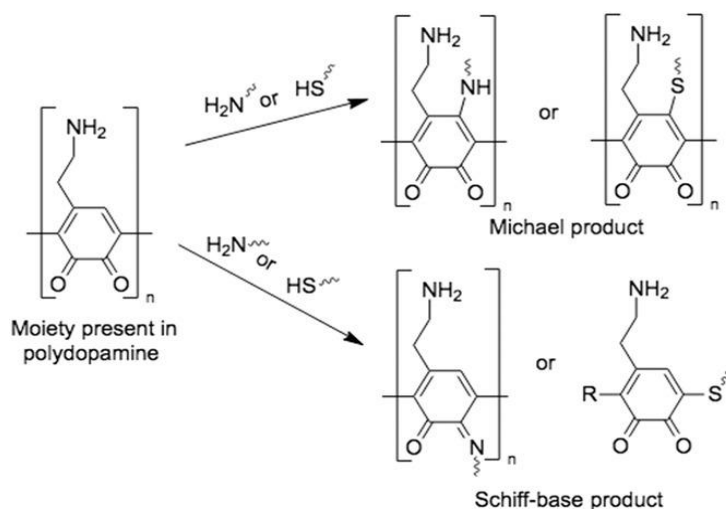
Figure 1.6 Reaction mechanisms for thiol or amine modified DNA relying on the dopamine–quinone moieties within the PDA structure. The conjugation is via either an amine or sulfide linkage or an imine species. The Schiff-base reaction with thiols occurs at a different position to amines. This requires a terminal dopamine–quinone species and forms a sulfide linkage adjacent to the carbonyl groups.

1.4.2 Low pH-Assisted DNA Adsorption

PDA is a zwitterionic material as it contains both amine groups and phenolic hydroxyl groups,[121] rendering a pH-switchable surface with an isoelectric point of ≈4.5.[122] Based on this, pH-responsive PDA was used for the adsorption of charged molecules.[123] Below the isoelectric point the PDA surface charge becomes positive, while DNA is negatively charged above pH 2 due to the phosphate backbone.[124] Hence, over a certain acidic pH range, PDA and DNA can attract, leading to DNA adsorption.[124]

1.4.3 Metal-Mediated DNA Adsorption

Catecholamines are good metal ligands.[75, 77-78, 125-126] On the other hand, DNA interacts with different metal ions through its nucleobases and phosphate backbone with different affinities.[2] Hence, it is reasonable to explore metal-mediated DNA adsorption. Through a careful reading of the literature, we noticed that divalent metal ions were present in buffers used in previous works, although the authors only claimed hydrogen bonding and π–π stacking interactions to be the reasons for DNA adsorption (Table 1.1).

11

Table 1.1 Metal ions in buffers for promoting DNA adsorption on PDA.

Binding buffer	Divalent metal	Application	Year	Ref.
Tris-HCl (pH 7.4)	5 mM Mg^{2+}	DNA biosensor	2013	[127]
20 mM Tris-HCl (pH 7.4)	1 mM Mg^{2+} + 1 mM Ca^{2+}	DNA/thrombin biosensor	2014	[128]
20 mM Tris-HCl (pH 8)	5 mM Mg^{2+} + 5 mM Ca^{2+}	miRNA biosensor	2014	[129]
20 mM Tris-HCl (pH 7.4)	1 mM Mg^{2+} + 1 mM Ca^{2+}	DNA biosensor	2015	[130]
1×PBS	5 mM Mg^{2+}	Intracellular delivery & Cell ATP imaging	2015	[131]
5 mM Tris-HCl (pH 8)	50 mM Mg^{2+}	DNA biosensor	2015	[132]
20 mM Tris-HCl (pH 8)	10 mM Mg^{2+}	Logic gate	2016	[133]
20 mM Tris-HCl (pH 8)	10 mM Mg^{2+}	DNA/ATP biosensor	2016	[134]
10 mM HEPES (pH 7.4)	20 mM Mg^{2+}	Intracellular delivery & Cell miRNA imaging	2017	[135]
20 mM Tris-HCl (pH 8)	10 mM Mg^{2+}	T4 PNK biosensor	2017	[136]

In 2018, Meng et al. investigated the role of polyvalent metal ions in DNA adsorption on PDA NPs.[32] At pH 7.6 in the absence of metal ions, the PDA cannot adsorb DNA at all. Hence, hydrogen bonding and π–π stacking alone were insufficient for DNA adsorption on PDA. Moreover, even up to 200×10^{-3} M monovalent metal ions could not promote DNA adsorption either, even though they can promote DNA adsorption on graphene oxide[31, 137-138] and AuNPs.[48]

Although in previous works (as presented in Table 1.1) Mg^{2+} was more commonly used than Ca^{2+}, Meng et al. showed that at the same concentration, Ca^{2+} was more effective than Mg^{2+} in promoting DNA adsorption on PDA.[32] They also used Cu^{2+} and Ce^{3+} to adsorb DNA and suggested these ions were even more efficient than Ca^{2+}, since adding cDNA can desorb the adsorbed DNA in the presence of Ca^{2+} but not in the presence Cu^{2+} or Ce^{3+}.

1.4.4 Applications of DNA/PDA Conjugates

1.4.4.1 DNA Extraction

Magnetic solid phase DNA extraction (MSPE) has advantages such as direct isolation from a crude sample, compatibility with large scale purification, and easy separation of biological debris.[139-140] To extract DNA from cell lysates of foodborne pathogens, Wang et al. coated a thin layer of PDA on magnetic Fe_3O_4 NPs.[124] They used the aforementioned low-pH (pH 4) adsorption method for the capture of DNA on the PDA surface, and the DNA–NP conjugates were collected by magnetic separation. For the elution step, Tris-HCl buffer (pH 8) was used to induce the desorption of extracted DNA.
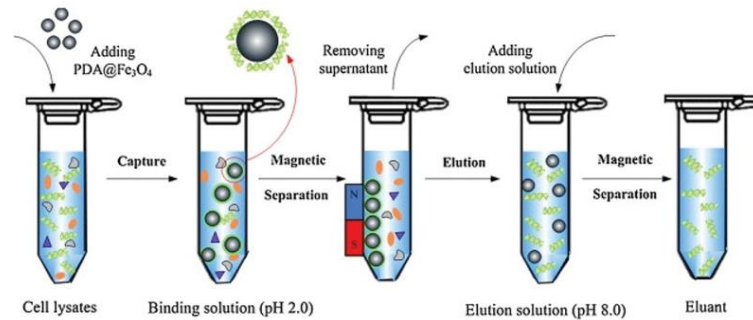
Figure 1.7 Scheme of DNA extraction procedure by Fe_3O_4@PDA core–shell NPs. Figure adapted with permission.[124] Copyright ©2015, Elsevier B.V.

The same group later simplified the DNA extraction method by avoiding magnetic separation.[141] They coated PDA on the inner surface of microfuge (MF) tubes and used it for DNA extraction via the pH-assisted method.[124] Although only the pH-assisted method was used for DNA extraction by PDA, other methods are also possible. For example, if metal-mediated DNA adsorption is used for the capture step, it might be possible to release the DNA by using EDTA.

1.4.4.2 Biosensors

One of the most common applications of PDA-DNA conjugates is biosensing. As shown in Figure 1.8, in a typical on–off biosensor, a fluorophore labeled (F-labeled) probe DNA is adsorbed on and quenched by PDA.[128] The presence of the target complementary DNA (cDNA) leads to hybridization and desorption of the probe DNA due to the lower affinity of dsDNA to the PDA surface. Using aptamers, non-nucleic acid targets can be detected.
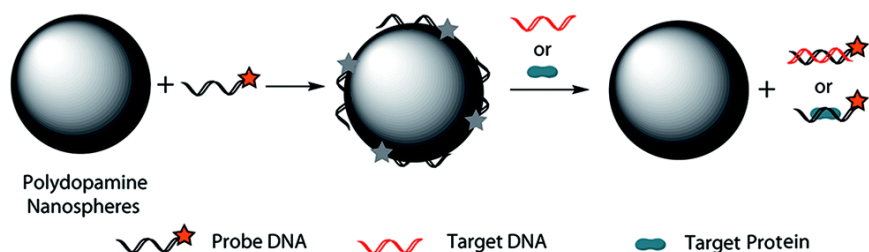
Figure 1.8 A scheme representing the principle of a typical on-off fluorescent-based biosensor using PDA. Figure adapted with permission.**[128]** Copyright ©2014, Royal Society of Chemistry.

Since noncovalent sensors may suffer from nonspecific probe desorption, efforts have also been made to covalently link DNA to PDA. In this method, amino- or thiol-modified DNA is immobilized onto PDA. Then the complementary target DNA (normally accompanied with a AuNP core) can hybridize with it to enhance different signals for surface plasmon resonance (SPR)[142] or electrochemical detection.[143] PDA-DNA biosensors have also been used for detection of cells as target where the probe DNA was conjugated with PDA through physical adsorption[144] or covalent binding.[89]

1.4.4.3 Intracellular Delivery and Imaging

PDA is highly biocompatible. Its protection of adsorbed DNA and their ability to cross the cell membrane enables PDA-DNA conjugates to be used for intracellular delivery and imaging applications. Detection of ATP in living cells,[145] miRNA in human mesenchymal stem cells,[90] tumor-related mRNA,[135] reactive oxygen species (ROS)[146] have been achieved using PDA-DNA conjugates.

1.4.4.4 Therapeutics

As the intracellular delivery of PDA-DNA conjugate became well established, the conjugates also have been applied for cancer therapy. Lin et al. used Fe_3O_4@PDA core–shell NPs for delivering FAM-labeled probe DNA to detect overexpression of mRNA in MCF-7 breast cancer cells.[131] The iron oxide enhanced the MRI contrast to monitor the delivery of the probe DNA, and the PDA was used for photoacoustic imaging due to its NIR light absorption. Similarly, a PDA-based nanosystem carrying an Mn^{2+}-specific DNAzyme has been used for photothermal therapy, photoacoustic imaging, and magnetic imaging.[147]

1.4.4.5 DNA Origami

As mentioned earlier, dopamine polymerization typically happens in an uncontrolled manner. However, it has been reported that local dopamine polymerization around a DNA template can be achieved when dopamine aggregation is inhibited at low pH.[148] In Tokura's work (Figure 1.9), a DNA nanotile-based origami was designed to contain G-quadruplex sequences, which can bind hemin to form a peroxidase-mimicking DNAzyme. The DNAzyme, when mixed with H_2O_2, can accelerate dopamine polymerization. Additionally, the DNAzyme nanotile activity was improved by lowering the pH to 5.3, which concomitantly prevented uncontrolled PDA formation in the solution.
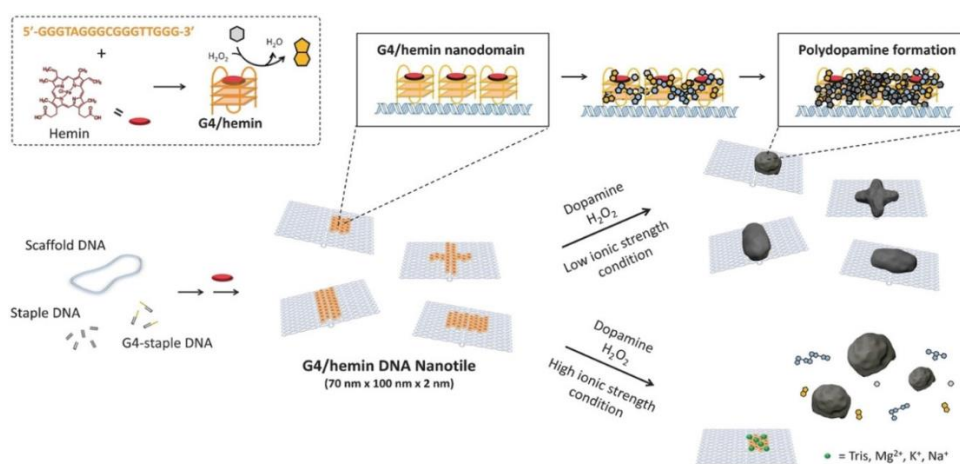
Figure 1.9 Scheme of the fabrication of PDA on a DNA origami. PDA is locally formed on the DNAzyme area attached to the nanotile carries, where the G-quadruplex DNA (orange) and hemin (red) are shown. At high ionic strength, the PDA formation on the DNAzyme is prevented. Figure adapted with permission.**[148]** Copyright © 2018 , Wiley-VCH.

Similarly, a phototriggered PDA formation on DNA origami has been reported.[149] A photosensitizer called protoporphyrin IX (PPIX) was anchored on G-quadruplex structures on the DNA template, which served as reaction centers for PDA formation. Dopamine polymerization by dissolved oxygen was avoided by adjusting the pH to 6.5. Upon irradiation with visible light, ROS were produced, which induce oxidative dopamine polymerization on the designated locations creating precise PDA patterns. Hence, a more straightforward controllable PDA synthesis was achieved by switching the light source on/off.

1.5 Introduction to Microplastics

Plastics are cheap, lightweight, durable, and versatile in manufacturing. Plastic production volume has been extensively growing from 1.5 million metric tons in 1950 to 370 million metric tons in 2020.[150] Plastics are polymers made from monomers which are derived from fossil hydrocarbons (e.g. ethylene). Chemical structures of the most common plastics are shown in Figure 1.10. Such polymers are not biodegradable, thereby the plastic waste accumulates in the environment.
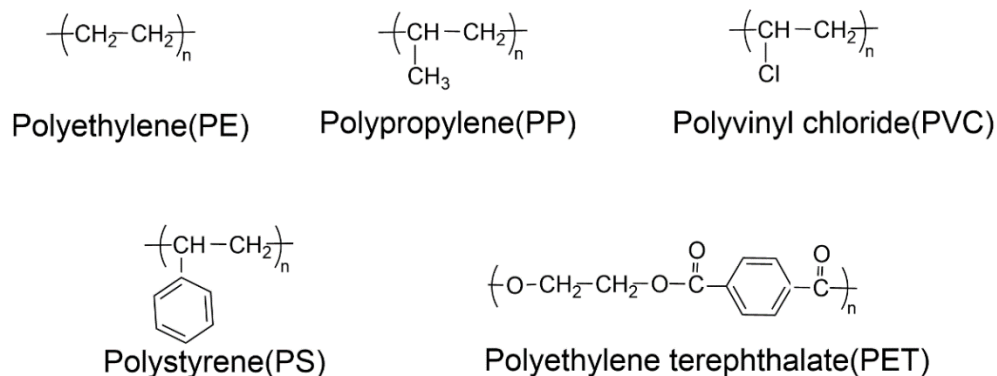
Figure 1.10 Molecular structures of the most common plastic materials including PE, PP, PVC, PS and PET.

   When plastic materials are shredded into submillimeter pieces via chemical or mechanical transformations, microplastics are generated.[151] Such microplastics are categorized as secondary microplastics. On the other hand, primary microplastics are the plastic microbeads that are primarily manufactured to be used in cleaning and cosmetic products. Primary microplastics issue seems to be easier to tackle, and there are already growing regulations to ban their use and to enforce the industries to replace biodegradable alternatives. Therefore, this thesis focuses on studying secondary microplastics.

   It is reported that an individual consumes the equivalent of a credit card worth of microplastics (~5 grams) every week by means of inhalation and ingestion.[152] Microplastics consumption can pose a threat to human health in long-term, and there are evidence that they can induce infertility, immune system disorders, and cancer.[153-154] Microplastics have high surface-to-volume ratio, and they are prone to adsorption of heavy metals, invasive microorganisms, and other pollutants in the environmental waters. Therefore, not only they have intrinsic detrimental effects on the ecosystem, but they also serve as a vector facilitating the spreading of other pollutants.[155]

The detrimental effects of microplastics on environment and human health motivated a variety of research regarding detection, removal, and degradation of the microplastics. To achieve any of these, studying the surface science and adsorption behavior of microplastics can be helpful. Following, I first discuss the adsorption behavior of microplastics for metal ions. Then, I review the literature of the microplastics-DNA interface and delineate our research purposes.

1.5.1 Adsorption of Metal ions onto Microplastics

Metal pollution is a common issue of environmental waters due to wastewater discharges.[156] Adsorption of many heavy metals on microplastics have been reported. Microplastics have typically a negatively charged surface. Therefore, adsorption of many divalent metals such as Ni^{2+}, Zn^{2+}, and Cu^{2+} via the electrostatic interactions with carboxylate groups of the microplastics have been reported.[157] Diffusion of metal ions into pores of the microplastics is another adsorption mechanism.[158] Moreover, co-precipitation and adsorption of hydrated oxides of Fe and Mn ions have also been reported.[159] Figure 1.11 is a scheme demonstrating the possible interactions involved in the adsorption of metal ions onto microplastics.[160]
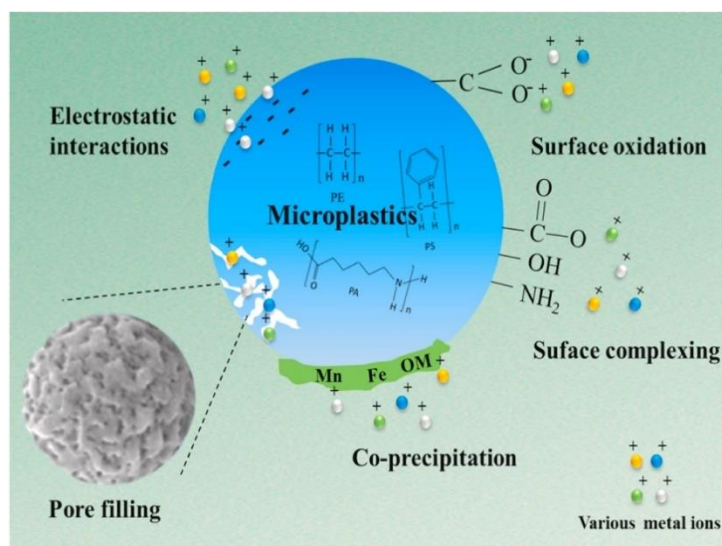
Figure 1.11 A scheme representing the possible adsorption mechanism of metal ions on microplastics. Figure adapted with permission.[160] Copyright ©2018, Elsevier B.V.

Moreover, the aging conditions of the microplastics creates more oxygen- containing functional groups on the surface, induces porosity and hydrophilicity, thereby affecting their adsorption

behavior.[161] For instance, UV-induced aging of microplastics can enhance their adsorption of Cu^{2+}, Pb^{2+}, Cd^{2+}, Ni^{2+} and Zn^{2+}.[162-163]

Similar to PDA, binding of metal ions to microplastics provides the opportunity to bridge the interactions between DNA oligonucleotides and microplastics.

1.6 DNA and Microplastics

1.6.1 Indirect DNA Interactions with Microplastics

Most of the literature about DNA and microplastics focuses on: 1.biological DNA extraction from microplastics,[164] or 2.DNA damage by microplastics.[165] Both attributes to indirect interactions between microplastics and DNA.

1.6.1.1 Biological DNA Extraction from Microplastics

As mentioned earlier, microplastics provide a stable substrate for adsorption of wide range of invasive pollutants such as living organisms. Therefore, extraction of nucleic acids such as biological DNA from microplastics biofilm is a common technique to gain insights into the composition of living organisms. The extraction is typically followed by sequencing and PCR amplification of the selected genes. Using DNA extraction from microplastics, the presence of many organisms including diatoms, bacteria, coccolithophores, and even some invertebrate groups have been identified.[166]

1.6.1.2 DNA Damage by Microplastics

On the other hand, it is reported that microplastics can induce damage and cleavage of DNA.[167-168] For instance, it is reported that photo-degraded PS microplastics have more toxicity than pristine PS and the produced toxicants can induce DNA damage of a model organism.[169] In another work, it is reported that under a solar simulator, PS nanoplastics modified with NH_2 can generate reactive oxygen species (ROS) which induce DNA damage.[170]

1.6.2 DNA Adsorption onto Plastics

Direct adsorption of DNA onto plastics has been reported when DNA was stored in PP microtubes.[171-172] PP is highly hydrophobic, and PP and DNA are highly negatively charged. Therefore, the DNA adsorption should be minimal. However, it has been observed that 180 bp ssDNA can remarkably adsorb onto the PP tube walls at high ionic strength conditions (e.g. 2.5 M NaCl).[171] Later, it was

reported that although differently manufactured PP tubes show different affinities for DNA adsorption, DNA adsorption on most PP tubes can be minimized by storing at low or moderate ionic strength.[172] It was implied that metal-mediated interactions might be crucial for adsorption of DNA onto plastics.

On the other hand, covalent immobilization of amino-modified ssDNA on carboxyl rich polycarbonate (PC) substrate can be achieved.[173] Unlike, PDA-DNA conjugates, the study of interactions of ssDNA onto plastics is as limited as it is discussed here.

1.6.3 Biological dsDNA (Genes) Adsorption onto Microplastics

Microplastics can act as a vector for antibiotic resistance genes (ARGs) and enhance their cell permeability.[174] Most of the studies in this regard focus on the detrimental effect of such conjugate on the ecosystem and little insights into the nature of interactions have been provided.

It has been reported that the UV-induced aged PS microplastics can more effectively adsorb ARGs.[175] They claimed that PS microplastics can adsorb ARGs via hydrophobic interactions as well as π-π stacking, whereas the aged PS microplastics contain more oxygen-containing groups (such as hydroxyl and carboxyl) which can form more hydrogen bonding with the ARGs.

Overall, systematic study of ssDNA adsorption on microplastics and investigation of the nature of interactions is missing in the literature. In this thesis (Chapters 4 and 5), we aim to systematically investigate DNA adsorption on microplastics with a focus on the effect of metal ions.

1.7 Thesis Goals and Outline

In this Chapter, we discussed the fundamental concepts about DNA oligonucleotides, PDA, and microplastics. The thesis focuses on studying the metal-mediated adsorption of DNA on two important polymeric materials. Chapters 2 and 3 are about DNA adsorption on PDA. Chapters 4 and 5 are about DNA adsorption on microplastics. These polymers and exploring their interactions with DNA are important from different viewpoints.

On one hand, PDA is known as a universal coating material that has been used for a wide range of biomedical applications. Therefore, DNA-PDA conjugates are useful in applications such as biosensing and drug delivery. On the other hand, microplastics are an environmentally related

concern. Therefore, understanding the interactions of DNA and microplastics can pave the way towards the DNA aptamer selection for microplastics detection.

In Chapter 2, we synthesize metal-doped PDA by adding Ca^{2+}, Ni^{2+}, Zn^{2+}, Fe^{3+}, or Gd^{3+} during the dopamine polymerization. We compare the DNA adsorption efficiency of metal-doped PDA with metal-adsorbed PDA (where metal ions are added after the PDA synthesis and to the reaction buffer). We find that metal-doped PDA adsorbs more DNA than metal-adsorbed which can be attributed to a higher metal loading on the surface of metal-doped NPs. Metal leaching from metal-doped NPs is negligible. Moreover, we show that the metal-doped PDA NPs promote a tighter and more robust DNA adsorption with high stability in serum and PBS. Finally, we show that metal-doped PDA NPs has an improved DNA sensing functionality compared to the metal-adsorbed PDA.

In Chapter 3, we introduce SNA and show that the adsorption of SNA on PDA is dependent on the cooperative effect of multiple metal ions whereas the linear DNA adsorption follows one-site metal binding behavior. SNA adsorption on PDA is extremely stable comparable to covalent binding. We then design a three-component hybrid material consisting of: a Fe_3O_4 core (to provide magnetic separation), a PDA shell (to achieve specific DNA extraction) and a SNA decoration (to achieve efficient hybridization of target DNA). This hybrid material is used for highly selective DNA extraction and detection.

In Chapter 4, we investigate the adsorption of linear DNA and SNA onto the most common microplastics including PE, PP, PVC, PS and PET. The vital role of environmentally abundant metal ions (Na^+, Mg^{2+}, and Ca^{2+}) to promote such adsorption is shown. PET and PS have the highest efficiency for DNA adsorption probably due to the extra interactions provided by their aromatic rings. The desorption studies reveal that hydrogen bonding and metal-mediated interactions are dominant for DNA adsorption onto microplastics.

In Chapter 5, we discuss an important parameter that affects adsorption behavior of microplastics: wetting. By using SNA and its strong interactions with microplastics, we reveal that wettable microplastics adsorb more efficiently. Spectroscopic data approves that upon the wetting conditions, no chemical change occurs on the microplastics. We reason that the wettable microplastics are more hydrophilic allowing SNA to come close to surface and be adsorbed, whereas fresh microplastics are hydrophobic and the trapped air at the surface disallows SNA interactions with microplastics surface. Finally, we propose SNA adsorption as a simple method to quantify the wettability of microplastics.

Chapter 2

Metal-Doped versus Metal-Adsorbed Polydopamine Nanoparticles for Adsorption and Sensing of DNA Oligonucleotides

The results presented in this chapter have been published as:

Mohamad Zandieh and Juewen Liu. "Metal-Doped Polydopamine Nanoparticles for Highly Robust and Efficient DNA Adsorption and Sensing". *Langmuir* **2021**, 37, 30, 8953−8960

2.1 Introduction

Adsorption of DNA oligonucleotides onto nanomaterials is highly important for biosensing,[8, 176-178] DNA extraction,[179-182] gene delivery,[183-186] and DNA-directed assembly.[41, 148, 187-188] The majority of nanomaterials are negatively charged at neutral pH, which would repel polyanionic DNA. To promote DNA adsorption on such nanomaterials, adding salt (e.g., NaCl) for charge screening[31, 42] or lowering pH[43, 49, 124] are the commonly used methods. Recently, polyvalent metal ions also have been used to bridge DNA adsorption.[34, 189-191]

PDA NPs are synthesized via oxidative polymerization of dopamine under alkaline conditions. Mild synthesis conditions, strong light absorption properties, and high biocompatibility are among the attracting properties of PDA.[92, 192] In addition, PDA is best known for its exceptional adhesive property, providing a functional coating on various surfaces.[58, 193-194] Therefore, PDA can mediate DNA attachment to various types of nanomaterials, and there is a high level of interest in attaching DNA to PDA.

DNA can interact with PDA via π–π stacking (between DNA nucleobases and PDA aromatic rings) and hydrogen bonding. From the standpoint of charge interactions, since PDA is negatively charged at physiological pH, it repels negatively charged DNA.[195] Polyvalent metal ions such as Ca^{2+},[32] and Ni^{2+} and Zn^{2+} are quite efficient to bridge DNA adsorption on PDA NPs.[196-197] Since catecholamines are strong metal ligands,[125-126, 198] an interesting question is whether metal ions can be doped in PDA NPs (as compared to add externally) to achieve DNA adsorption. In this case, metal ions need to be stably embedded in PDA without leaching. At the same time, a fraction of the metal ions need to be present on the surface of PDA. Metal ions have been previously used during PDA synthesis mainly

21

for producing paramagnetic NPs.[77-78] Wang and co-workers showed that a remarkably higher metal content (e.g., 20-fold more for Zn^{2+}) was loaded within the PDA NPs during the synthesis compared to when metal ions were added to PDA after the synthesis.[77]

In this work, we compared the effect of adding polyvalent metal ions during (metal-doped) and after (metal-adsorbed) the synthesis of PDA NPs with a focus on Zn^{2+} (Figure 2.1A). We showed that, for the metal-doped NPs, the metal ions were loaded on the surface more tightly and likely with a higher content. A higher DNA adsorption affinity and robustness were observed for the metal-doped PDA NPs, which were useful for the detection and extraction of DNA.Materials and Methods

2.2 Materials and Methods

2.2.1 Chemicals

All of the DNA samples were purchased from Integrated DNA Technologies (IDT, Coralville, IA, USA), and their sequences are presented in Table 2.1. Various metal chloride salts, dopamine hydrochloride, ethylenediaminetetraacetic acid (EDTA), 8- hydroxy-5-quinolinesulfonic acid (HQS), bovine serum albumin (BSA), and fetal bovine serum (FBS) were obtained from Sigma- Aldrich. Sodium phosphate dibasic heptahydrate, 4-(2-hydroxyethyl) piperazine-1-ethanesulfonate (HEPES), urea, and adenosine were purchased from Mandel Scientific (Guelph, ON, Canada). Milli-Q water was used for all of the buffer and solution preparations.

Table 2.1 DNA sequences used in this Chapter.

DNA Names	Sequences (from 5′ to 3′)
FAM-DNA	AAA AAA AAA CCC AGG TTC TCT-FAM
cDNA	AGA GAA CCT GGG TTT TTT TTT
rDNA	TTT CAC AGA TGC GTC CCC CCC

2.2.2 Instrumentation

The fluorescence measurements were performed using a microplate reader (Spark, Tecan, Ex: 485 nm; Em: 535 nm for carboxyfluorescein (FAM), and Ex: 393 nm; Em: 521 nm for HQS).

The hydrodynamic size and ζ-potential of NPs were measured by a dynamic light scattering (DLS) instrument (Zetasizer Nano 90, Malvern). In a typical experiment, 50 μg/mL of PDA NPs were

dispersed in buffer (10 mM HEPES, pH 7.6), and the measurements were performed at 25 °C. The transmission electron microscopy (TEM) images were taken using a Phillips CM10 100 kV microscope.

2.2.3 Synthesis of PDA NPs

Our PDA NPs were synthesized via oxidative self-polymerization of 2 mg/mL dopamine in the presence of 8.5 mM NaOH at 50 °C. After 5 h, the NPs were centrifuged (15,000 rpm, 10 min) and washed four times with Milli-Q water. Finally, the NPs were dispersed in water and stored at 4 °C for future use.

2.2.4 Preparing Metal-Adsorbed PDA NPs

Metal-adsorbed PDA NPs were prepared by simple mixing of 50 μg/mL of the as-synthesized bare PDA NPs with different concentrations of Zn^{2+} in a buffer (10 mM HEPES, pH 7.6) followed by incubation for 30 min. No washing step was performed.

2.2.5 Synthesis of Metal-Doped PDA NPs

As metal ions accelerate the rate of PDA formation, we used a lower dopamine concentration and shorter synthesis time compared to the synthesis of the bare PDA NPs. Metal-doped PDA NPs were typically prepared by oxidation of 1.5 mg/mL dopamine in the presence of 8.5 mM NaOH and 0.4 mM different metal ions at 50 °C. After 1.5 h, the NPs were centrifuged (15,000 rpm, 10 min) and washed four times with Milli-Q water to remove free metal ions. Finally, the NPs were dispersed in water and stored at 4 °C for future use.

2.2.6 DNA Adsorption Studies

Different concentrations of FAM-DNA were incubated with 50 μg/mL NPs in a buffer (10 mM HEPES, pH 7.6). After 30 min, the samples were centrifuged (15,000 rpm, 10 min), and the fluorescence intensity of the supernatants was measured to back calculate the adsorbed DNA. The fraction of adsorbed DNA was calculated by $(F_0 - F)/F_0$, where F_0 represents the fluorescence of the supernatant of FAM-DNA in the absence of the NPs and F is the fluorescence of the supernatant after DNA adsorption on the NPs. For the comparison studies, FAM-DNA was incubated with 50 μg/mL metal-doped PDA(Zn^{2+}) NPs, or 50 μg/mL PDA plus 100 μM Zn^{2+} ions (metal-adsorbed). 100 μM free Zn^{2+} ions were chosen, as it was the initial Zn^{2+} concentration used for the synthesis of the

23

PDA(Zn^{2+}) NPs (when diluted to 50 μg/mL). For the Zn^{2+}-adsorbed NPs, 10 mM EDTA was added to the supernatants for 30 min to eliminate the fluorescence quenching effect by the free Zn^{2+} ions. No salt was added to the buffer for DNA adsorption to the metal-doped PDA NPs. For the kinetic studies, 10 nM FAM-DNA was added to 5 μg/mL of the NPs.

2.2.7 Detection of cDNA

First, 10 nM FAM-DNA as a probe DNA was adsorbed on the PDA(Zn^{2+}) or PDA+Zn^{2+} NPs. Then, various concentrations of nonlabeled target cDNA were added to hybridize with the probe DNA and induce fluorescence recovery. To detect the cDNA in biological environments, the cDNA was first mixed with BSA or dispersed in serum and then added to the probe.

2.3 Results and Discussion

2.3.1 Synthesis of Metal-Doped PDA NPs for DNA Adsorption

To prepare metal-doped PDA NPs, metal ions were added during the polymerization of dopamine. After polymerization, the resulting NPs were washed to remove the free metal ions. We used the following nomenclature in the manuscript: PDA(M^{n+}) for the metal-doped and PDA+M^{n+} for the metal-adsorbed NPs (prepared by mixing as-synthesized bare PDA NPs and metal ions without removing free metal ions).

We then tested the adsorption of 100 nM carboxyfluorescein (FAM)-labeled DNA onto different PDA NPs. In the absence of metal ions in the buffer, the bare PDA NPs were unable to adsorb the DNA (Figure 2.1B, black curve). On the other hand, the metal-doped PDA NPs adsorbed the DNA to different extents, suggesting the role of the doped metal ions. Among the metals, Fe^{3+}, Ca^{2+}, and Ni^{2+} showed relatively lower DNA adsorption efficiency (15, 35, and 52%, respectively). On the other hand, Gd^{3+} and Zn^{2+} showed the highest adsorption efficiency of 84 and 73% DNA, respectively. The higher DNA adsorption on PDA(Gd^{3+}) was probably due to the stronger binding affinity between lanthanides and DNA,[2, 199] as well as the higher affinity of PDA for Gd^{3+}.[67, 75] The general trend of the effectiveness of metal ions in the metal-doped NPs was similar to that on metal-adsorbed PDA NPs,[32, 196-197] where a higher DNA adsorption efficiency of lanthanides and transition metal ions was observed compared to Ca^{2+}.

The ζ-potentials of the PDA NPs were measured at pH 7.6 (Figure 2.1C), and the doping of metal ions led to only a slightly less negative surface charge than the bare PDA NPs. Therefore, although a fraction of the doped metal ions were likely present on the surface, they were not enough to reverse or even neutralize the surface charge. In addition, no direct correlation was observed between the surface charge and the DNA adsorption efficiency (compare parts B and C of Figure 2.1), highlighting that the role of the metal ions for DNA adsorption was beyond charge screening.[34]

Furthermore, we noticed that the DNA adsorption efficiency was dependent on the duration of PDA synthesis. As shown in Figure 2.1D, for all of the metal ions, after 2 h of polymerization, the DNA adsorption efficiency drastically decreased. Likely, with longer synthesis time, more metal ions were buried inside the NPs, leaving fewer on the surface, since using this procedure, an average of ~10 nm PDA layer could be formed per hour.[182] To achieve a high DNA adsorption efficiency, we chose 1.5 h for our synthesis.
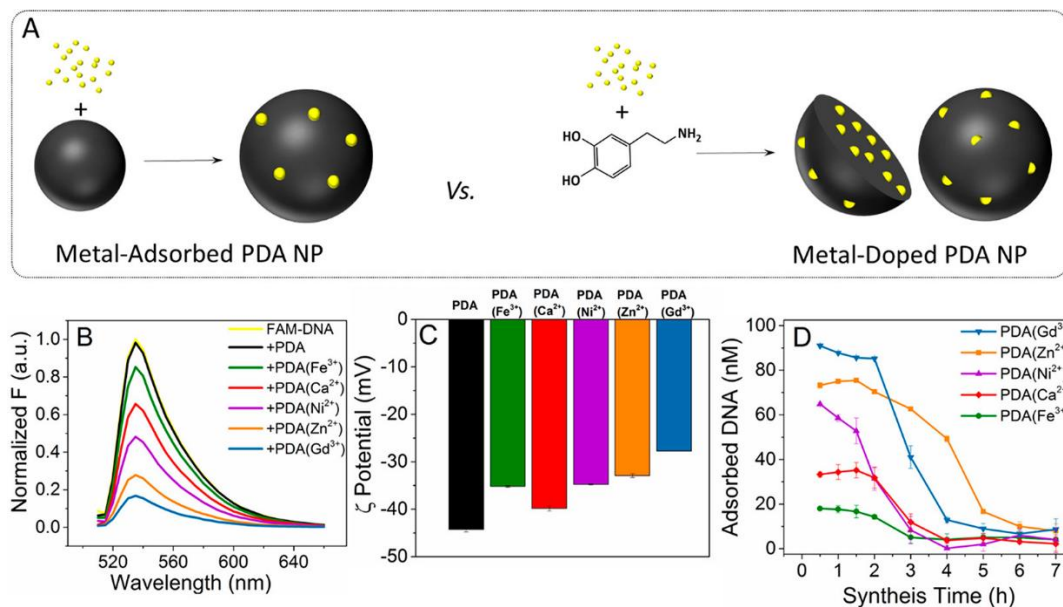
Figure 2.1 (A) Scheme illustrating the difference between metal ions (the yellow dots) loading on the surface of metal-adsorbed PDA NPs, versus inside and on the surface of metal-doped PDA NPs. (B) Fluorescence spectra of the supernatant of 100 nM FAM-DNA after adsorption on different PDA NPs for 30 min. (C) ζ-Potential of different NPs in 10 mM HEPES buffer, pH 7.6. (D) Effect of the synthesis time on the DNA adsorption property of different PDA NPs. 50 μg/mL PDA NPs were used for all of the experiments in this figure.

The pH of the solution would strongly affect the DNA adsorption efficiency on PDA. At lower pH values, due to the protonation of surface amino groups, PDA would more effectively adsorb negatively charged DNA.[124, 196] In this work, we focused on the effect of metal ions and performed all experiments at the physiological pH of 7.6.

Based on TEM, involving metal ions during the dopamine polymerization reaction led to the production of spherical NPs similar to the bare PDA NPs yet with slightly different size distributions (Figure 2.2). The highest uniformity was observed for the PDA(Fe^{3+}) and PDA(Ni^{2+}) NPs by both TEM and DLS (Figure 2.3). Moreover, except for Gd^{3+}, the DLS data (Figure 2.3) were comparable to the TEM images, confirming the good dispersity in water. The average size of the PDA(Gd^{3+}) NPs was measured to be 390 nm by DLS (Figure 2.3F), while much smaller nanospheres were observed under TEM that tended to aggregate (Figure 2.2F). The lower water dispersity of PDA(Gd^{3+}) was in agreement with the literature.[75]
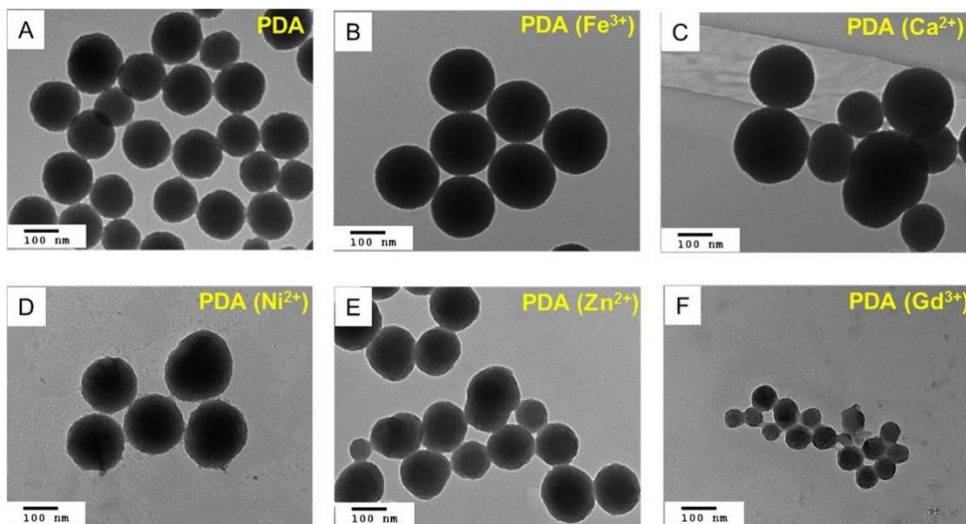
Figure 2.2 TEM micrographs depicting spehrical (A) PDA, (B) PDA(Fe^{3+}), (C) PDA(Ca^{2+}), (D) PDA(Ni^{2+}), (E) PDA(Zn^{2+}), and (F) PDA(Gd^{3+}) NPs.
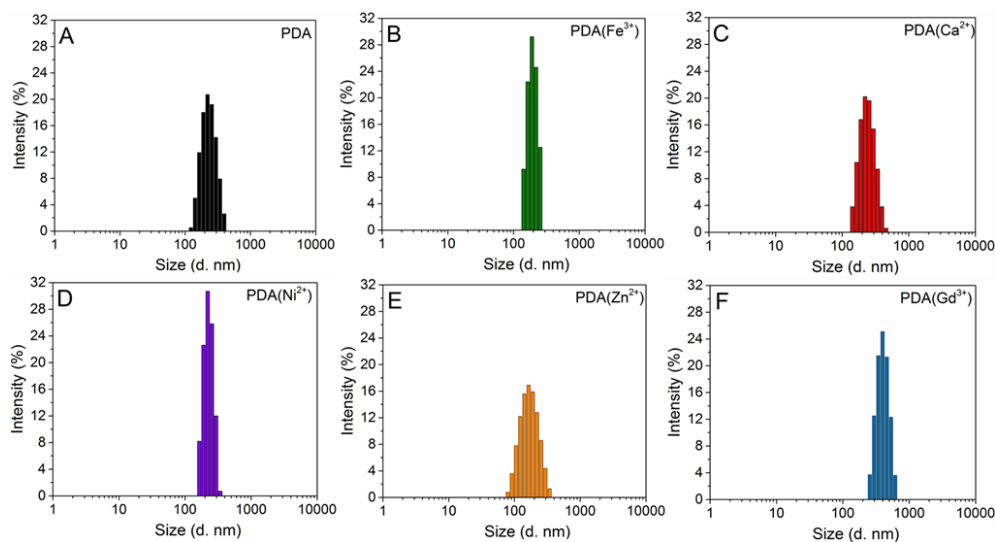
Figure 2.3 Size distribution of (A) PDA, (B) PDA(Fe^{3+}), (C) PDA(Ca^{2+}), (D) PDA(Ni^{2+}), (E) PDA(Zn^{2+}), and (F) PDA(Gd^{3+}) NPs characterized by DLS. The difference between the TEM image and DLS measurement for the PDA(Gd^{3+}) NPs inferred aggregation. For the other NPs, the DLS data agreed with the TEM images, and PDA(Fe^{3+}) and PDA(Ni^{2+}) showed the highest monodispersity among the metal-doped NPs

2.3.2 Embedded Metal Ions were Responsible for the DNA Adsorption on the Metal-Doped NPs

One concern of using metal-doped PDA NPs is the potential leaching of metal ions. To investigate it, we took the PDA(Zn^{2+}) and PDA(Gd^{3+}) NPs as the most efficient ones for DNA adsorption. After 2 days of incubation in water, the NPs were centrifuged, and the supernatants were collected (note that the NPs were already washed four times after the synthesis to remove free metal ions). To quantify the concentration of leached Zn^{2+} ions, 8-hydroxy-5-quinolinesulfonic acid (HQS) was used as a fluorescent probe, since Zn^{2+} can induce its fluorescent emission at 521 nm (Figure 2.4A).[200-201] Using this standard curve, the Zn^{2+} concentration in the supernatant of the 50 μg/mL PDA(Zn^{2+}) was measured to be ~0.7 μM (Figure 2.4A). Such a low concentration of free Zn^{2+} ions was not expected to promote DNA adsorption.[196-197]
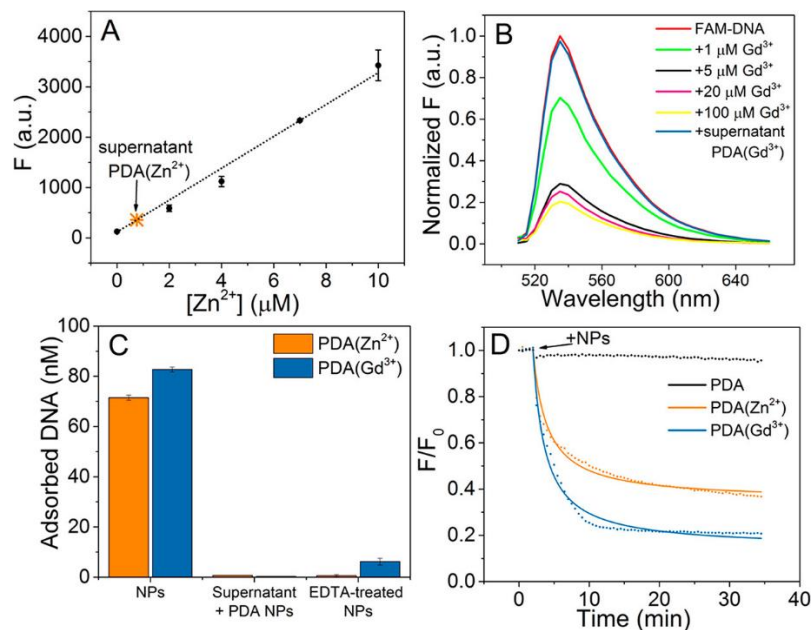
Figure 2.4 (A) A standard curve created by mixing different concentrations of Zn^{2+} with 2 mM HQS in 10 mM HEPES buffer, pH 7.6. The orange dot points out the concentration of Zn^{2+} in the supernatant of 50 μg/mL PDA(Zn^{2+}) NPs. (B) Quenching of 100 nM FAM-DNA induced by different concentrations of Gd^{3+}. The blue curve is related to the concentration of Gd^{3+} in the supernatant of 50 μg/mL PDA(Gd^{3+}) NPs. (C) Adsorption of 100 nM FAM-DNA on 50 μg/mL PDA(Zn^{2+}) or PDA(Gd^{3+}) NPs, the supernatant of the NPs plus 50 μg/mL PDA NPs, and EDTA-treated NPs with free EDTA washed away. (D) Kinetics of 10 nM DNA adsorption on 5 μg/mL PDA, PDA(Zn^{2+}), and PDA(Gd^{3+}) NPs in 10 mM HEPES buffer, pH 7.6. The dotted lines are the experimental data, and the solid lines represent the fitting curves following the pseudo second order (PSO) kinetic model. F_0 is the fluorescence intensity of the sample at time 0, and F is the intensity at time t.

We then estimated the concentration of the free Gd^{3+} ions in the supernatant of the PDA(Gd^{3+}) NPs by taking advantage of the strong fluorescence quenching property of Gd^{3+}. As shown in Figure 2.4B, even 1 μM Gd^{3+} led to ~30% quenching of 100 nM FAM-DNA. However, the supernatant of the 50 μg/mL PDA(Gd^{3+}) NPs did not affect the FAM fluorescence, suggesting that the concentration of free Gd^{3+} ions was also less than 1 μM.

To further test the effect of the leached metal ions, the supernatants of the PDA(Zn^{2+}) and PDA(Gd^{3+}) NPs were then obtained and separately added to 50 μg/mL bare PDA NPs. As expected, due to the very low concentrations of the free ions, no DNA adsorption was observed (Figure 2.4C), confirming that, for the metal-doped PDA NPs, it was the embedded metals instead of the leached free metals responsible for the DNA adsorption. We also incubated the metal-doped NPs with 10 mM

28

EDTA for 30 min and then washed them to remove EDTA. The resulting NPs lost the DNA adsorption function (Figure 2.4C), likely because EDTA chelated away or capped the doped metal ions on the surface. Taken together, the embedded metal ions were solely responsible for the DNA adsorption onto these metal-doped NPs.

To gain more insights, we then investigated the kinetics of DNA adsorption on these NPs (10 nM DNA, 5 μg/mL NPs). As shown in Figure 2.4D, the bare PDA NPs had almost no effect on the fluorescence signal, emphasizing that no DNA adsorption occurred. On the other hand, the PDA(Zn^{2+}) and PDA(Gd^{3+}) NPs adsorbed 65 and 80% of the DNA after 30 min. Moreover, the adsorption on PDA(Gd^{3+}) happened faster. Based on the kinetic traces, the half-saturation time ($t_{1/2}$) was calculated to be 3.6 and 2.1 min for the PDA(Zn^{2+}) and PDA(Gd^{3+}) NPs, respectively. The kinetic data were then fitted with pseudo-second-order (PSO) (Figure 2.4D) adsorption kinetics model,[202] and the correlation coefficients (R^2) were calculated to be ~0.98. When studying the adsorption kinetics models, the physical interpretation and assumptions should also be considered instead of evaluation solely based on the R^2 value.[203] Since in our system the DNA (the adsorbate) concentration was relatively low and changed dramatically during the adsorption, we concluded that the adsorption should be better described by the PSO kinetic model.[202]

2.3.3 Comparison between Metal-Doped and Metal-Adsorbed PDA

To compare the metal-doped and metal-adsorbed PDA NPs, we focused on Zn^{2+} to avoid the fluorescence quenching problem by Gd^{3+}. The quenching effect of Zn^{2+} can be eliminated by adding 10 mM EDTA to the supernatant. However, a high concentration of Gd^{3+} could irreversibly quench the FAM signal (Figure 2.5), which would affect our calculations. In fact, this revealed an advantage of metal-doped NPs, where free metal ions and their FAM-quenching effect were eliminated.
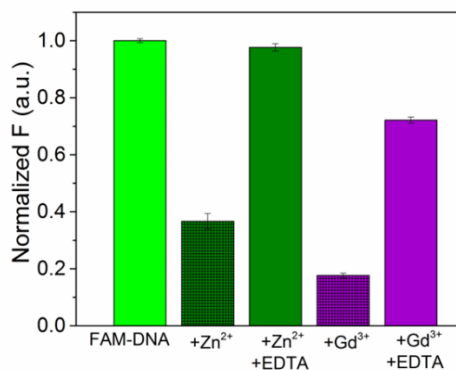
Figure 2.5 Fluorescence intensity of 100 nM FAM-DNA in the presence of 100 µM Zn^{2+} or 100 µM Gd^{3+}, before and after the addition of 10 mM EDTA. The FAM-signal was almost completely recovered by EDTA in the presence of Zn^{2+}, while a fraction of FAM was still quenched by 100 µM Gd^{3+}, even after adding EDTA.

The DNA adsorption isotherms were measured by incubating different concentrations of FAM-DNA with the metal-doped and metal-adsorbed NPs (Figure 2.6A-B), both prepared by the same initial concentration of 100 µM Zn^{2+}. For both methods, a higher initial DNA concentration resulted in a higher DNA adsorption until reaching the saturation points. The Langmuir (Figure 2.6A) and Freundlich (Figure 2.6B) adsorption models were applied to interpret the adsorption behavior. The fitted data agreed better with the Langmuir isotherm model ($R^2 > 0.97$) instead of the Freundlich isotherm ($R^2 \approx 0.78$). The Langmuir isotherm assumes monolayer DNA adsorption, whereas the Freundlich isotherm is not limited to a monolayer. Since metal ions need to mediate the adsorption, we believe that the monolayer assumption can be satisfied, which was supported by our fitting of the Langmuir model. Moreover, the adsorption of DNA was reversible (an assumption by both models). Using the Langmuir isotherm, after extrapolation to infinitely high DNA concentrations, the saturation DNA loading capacity was calculated to be 0.23 µM for the metal-doped PDA NPs and 0.16 µM for the metal-adsorbed PDA NPs. For the metal-doped NPs, although a fraction of the 100 µM Zn^{2+} ions were consumed by the inner moieties of the NPs, the surface metal ions were still more effective than when 100 µM Zn^{2+} was added after the synthesis (metal-adsorbed). This is a surprising result, since, although the total Zn^{2+} concentration could reach 100 µM for the Zn^{2+}-doped PDA NP, a fraction of the metal ions was likely in the interior of the NPs, while, for the metal-free PDA, its surface can access the full 100 µM Zn^{2+}. The higher metal loading in the doping strategy might be attributed to a higher electrostatic attraction force between PDA moieties and Zn^{2+} ions.[204]

30
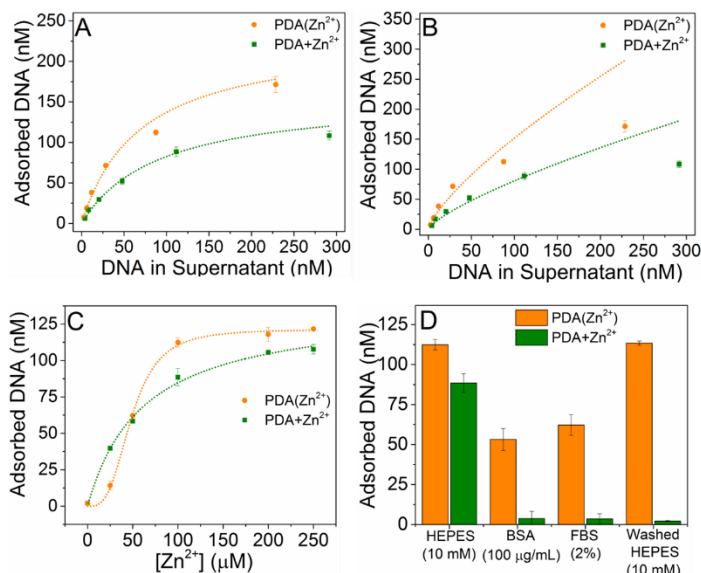
Figure 2.6 Adsorption isotherms of FAM-DNA on PDA(Zn^{2+}) and PDA+Zn^{2+} fitted with the (A) Langmuir model, and (B) Freundlich model. (C) Adsorption of 200 nM DNA on PDA(Zn^{2+}) and PDA+Zn^{2+} prepared with different concentrations of Zn^{2+}. (D) Comparison between the robustness of the PDA(Zn^{2+}) and PDA+Zn^{2+} for the extraction of 200 nM DNA in 10 mM HEPES, 100 μg/mL BSA, 2% FBS, and after washing twice with water. 50 μg/mL PDA NPs were used for all of the experiments in this figure.

The effect of metal concentration on DNA adsorption was also explored for the two metal-loading strategies (Figure 2.6C). At lower Zn^{2+} concentrations (lower than 50 μM), Zn^{2+} was more effective for the metal-adsorbed system. We reason that, under this condition, a large fraction of Zn^{2+} ions was consumed by the interior moieties of the 50 μg/mL of the metal-doped NPs, leading to a lower DNA adsorption compared to metal-adsorbed NPs. However, at higher Zn^{2+} concentrations, the metal-doped strategy established a higher DNA adsorption efficiency probably due to the higher content of Zn^{2+} ions on the surface. This created a sigmoidal binding curve for the metal-doped NPs.

We further compared the robustness of metal-doped and metal-adsorbed NPs. First, extraction of 200 nM DNA in complex biological environments such as in the presence of BSA (100 μg/mL) and in serum was investigated. For PDA+Zn^{2+}, DNA extraction drastically dropped to ~3 nM in both the BSA and serum solutions (Figure 2.6D), while PDA(Zn^{2+}) still adsorbed considerable amounts of 53 and 62 nM DNA in the BSA and serum, respectively. Moreover, we washed the metal-doped and metal-adsorbed NPs with water twice and then used them for DNA adsorption in 10 mM HEPES (Figure 2.6D). The PDA(Zn^{2+}) fully retained its adsorption efficiency, while PDA+Zn^{2+} fully lost it.

Taken together, the doped metal ions were tightly trapped on the PDA surface, facilitating DNA adsorption even in a biological environment, while the adsorbed metals were easily washed away, and thus were unable to adsorb DNA in biological environments.

2.3.4 DNA Desorption for Probing the Adsorption Mechanism

After achieving DNA adsorption, we then studied the stability of adsorption and methods for releasing the adsorbed DNA. The preadsorbed DNA strands were respectively exposed to 10 mM EDTA, 5 mM phosphate, and 5 mM adenosine, and the fraction of desorption was tracked by the enhancement of fluorescence intensity. These competing molecules were added to probe the effect of metal ions, the phosphate backbone, and the DNA base in the adsorption, respectively.

The adsorbed DNA was almost completely desorbed by EDTA regardless of the metal-loading strategy (Figure 2.7B), since EDTA can strongly bind to Zn^{2+} with a logarithmic stability constant of 16.4.[205] Moreover, the kinetics revealed very fast desorption from metal-doped NPs, reaching a plateau within 10 min (Figure 2.7A). Since polyvalent metal ions play vital roles for DNA adsorption on PDA, EDTA provides a convenient method to release DNA.
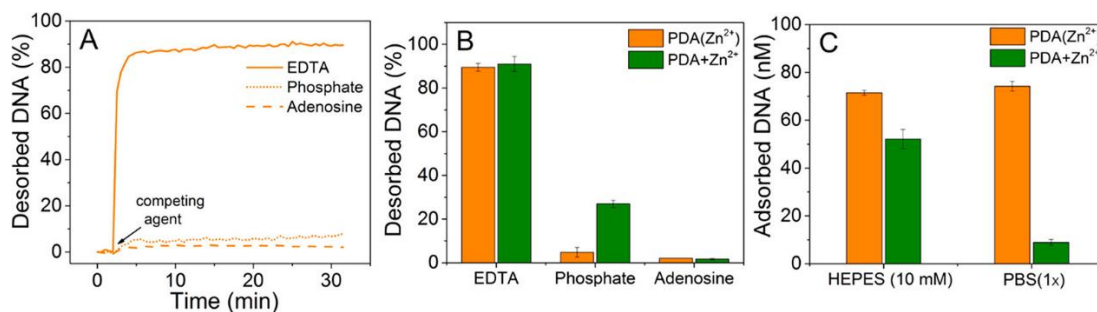
Figure 2.7 (A) Kinetics of 10 nM DNA desorption from PDA(Zn^{2+}) induced by 10 mM EDTA, 5 mM phosphate, and 5 mM adenosine, respectively. (B) Comparison between the desorption of 10 nM DNA from PDA(Zn^{2+}) versus PDA+Zn^{2+}. (C) Comparison between the adsorption efficiency of 100 nM DNA on the PDA(Zn^{2+}) versus PDA+Zn^{2+} NPs in HEPES (10 mM, pH 7.6) and in PBS ($1\times$, pH 7.6) buffers.

For the metal-adsorbed PDA NPs, phosphate-induced DNA desorption was much higher than adenosine-induced desorption (Figure 2.7B), suggesting a high contribution of the phosphate backbone for the DNA adsorption in the presence of Zn^{2+}. However, comparison between the metal-doped and metal-adsorbed NPs indicated that a significantly lower phosphate-induced desorption occurred from the metal-doped NPs (Figure 2.7B). This confirmed a tighter DNA adsorption on the

32

metal-doped NPs, which could be due to its higher metal loading. We previously showed that, for individual metal ions, higher metal concentrations can lead to higher resistance to phosphate-induced desorption.[196] Moreover, since inorganic phosphate competed with PDA for binding to Zn^{2+}, it appeared that the tightly doped Zn^{2+} ions on PDA were not affected by the added phosphate, while the loosely adsorbed Zn^{2+} ions were taken away by phosphate, leading to the DNA desorption.

The negligible phosphate-induced DNA desorption suggested that the metal-doped NPs are good candidates for applications in phosphate buffered saline (PBS), which is an important buffer in biological assays. We examined the adsorption of 100 nM DNA onto the metal-doped and metal-adsorbed PDA NPs in PBS buffer (pH 7.6) to challenge the DNA adsorption (Figure 2.7C). For the metal-adsorbed NPs, a drastic decrease in DNA adsorption was observed compared to the adsorption in HEPES buffer. On the other hand, the tightly Zn^{2+} doped NPs were not affected by PBS at all, resulting in the same DNA adsorption efficiency as in HEPES.

2.3.5 Selective DNA Detection

Given the excellent DNA adsorption and fluorescence quenching properties of the metal-doped PDA NPs, we then investigated this system for DNA detection. We first adsorbed the FAM-labeled probe DNA on the two types of PDA NPs. Then, a 21-mer nonlabeled complementary DNA (cDNA) or a random DNA (rDNA) was added as a target and control, respectively. Therefore, the hybridization or/and displacement of the preadsorbed FAM-DNA can be tracked by the fluorescence enhancement (Figure 2.8A). For the metal-doped NPs, time-dependent fluorescence signals were observed (Figure 2.8B), and the cDNA brought a stronger signal than the rDNA. Therefore, specific DNA hybridization allowed specific probe desorption.
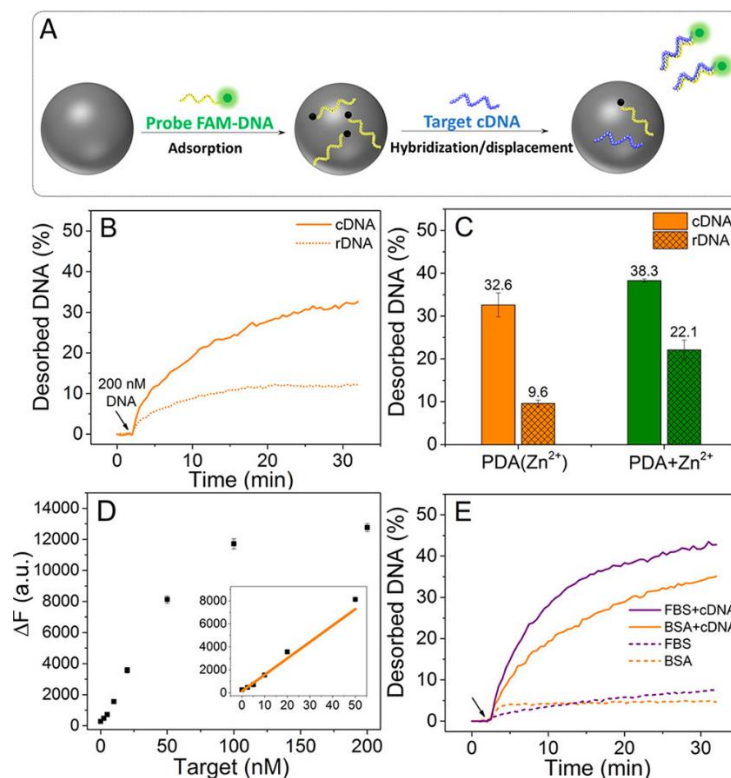
Figure 2.8 (A) A scheme depicting the preparation of the sensor and the mechanism of target cDNA detection. (B) Kinetics of the PDA(Zn^{2+}) sensor signaling induced by 200 nM cDNA or rDNA. (C) Comparison between the selectivity of the PDA(Zn^{2+}) versus PDA+Zn^{2+} sensors for detection of 200 nM cDNA. (D) Calibration curve of the PDA(Zn^{2+}) sensor for the detection of various concentrations of target cDNA. (E) Kinetics of the PDA(Zn^{2+}) sensor signaling induced by 100 μg/mL BSA and FBS (2%), in the absence or presence of 200 nM target cDNA.

To compare the selectivity, we calculated the ratio of FAM-DNA desorbed by cDNA over rDNA for both methods. As represented in Figure 2.8C, the metal-doped NPs showed a higher selectivity (3.4), compared to the metal-adsorbed NPs (1.7). The higher selectivity implied the more important role of DNA hybridization for DNA desorption, which was originated from the tighter DNA adsorption to the metal-doped PDA NPs.

Various concentrations of cDNA were then added to the preadsorbed probe DNA to obtain a calibration curve for the sensor. A linear concentration-dependent fluorescence enhancement was observed up to 50 nM of cDNA (Figure 2.8D), and the limit of detection (LOD) was calculated to be

0.45 nM (3σ/slope, where σ is the standard deviation of the background variation in the absence of target).

In the above sections, the robustness of DNA adsorption on metal-doped PDA NPs was confirmed. We also aimed to achieve target DNA detection in biological samples. When BSA was exposed to the probe as a model protein, less than 5% desorption happened, while the coexistence of BSA and the target cDNA led to ∼35% probe desorption (Figure 2.8E), providing a strong signal for detection similar to that produced in the clean buffer (Figure 2.8B). It appeared that BSA cannot effectively compete with the DNA on the surface. Therefore, the metal-doped PDA NPs were resistant to nonspecific protein-induced DNA desorption, unlike surfaces such as graphene oxide (GO) that suffer from such protein-induced DNA desorption.[206] Finally, we examined the sensor's function in serum. Even though the probe DNA desorption slightly increased, the signal was still ∼7-fold higher than the background, showing the efficiency of such sensors in complexed biological samples.

2.4 Conclusions

In summary, we have synthesized metal-doped and metal-adsorbed PDA NPs and compared their DNA adsorption. Metal-doped PDA NPs with spherical morphology were synthesized in the presence of various metal ions, and they showed different levels of DNA adsorption efficiency. Overall, Gd^{3+} and Zn^{2+} showed the highest efficiency among the tested metals. Metal leaching from the metal-doped NPs was negligible, while metals were easily removed from the metal-adsorbed NPs by washing with water. The metal-doped NPs showed higher DNA adsorption efficiency than the metal-adsorbed NPs. Furthermore, the tightly embedded metal ions in the metal-doped NPs led to a considerable DNA extraction even in complexed biological environments such as BSA or serum, while DNA extraction was almost completely inhibited for the metal-adsorbed NPs. When used as a sensor, the metal-doped NPs showed a 2-fold higher selectivity than the metal-adsorbed NPs for the detection of cDNA due to their tighter DNA binding, which minimized nonspecific probe displacement. The LOD was 0.45 nM cDNA for the Zn^{2+}-doped sensor. This study has revealed interesting metal coordination on the PDA surface and proposed PDA-based hybrid NPs for highly efficient DNA adsorption and robust and sensitive DNA detection.

Chapter 3

Spherical Nucleic Acid Functionalization of Polydopamine to Achieve Robust and Selective DNA Extraction and Detection

The results presented in this chapter have been published as:

Mohamad Zandieh and Juewen Liu. "Cooperative Metal Ion-Mediated Adsorption of Spherical Nucleic Acids with a Large Hysteresis". *Langmuir* **2020**, 36, 47, 14324–14332, and

Mohamad Zandieh and Juewen Liu. "Spherical Nucleic Acid Mediated Functionalization of Polydopamine-Coated Nanoparticles for Selective DNA Extraction and Detection". *Bioconjugate Chem.* **2021**, 32, 4, 801-809.

3.1 Introduction

Materials for sequence-specific extraction of nucleic acids are highly important for bioanalytical chemistry.[207-209] To achieve separation in resource-limited regions, magnetic separation is desirable to avoid the need for high-speed centrifugation.[210-211] Moreover, by using magnetic separation for biological samples, direct isolation from crude samples and large-scale purification can be achieved.[211-212] Therefore, many works have used magnetic nanoparticles (NPs) for DNA extraction.[181, 213-215] At the same time, the surface property of magnetic NPs needs to be adjusted to avoid nonspecific DNA adsorption. Since common magnetic particles such as iron oxide can nonspecifically adsorb DNA,[176, 206] coating the surface with a nonadsorbing material is needed. Polydopamine (PDA) is a popular biocompatible coating material, which already has been used to coat magnetic iron oxide NPs, and such conjugates were well-characterized.[60, 180, 216-217]

To extract DNA from cell lysates, Wang and co-workers synthesized Fe_3O_4@PDA core–shell NPs.[124] In buffers without polyvalent metal ions, PDA does not adsorb DNA.[32, 196] Hence, they used a low pH-assisted adsorption method (pH 2) for the direct capture of DNA on PDA. They also effectively released the captured DNA by adjusting the pH back to neutral and switching the PDA surface charge. However, this method suffered from a lack of sequence selectivity.

We reason that spherical nucleic acids (SNA) may solve the above-mentioned challenges. Attaching a high density of DNA oligonucleotides to a nanoparticle creates an interesting structure termed SNA.[218] Since DNA is a highly negatively charged polymer, SNA can accumulate an

extremely high density of negative charges. Because of this and other DNA-related properties, SNA have many interesting properties distinct from typical linear nucleic acids of the same sequence. Sharper melting transitions,[39] tighter binding of the complementary DNA,[40-41] and much higher efficiency of cellular uptake[38, 219] are some commonly cited and used special properties of SNA enabling their widespread applications.[3, 220-225]

Building on these progresses, in this work, we first studied the difference between the adsorption of linear and spherical DNA on PDA. We found different trends of metal-dependent adsorption for linear and spherical DNAs, indicating an effect of geometric confinement in spherical DNA.[226] In particular, SNA showed cooperative metal-mediated adsorption. Then, we designed a three-component hybrid material consisting of a Fe_3O_4 core, a PDA shell, and a SNA decoration. We compared this conjugate with directly attached linear DNA to Fe_3O_4@PDA and found several advantages of using the SNA. The resulting hybrid nanomaterial showed excellent selectivity for DNA extraction and detection.

3.2 Materials and Methods

3.2.1 Chemicals

The DNA samples were all purchased from Integrated DNA Technologies (IDT, Coralville, IA, USA), and their sequences are presented in Table 3.1. Dopamine hydrochloride, various metal chloride salts, $HAuCl_4$, ethylenediaminetetraacetic acid (EDTA), reduced glutathione (GSH), polyethylene glycol (PEG-1000), tris(2-carboxyethyl) phosphine hydrochloride (TCEP), bovine serum albumin (BSA), and potassium cyanide (KCN) were from Sigma-Aldrich. Using citrate reduction, citrate-capped AuNPs (13 nm) were prepared based on the literature,[227] and citrate-capped AuNPs of other sizes (5 and 30 nm) were purchased from BBI Solutions (Cardiff, UK). Sodium acetate, 4-(2- Hydroxyethyl)piperazine-1-ethane sulfonate (HEPES) and urea were purchased from Mandel Scientific (Guelph, ON, Canada), and ethylene glycol was from Fischer Scientific. Milli-Q water was used for preparing all the buffers and solutions.

Table 3.1. The DNA sequences and modifications used in this Chapter.

DNA Names	Sequences (from 5′ to 3′)
FAM-DNA	**AAA AAA AAA CCC AGG TTC TCT-FAM**
SH-DNA	**SH-AAA AAA AAA CCC AGG TTC TCT**
SH-DNA-FAM	**SH-AAA AAA AAA CCC AGG TTC TCT-FAM**
FAM-cDNA	**FAM-AGA GAA CCT GGG**
FAM-rDNA	**FAM-AAA AAA AAA AAA**
Target DNA	**AGA GAA CCT GGG TTT TTT TTT**
21-mer rDNA	**TTT CAC AGA TGC GTC CCC CCC**

3.2.2 Instrumentation

The transmission electron microscope (TEM) images were acquired using a Phillips CM10 100 kV microscope. The ζ-potentials of the NPs were measured using a dynamic light scattering (DLS) instrument (Zetasizer Nano 90, Malvern). In an experiment, different NPs (final concentration of 50 μg/mL) were dispersed in 1 mL HEPES buffer (25 mM, pH 7.6), and the measurement was performed at 25 °C. The fluorescence measurements were performed using a microplate reader (Spark, Tecan) with 485 nm excitation and 535 nm emission. UV−vis absorption spectra were collected by a spectrometer (Agilent 8453A).

3.2.3 Synthesis of PDA NPs (~400 nm)

The PDA NPs were produced by polymerization of 2.2 mg/mL dopamine in the presence of a final of 8.5 mM NaOH at 20 °C. After 5 h of polymerization, the obtained PDA NPs were centrifuged (10,000 rpm, 10 min) and washed with Milli-Q water three times. Finally, the NPs were dispersed in water and stored at 4 °C for future use.

3.2.4 Synthesis of Fe_3O_4 NPs

The Fe_3O_4 NPs were synthesized based on a reported protocol.[228] First, 338 mg of $FeCl_3 \cdot 6H_2O$ was dissolved in 10 mL of ethylene glycol through a brief sonication to obtain a clear yellowish solution. Then, 900 mg of sodium acetate and 250 mg of PEG-1000 were added, and the solution was stirred

for 30 min. Finally, the mixture was stirred at 200 °C under a reflux-condenser setup for 8 h. The final products were magnetically separated and washed several times with water.

3.2.5 Synthesis of Fe₃O₄@PDA and PDA NPs (~200 nm)

Fe_3O_4@PDA NPs were prepared by mixing 2 mg/mL dopamine and 250 μg/mL Fe_3O_4 NPs in the presence of a final of 8.5 mM NaOH. After 6 h of polymerization at 20 °C, a PDA shell was coated on the Fe_3O_4 NPs and the core−shell NPs were magnetically separated and washed several times with water. Similarly, by polymerization of 2 mg/mL dopamine in the basic solution (no Fe_3O_4 NPs), bare PDA NPs were obtained, which were washed by centrifugation (15,000 rpm, 10 min).

3.2.6 SNA Preparation

The SNAs were prepared by the salt-aging method.[42, 49] In this method, 3 μM SH-DNA was incubated with 12 nM AuNPs overnight. Then, a final concentration of 0.25 M NaCl was gradually added over 7 h. After another overnight incubation, the SNAs were centrifuged at 20 °C (5 nm AuNPs: 50,000 rpm for 20 min; 13 and 30 nm AuNPs: 14,000 rpm for 15 min) and washed three times with a buffer (5 mM HEPES, pH 7.6). The concentration of the AuNPs was calculated based on the extinction coefficients of 1.1×10^7 M^{-1} cm^{-1} at 518 nm, 2.7×10^8 M^{-1} cm^{-1} at 520 nm, and 3.36×10^9 M^{-1} cm^{-1} at 526 nm for 5, 13, and 30 nm AuNPs, respectively. In addition, the low-density (LD) SNA was prepared by incubation of the 13 nm AuNPs with 0.5 μM SH-DNA overnight followed by incubation with 200 μM GSH as a backfilling agent for 3 h. This way, it was ensured that the DNA was adsorbed via its thiol group instead of the bases. Then, the same washing steps were performed. Using a FAM and SH dual labeled DNA (SH-DNA-FAM), and after dissolving the AuNP core by adding KCN (a final of 10 mM), the density of attached DNA on each SNA was measured.[229]

3.2.7 Linear DNA Adsorption

In a typical experiment, 150 nM 3′- FAM DNA was mixed with 50 μg/mL of the large PDA (~400 nm) in the presence of different metal ions in buffer (20 mM HEPES, pH 7.6). After 30 min, the samples were centrifuged (15000 rpm, 10 min), and the supernatants were completely separated. The supernatant was then incubated for 30 min with 10 mM EDTA to eliminate the quenching effect by the free metal ions. Finally, the fluorescence intensity of the supernatant was measured to back calculate the adsorbed DNA.

3.2.8 SNA Adsorption

In a typical experiment, the SNA (final of ~150 nM DNA) was incubated with 50 μg/ mL of the large PDA (~400 nm) in the presence of different metal ions in buffer (20 mM HEPES, pH 7.6). After 30 min, the samples were centrifuged for 5 min at 3000, 1200, and 800 rpm for 5, 13, and 30 nm AuNPs respectively. Then, the adsorbed DNA was calculated according to the decrease of AuNP absorbance of the supernatant. Different centrifugation speeds were chosen to avoid the precipitation of nonadsorbed DNA.

3.2.9 Desorption Studies

For the DNA desorption experiments, first, DNA was adsorbed on the large PDA (~400 nm) in the presence of 100 mM Na^+, 2 mM Ca^{2+}, or 0.6 mM Zn^{2+} for 30 min. Then, 4 M urea or 4 mM EDTA in the buffer was exposed to the samples. After incubation for 30 min, the supernatants of the samples were collected based on the mentioned conditions for the linear/SNA, and the desorbed DNA was calculated according to the signal increase.

3.2.10 DNA Functionalization of Fe_3O_4@PDA NPs

In the covalent method, SH-DNA was first TCEP-treated in 25 mM HEPES (pH 7.6) or acetate buffer (pH 5) for 90 min (TCEP:DNA = 100:1) to cleave the disulfide bond. Then different concentrations of the DNA were incubated with 50 μg/mL of the Fe_3O_4@PDA NPs in 25 mM HEPES buffer (pH 7.6, 300 mM Na^+) overnight. To quantify the covalent attachment, SH-DNA-FAM was used. After incubation, the NPs were separated by a magnet and the fluorescence intensity of the supernatant was measured to back calculate the loaded DNA. In the physisorption method, different concentrations of SNA were incubated with 50 μg/mL of the Fe3O4@PDA NPs in 25 mM HEPES buffer (pH 7.6, 300 mM Na^+) for 30 min, and the adsorption was back calculated based on the decrease of AuNP absorbance of the supernatant. For both methods, the same DNA sequence was used.

3.2.11 DNA Extraction and Detection

For DNA extraction, first, Fe_3O_4@PDA NPs were functionalized with a final concentration of 150 nM SNA or SH-DNA. Then, different concentrations of FAM-labeled complementary (FAM-cDNA) or random DNA (FAM-rDNA) were incubated with the NPs in 25 mM HEPES buffer (pH 7.6, 300 mM Na^+) for 30 min. After that, the pellets were separated by a magnet and the supernatants were collected to back-calculate the extracted DNA. For DNA detection, first, 200 nM 12-mer FAM-

cDNA (reporter DNA) was incubated with the SNA or SH-DNA functionalized Fe_3O_4@PDA NPs in 25 mM HEPES buffer (pH 7.6, 300 mM Na^+) for 30 min. Then, the probe was incubated with 1 mg/mL BSA for another 30 min and washed with the same buffer. Finally, the pellets were dispersed in different concentrations of nonlabeled 21-mer cDNA (target DNA) in the same buffer to displace the reporter DNA and produce fluorescence signals.

3.3 Results and Discussion

3.3.1 Adsorption of Linear DNA and SNA on PDA

To track the adsorption of the 21-mer linear DNA (Figure 3.1A), a FAM fluorophore was labeled on the 3′ end. The same DNA sequence bearing a 5′-HS was used to prepare the SNA (Figure 3.1B). On each 13 nm AuNP, an average of 98 DNA strands were attached. During our experiment, the SNA was used at roughly the same concentration as the linear DNA in terms of the total DNA concentration. Our PDA NPs were synthesized based on a previously reported method,[69] and they had an average size of ~400 nm under TEM (Figure 3.1C). According to DLS, the average size of the PDA NPs was 458 nm (Figure 3.1D), which was comparable with the data from TEM, confirming their good water dispersity. We prepared such large PDA NPs so that they can be easily precipitated without precipitating the AuNPs. At a reaction pH of 7.6, the ζ potential of the PDA NPs was −31 mV, and thus they electrostatically repelled DNA. Therefore, metal ions were used to screen charge repulsion for DNA adsorption.[34]
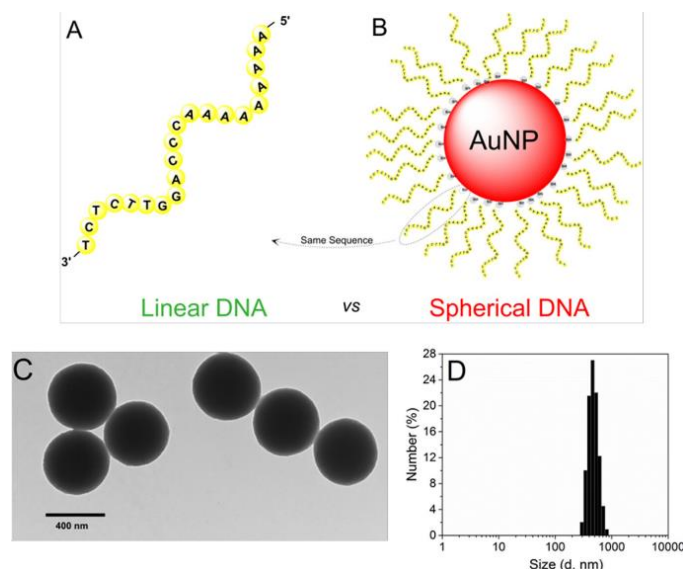
Figure 3.1 (A) Scheme of the linear DNA and its sequence. (B) Scheme indicating that the spherical DNA consisted of an AuNP core and thiolated DNA with the same sequence. (C) TEM micrograph depicting uniform PDA NPs. (D) Size distribution of the PDA NPs characterized by DLS.

We first used NaCl as the salt to promote DNA adsorption. As shown in Figure 3.2A, the linear DNA was not adsorbed on the PDA NPs in the presence of up to 100 mM Na^+, which is in agreement with the literature.[32, 195-196] Interestingly, by using the SNA, Na^+-dependent adsorption was observed, and 100 mM Na^+ was enough for adsorption of almost all of the SNA(150 nM DNA on 1.53 nM of 13 nm AuNPs). This result implied a weak binding force between the linear DNA and PDA, which was not strong enough to hold the DNA on the PDA. The polyvalent binding of the SNA has amplified individual weak interactions to allow stable adsorption. In addition, the densely packed DNA may favor π-π stacking between the terminal bases and the PDA surface.

We then tested divalent Ca^{2+} since it can promote linear DNA adsorption on PDA.[32] Indeed, both types of DNA were adsorbed (Figure 3.2B). At low concentrations of Ca^{2+} (below 0.5 mM), the linear DNA was adsorbed even more than the SNA. However, the SNA caught up and surpassed with more than 0.5 mM Ca^{2+}. Studies have indicated that Ca^{2+} might bridge DNA base and PDA to facilitate adsorption, and Ca^{2+} can also interact with the phosphate backbone of DNA.[2, 26] For the SNA, the effect of Ca^{2+} was close to that of Na^+ but the required concentration was around 55-fold lower by comparing the metal concentration required to reach half saturation. Figure 3.2D shows a TEM micrograph of the SNA adsorbed on the PDA NPs.
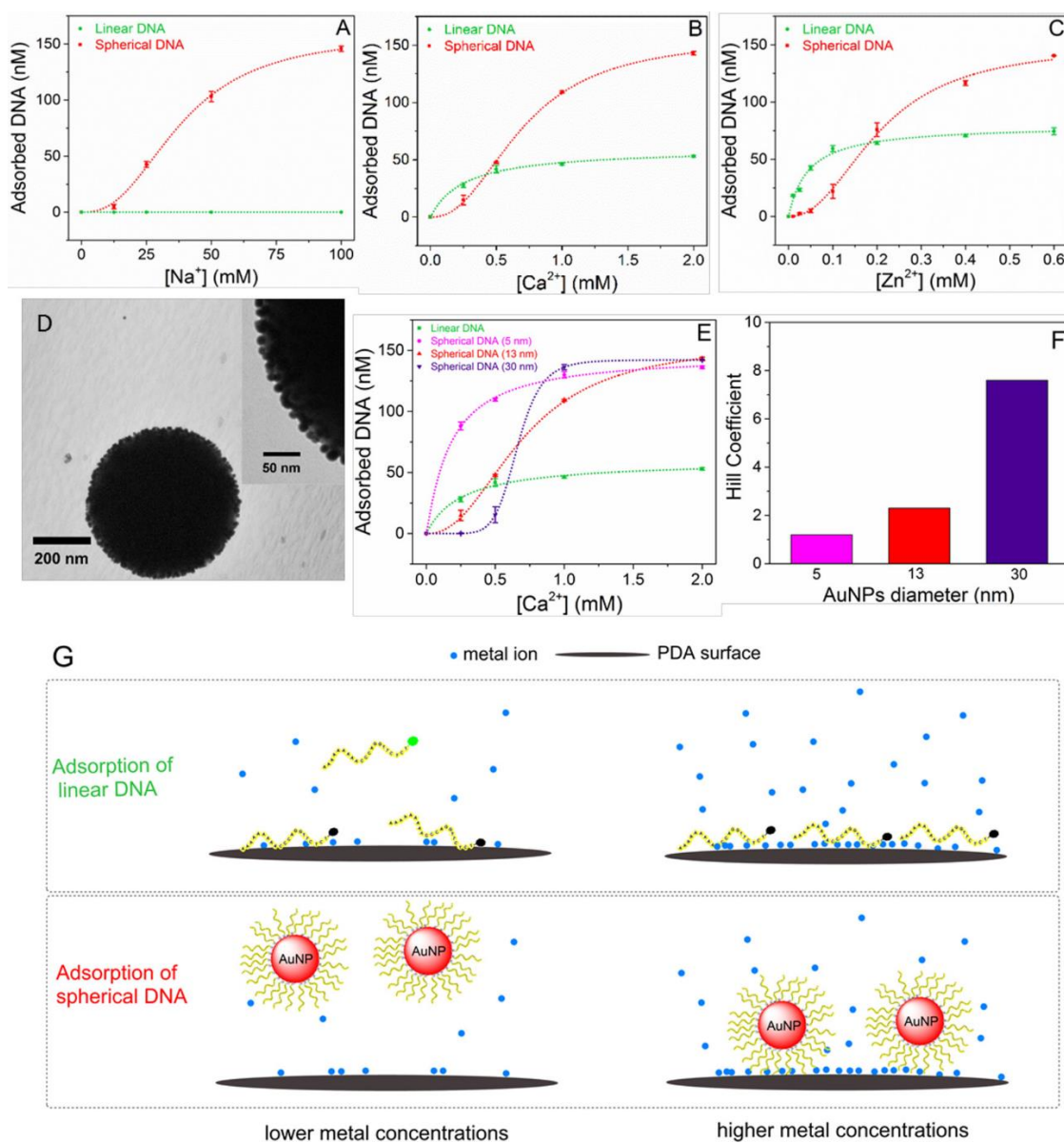
Figure 3.2 Adsorption of the linear and spherical DNA (150 nM DNA) on 50 μg/mL PDA in the presence of different concentrations of (A) Na$^+$, (B) Ca^{2+}, and (C) Zn^{2+}. (D) TEM micrograph depicting spherical DNA attached to the PDA NPs in the presence of 2 mM Ca^{2+}. Inset: a higher magnification. (E) Effect of the size of the AuNP core on the adsorption in the presence of different concentrations of Ca^{2+}. (F) Hill coefficient for Ca^{2+} of the spherical DNA of different sizes. (G) Scheme illustrating the differences between the metal-dependent normal adsorption of linear DNA and cooperative adsorption of spherical DNA on PDA. In the top row, the 3′-FAM is quenched upon the adsorption of linear DNA.

43

We recently showed that transition metal ions can drastically enhance DNA adsorption on PDA,[196] thus Zn^{2+} was further tested. In the presence of low concentrations of Zn^{2+}, adsorption of the linear DNA was also more efficient than the SNA (Figure 3.2C), while with sufficient metal ions (>0.2 mM), the SNA also caught up. Since the concentration range used for Zn^{2+} was even lower than that for Ca^{2+}, Zn^{2+} was a more efficient metal ion for DNA adsorption. For the SNA, we noticed sigmoidal metal binding curves for all these metal ions, suggesting the binding of multiple metal ions to achieve the adsorption of the SNA. We did a quantitative fitting and obtained Hill coefficients for Na^+ (2.5), Ca^{2+} (2.3), and Zn^{2+} (2.2). Therefore, two to three metal ions on the surface were simultaneously required, and this is also consistent with the model of polyvalent interactions. For the linear DNA, they can all fit to a normal binding curve with binding of just one Ca^{2+} or Zn^{2+}. This does not rule out that the linear DNA can also utilize multiple metal ions for adsorption, but the effect of the metal ions was not cooperative, and they were likely to act individually.

We then studied the effect of size of SNA on the adsorption. On average, 10, 98, and 390 DNA strands were attached on each of the 5, 13, and 30 nm AuNPs, respectively. The SNAs with different sizes but equal total DNA concentration (150 nM) were incubated with the PDA NPs in the presence of different concentrations of Ca^{2+}. As shown in Figure 3.2E, the cooperative effect of metal ions was even stronger for the larger SNAs. For the 5 nm, the curve appeared similar to a normal binding (Hill coefficient of 1.2), but the adsorption capacity was still much higher than the AuNP-free linear DNA. On the other hand, the adsorption of the 30 nm spherical DNA was more dependent on the cooperative effect of metal ions with a Hill coefficient of 7.6. In Figure 3.2F, we plotted the Hill coefficients as a function of AuNP size. Based on this understanding, we described the adsorption of linear and SNA on PDA in Figure 3.2G. In the above discussion, we only considered the effect of metal ions in adsorbing DNA. Metal ions can also reduce charge repulsion among DNA strands, allowing a high density packing of DNA on AuNPs.

3.3.2 DNA Desorption from the PDA NPs

The above studies measured DNA adsorption capacity, which indirectly reflected adsorption affinity. To probe adsorption affinity directly, we then used denaturing agents to wash preadsorbed DNA. For the linear DNA, desorption was followed using its fluorescence, while for the SNA on 13 nm AuNPs, desorption was tracked using the color of the AuNPs. First, both types of DNA were respectively adsorbed on the PDA NPs in the presence of 100 mM Na^+, 2 mM Ca^{2+}, or 0.6 mM Zn^{2+}. Then, 4 M

urea was added to probe possible hydrogen bonding interactions, since urea can disrupt hydrogen bonds. The UV–vis spectra of the supernatants are presented (Figure 3.3A), where a sharp peak at 520 nm was observed for the control sample without PDA (red spectrum). For the rest of the samples, the higher the peak, the more desorption of the SNA. The SNA desorbed less than 20% in the case of divalent metal ions; and therefore, hydrogen bonding was unimportant for such metal-mediated adsorption.
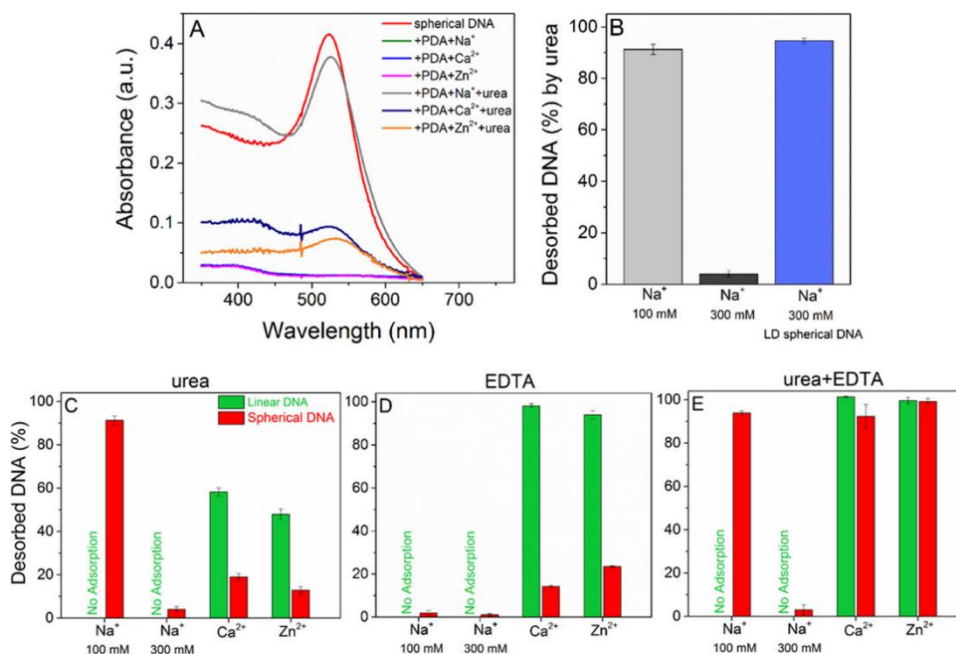

Figure 3.3. (A) UV–vis spectra of the supernatants collected from different samples after centrifugation at 1200 rpm for 5 min at which speed the spherical DNA was not precipitated. The red curve is the spherical DNA alone without PDA. In the presence of 50 µg/mL PDA (100 mM Na^+, 2 mM Ca^{2+}, or 0.6 mM Zn^{2+}), the spherical DNA fully adsorbed. After adding 4 M urea, the UV–vis spectra showed different levels of desorption. (B) Effect of Na^+ concentration and DNA density on desorption of the spherical DNA by urea. The desorption of the linear and spherical DNA from the PDA in the presence of different metal ions induced by (C) 4 M urea, (D) 4 mM EDTA, and (E) 4 M urea plus 4 mM EDTA.

On the other hand, almost 90% of the spherical DNA desorbed in the sample with 100 mM Na^+, showing that hydrogen bonding contributed significantly, probably between the amine and carbonyl groups of the DNA and amine and hydroxyl of the PDA. Hence, the weak hydrogen bonding was amplified by polyvalent binding in the SNA. Increasing the concentration of Na^+ to 300 mM resisted urea-induced desorption (Figure 3.3B), suggesting that although the initial driving force for

adsorption with Na^+ was hydrogen bonding, increasing the Na^+ concentration could enable other types of binding forces.

To further understand the importance of DNA density, SNA with a lower DNA density (LD) was prepared. Compared to the original 98 DNA strands on each 13 nm AuNP, this sample had only 29 DNA strands; only ~30% of the original density. Complete adsorption still occurred for the LD SNA in the presence of 300 mM Na^+. However, after adding 4 M urea, the LD SNA was almost completely desorbed (Figure 3.3B). Therefore, a high density of DNA was required to achieve stable adsorption of the SNA.

For divalent metal-mediated adsorption, when challenged by urea, the linear DNA was also desorbed more than the SNA (Figure 3.3C).[50] This data also confirmed the importance of polyvalent hydrogen bonding on the adsorption affinity of SNA on PDA. The densely packed SNAs are more rigid and would have a smaller loss in entropy upon adsorption, which are also favorable for adsorption. We reason that the confinement of SNA would favor the entropy term relative to the linear DNA. The effect of densely packed SNA on its tighter hybridization with cDNA was recently articulated to be mainly enthalpy-driven. The high DNA density caused geometric confinements, which was found to cost a high entropic penalty for binding to the complementary DNA.[226] For adsorption, no such hybridization is needed, and this is a difference between the adsorption we studied here and the hybridization of DNA studied in the literature.

To further probe the effect of metal ions, we then added EDTA. EDTA had no effect on the Na^+-mediated SNA (Figure 3.3D, first two red bars). As a strong metal chelator, EDTA almost completely desorbed all the linear DNA in the case of the divalent metal samples. On the other hand, only 14 (for Ca^{2+}) and 23% (for Zn^{2+}) of the SNA desorbed. The stability constants (logarithm) of EDTA binding to Ca^{2+} and Zn^{2+} are 10.6 and 16.4, respectively, and thus the free metal ions should be in the nanomolar region or even lower.[230] Based on the data in Figure 3.2B, C, such low metal concentrations cannot support the adsorption of the SNA. The fact that most of the SNAs were still adsorbed suggested that either the metal was coordinated by even stronger affinity binding sites or after the adsorption, the metals may leave the structure, and other forces can still support the adsorption. To test these hypotheses, we then combined urea and EDTA, which almost completely desorbed the SNA in the case of divalent metal ions (Figure 3.3E), supporting the second hypothesis. After removing the divalent metal ions, the SNA can no longer resist the urea-induced desorption.

3.3.3 Magnetic Fe$_3$O$_4$@PDA NPs Free of Nonspecific DNA Adsorption

Based on a reported protocol,[228] Fe$_3$O$_4$ NPs with an average size of ~120 nm were synthesized and observed under TEM to have a spherical morphology (Figure 3.4A). No surfactants were used during the synthesis and thus the native oxide surface was exposed. At pH 7.6, the ζ-potential of the Fe$_3$O$_4$ NPs was −22 mV (Figure 3.4D). Despite the negative surface charge, the bare Fe$_3$O$_4$ NPs could nonspecifically adsorb single-stranded DNA in the presence of salt, such as NaCl (Figure 3.4E), likely via the phosphate backbone of DNA after screening of charge repulsion.[57] To inhibit such nonspecific adsorption, we then coated the NPs with PDA.
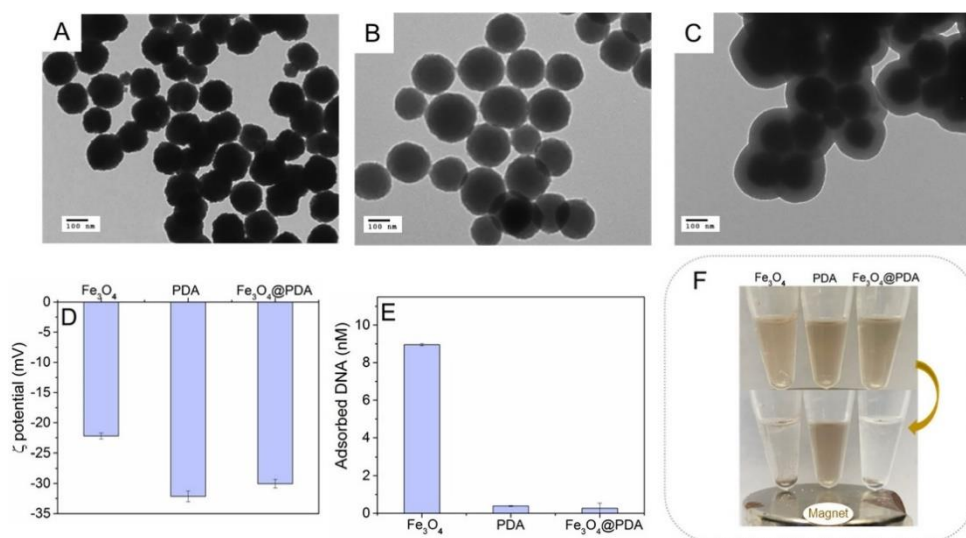

Figure 3.4 TEM micrographs depicting spherical (A) Fe$_3$O$_4$, (B) PDA, and (C) Fe$_3$O$_4$@PDA NPs. (D) ζ-potentials of the NPs in 25 mM HEPES, pH 7.6. (E) Adsorption of 10 nM FAM-cDNA on different NPs in the presence of 300 mM Na$^+$. (F) Photographs of the NPs before and after magnetic separation showing that Fe$_3$O$_4$@PDA NPs retained the magnetic property of the core.

After 6 h of dopamine polymerization in a basic condition, a PDA shell with a thickness of ~40 nm was formed over the Fe$_3$O$_4$ NP core (Figure 3.4C). During the growth of the PDA shell on the Fe$_3$O$_4$ NPs, some particles merged and formed aggregated products. For comparison, we also prepared pure PDA NPs without a Fe$_3$O$_4$ core in the same condition over 6 h (Figure 3.4B). At pH 7.6, the surface charge of Fe$_3$O$_4$@PDA NPs was −30 mV (Figure 3.4D), close to that of the pure PDA NPs, suggesting the successful PDA coating on the Fe$_3$O$_4$ NPs.

We then studied the adsorption of DNA. After the PDA coating, almost no DNA was adsorbed (Figure 3.4E), and the sample behaved similarly to the pure PDA NPs (Figure 3.4E). This experiment also indicated that the surface was fully covered by PDA and the nonspecific DNA adsorption was inhibited. It is well-known that PDA cannot adsorb DNA in the absence of divalent metal ions.[32, 195]

The Fe_3O_4 NPs had strong superparamagnetic properties,[228] and can be easily pulled down by a magnet within 30 s (Figure 3.4F). After coating a PDA shell, the magnetic property was retained, and nonspecific DNA adsorption was avoided (Figure 3.4E,F). It should also be considered that the duration of dopamine polymerization may affect PDA's DNA adsorption property, since different extent of PDA oxidation have different surface properties.[73, 195] To avoid nonspecific DNA adsorption, we chose 6 h polymerization.

3.3.4 DNA Functionalization of Fe_3O_4@PDA NPs

After preparing the NPs without nonspecific DNA adsorption, we then compared two methods for the conjugation of DNA and specific DNA extraction. In the covalent method, a thiol-modified DNA was used. Figure 3.5A (the top row) illustrates the Michael addition and Schiff-base reactions between a thiol residue and different positions of the dopamine-quinone moiety.[89, 231] Before the reaction, the DNA was first treated with TCEP in two different pH values to cleave the disulfide bond. As shown in Figure 3.5C, the TCEP-treated DNA in pH 5 showed higher activity, and ~75 nM of the initial 150 nM DNA was attached to the NPs after overnight incubation. This is consistent with the understanding that TCEP has stronger reducing power at mildly acidic pH.[232] On the other hand, at the same buffer conditions, the non-TCEP-treated DNA or nonthiolated DNA (FAM-DNA) could not be attached to the NPs, ruling out the possibility of noncovalent DNA adsorption (Figure 3.5C).

In the physisorption method, we first attached the same thiolated DNA to 13 nm AuNPs by the salt-aging method to prepare SNAs (Figure 3.5B), where on average, ~100 DNA strands were attached on each AuNP.[49] To screen the charge repulsion between the negatively charged SNA and Fe_3O_4@PDA NPs, 300 mM Na^+ was used in the buffer. Then, simple mixing of the SNA and the Fe_3O_4@PDA resulted in highly stable conjugates.[50] Since no divalent metal ions were added, the SNA adsorbed on the Fe_3O_4@PDA NPs based on weak interactions between DNA and PDA such as hydrogen bonding and π–π stacking, which were significantly enhanced by simultaneously involving multiple binding sites in the dense DNA layer.[50] Different densities of the SNA can be attached onto the Fe_3O_4@PDA NPs by simply varying the ratio between the SNA and Fe_3O_4@PDA. Figure 3.5 includes the TEM

48

images depicting 50 µg/mL of the Fe$_3$O$_4$@PDA NPs after functionalization with 150 (Figure 3.5D) and 300 nM (Figure 3.5E) SNA, respectively.

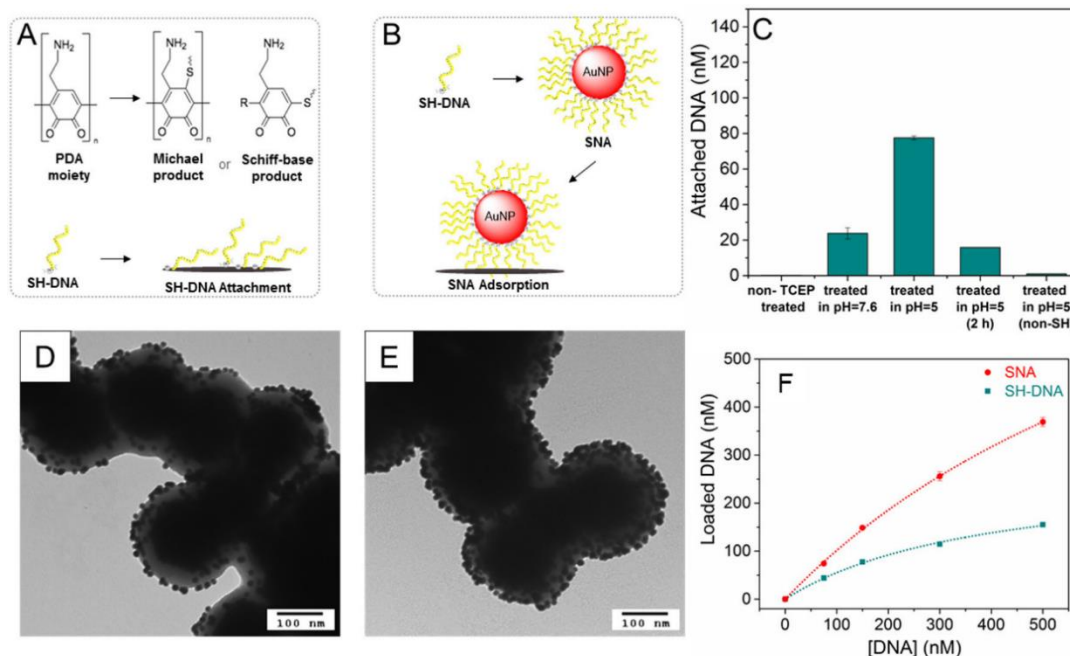**Figure 3.5** (A) Chemical reaction mechanisms and scheme of SH-DNA attachment to the Fe$_3$O$_4$@PDA NPs. (B) A scheme depicting SH-DNA attachment to AuNPs to form SNA and subsequent adsorption of the SNA on a surface. (C) Investigation of effects of TCEP treatment, pH and incubation time on the efficiency of SH-DNA attachment to the NPs. The incubation happened overnight unless otherwise mentioned. TEM micrographs depicting 50 µg/mL Fe$_3$O$_4$@PDA NPs after incubated with (D) 150 and (E) 300 nM SNA. (F) Probe DNA loading capacity on 50 µg/mL Fe$_3$O$_4$@PDA NPs, where different concentrations of probe SNA or SH-DNA were exposed to the NPs.

After establishing the two bioconjugation methods, we then compared their DNA functionalization capacity by exposing different concentrations of the SH-DNA and SNA to the Fe$_3$O$_4$@PDA NPs. We kept the total DNA concentration to be the same for them to have a fair comparison, where the loading capacity of the SNA was higher than of the linear SH-DNA (Figure 3.5F). All of the 150 nM SNA was adsorbed on the surface, while 500 nM SH-DNA was needed to achieve ~150 nM probe DNA on the surface.

To gain more insights, we then investigated the adsorption isotherms. For both SH-DNA and SNA, a higher initial DNA concentration resulted in more DNA conjugation, and the data were fitted to the

Langmuir isotherm (Figure 3.5F). After extrapolation to infinitely high DNA concentration, the saturation DNA loading capacity on 50 μg/mL of the Fe_3O_4@PDA NPs was calculated to be 0.28 μM for the linear SH-DNA and 1.1 μM for the SNA. This pointed out that the SNA functionalization of the NPs was remarkably more efficient than the linear DNA. Of note, the fitting here was only for mathematic treatment since DNA adsorption here is considered to be irreversible, which did not satisfy the requirements of the Langmuir model. Moreover, the SNA conjugation was accomplished within 30 min, while overnight incubation was needed for the attachment of SH-DNA, suggesting a kinetic disadvantage of the latter. As shown in Figure 3.5C, after 2 h, only ~15 nM of the initial 150 nM SH-DNA was attached to the Fe_3O_4@PDA NPs.

3.3.5 Selective Extraction of DNA

To extract DNA from biological samples, magnetic separation has often been used due to the mild, straightforward, and efficient reaction conditions.[124, 213, 233-234] However, such methods often overlooked sequence selectivity. Hence, we aimed to design magnetic NPs for highly selective extraction of DNA using Fe_3O_4@PDA/DNA conjugates. Since in the absence of divalent metal ions, PDA does not adsorb DNA, this would prevent nonspecific extraction of DNA. To test this idea, we used a 21-mer probe DNA containing a 12-mer block for hybridization and a 9-mer spacer. For comparison, Fe_3O_4@PDA NPs were functionalized with a final concentration of 150 nM probe SNA or SH-DNA. Then, different concentrations of FAM-labeled 12-mer DNA (FAM-cDNA) complementary to the 21-mer probe DNA was incubated with the NPs.

As shown in Figure 3.6A, the SNA-functionalized NPs were remarkably more effective for the extraction of the cDNA. Of 200 nM FAM-cDNA, ~ 80 nM was captured by the SNA-functionalized NPs, while only around 20 nM was captured by the SH-DNA functionalized NPs. The data were fitted with Langmuir isotherms, and after extrapolation, the saturation extraction capacity was 110 nM and 36 nM for the SNA and SH-DNA probes, respectively. The higher extraction efficiency of the SNA than SH-DNA was even despite the fact that a portion of the 150 nM probe on the SNA were located in the anchoring face to interact with the PDA (Figure 3.5B), while all of the 150 nM probe SH-DNA was expected to be accessible for hybridization with the FAM-cDNA. The lower DNA capture for NPs@SH-DNA system was probably due to the unfavorable conformation of attached DNAs on the surface for hybridization (Figure 3.5A), whereas for the SNA, the DNA strands were in a favorable upright conformation, and they have stronger affinity to the cDNA.
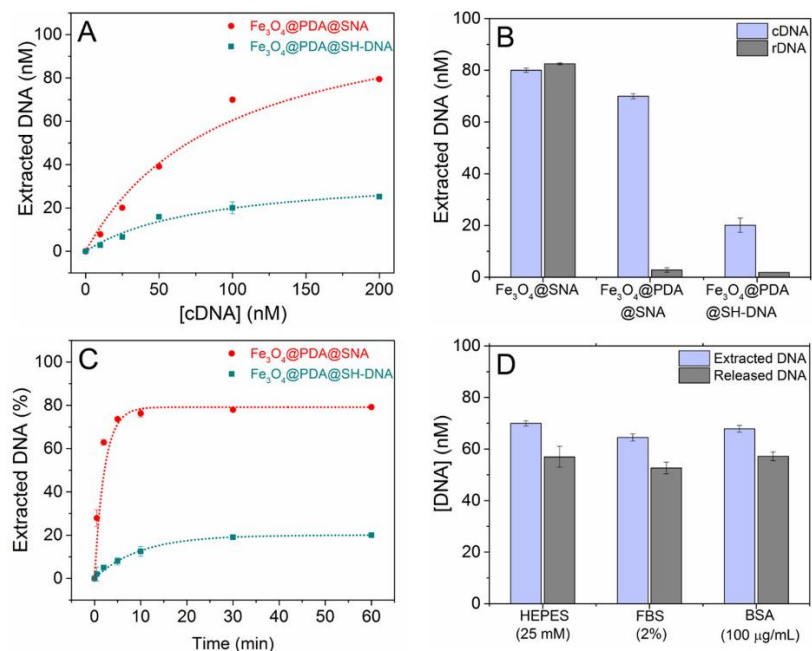
50

Figure 3.6 (A) Extraction capacity of FAM-cDNA by Fe_3O_4@PDA NPs functionalized with 150 nM of probe SNA or SH-DNA. (B) Selectivity of different nanoprobes exposed to 100 nM FAM-cDNA or FAM-rDNA. (C) Kinetics of 10 nM FAM-cDNA extraction by Fe_3O_4@PDA NPs functionalized with 150 nM of probe SNA or SH-DNA. The data were fitted with a PFO adsorption kinetic model. (D) Fe_3O_4@PDA@SNA efficiency for the capture and release of 100 nM FAM-cDNA in different solutions

The selectivity of DNA capture was studied by using 100 nM of the FAM-cDNA or a noncomplementary DNA (FAM-rDNA), and we calculated the ratio of the captured FAM-cDNA over FAM-rDNA. First, the SNA-functionalized Fe_3O_4 NPs (without a PDA shell) were tested, and both FAM-cDNA and FAM-rDNA were captured similarly (selectivity of ~1) due to the nonspecific adsorption of DNA on the Fe_3O_4 NPs (Figure 3.6B). On the other hand, SNA-functionalized Fe_3O_4@PDA NPs highly selectively captured FAM-cDNA over FAM-rDNA, where the selectivity was calculated to be 27.6. Hence, by coating the Fe_3O_4 NPs with PDA, only the complementary DNA was extracted. When the Fe_3O_4@PDA NPs were directly functionalized with SH-DNA, a high selectivity of 13.2 was still achieved, although the extraction capacity was lower (~20 nM; Figure 3.6B).

The kinetics of hybridization of cDNA with the probe DNAs were also studied (Figure 3.6C). The data were fitted well to a pseudo first order (PFO) adsorption kinetic model[235] with correlation coefficients (R^2) of greater than 0.999 for both SH-DNA and SNA. Based on the fitting calculations,

DNA extraction on the SNA probe was 5-fold faster than on the SH-DNA probe to reach half-saturation, since the $t_{1/2}$ was 1.4 min for the SNA and 7.1 min for the SH-DNA.

Finally, the robustness of the DNA extraction on Fe_3O_4@PDA@SNA probe was studied in complex biological environments such as FBS (2%) and BSA (100 μg/mL) (Figure 3.6D). This probe can successfully extract DNA in both. In addition, ∼ 80% of the extracted DNA can be released by simply dispersing the NPs in a buffer of low ionic strength (HEPES 25 mM, pH 7.6, devoid of NaCl). When the NPs were functionalized with 150 nM SNA, and 100 nM cDNA was added, the captured cDNA was 69, 64, and 67 nM in HEPES, FBS (2%), and BSA (100 μg/mL), respectively (Figure 3.6D). Overall, the designed magnetic hybrid nanoprobe seemed to be a promising candidate for sequence-specific DNA extraction in biological samples.

3.3.6 Detection of Target DNA

Due to the selective DNA hybridization, the same platform could further be used for sensing purposes.[3, 236] In Figure 3.7A, the sensor design is demonstrated. First, the Fe_3O_4@PDA NPs were functionalized with 150 nM SH-DNA or SNA. Then, 200 nM 12-mer FAM-cDNA (reporter DNA) was incubated with the functionalized NPs to hybridize with the probe DNA forming a nanoflare probe.[37] Then, 1 mg/mL BSA was added as a competing agent to block the unoccupied probe DNAs. Finally, the pellets were dispersed in different concentrations of nonlabeled 21-mer cDNA (target DNA) to displace the reporter DNA and produce fluorescence signals.
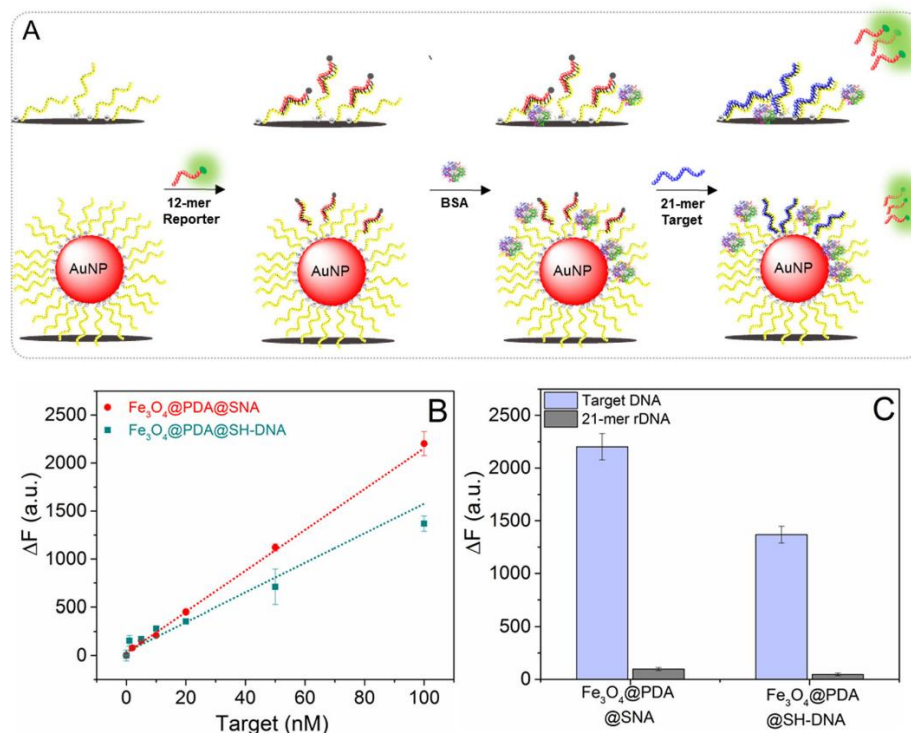
Figure 3.7 (A) Design of the detection procedure for both SH-DNA and SNA functionalized Fe_3O_4@PDA NPs. The shorter FAM-cDNA (reporter) hybridized with the probe DNA strands and was released upon displacement with the nonlabeled longer target cDNA. (B) The response signal of the biosensors to different concentrations of target DNA. (C) Selectivity of the biosensors to the target DNA over a 21-mer random DNA.

The calibration figures for both biosensors were obtained (Figure 3.7B), where the limit of detection (LOD) was calculated to be 10.7 and 4.4 nM for the linear SH-DNA and SNA-functionalized NPs, respectively (3σ/slope; σ being the standard deviation of the background variation in the absence of target). Moreover, at the same target concentrations, the biosensors' signal was stronger for the SNA-functionalized sensor. The lower LOD and the stronger signal can be attributed a higher reporter DNA density on the SNA probe (~80 nM reporter DNA) than on the linear DNA probe (~20 nM reporter DNA).

Furthermore, we showed that both detection methods were highly selective toward the target DNA when 100 nM target and random DNA separately were exposed to the sensor (Figure 3.7C). This high selectivity was assured by nonadsorbing surface of the NPs as well as using BSA as a competing and bocking agent.

3.4 Conclusions

In summary, we have compared the adsorption of the linear and SNA by PDA NPs. The linear DNA showed the normal metal-dependent binding behavior in the presence of different metal ions. However, a cooperative binding of multiple metal ions was needed for the adsorption of SNA as reflected by the sigmoidal binding curves. The extraordinary adsorption stability of spherical DNA was present only if the cooperative effect was fulfilled at high metal ion concentrations. Then, Fe_3O_4@PDA core–shell NPs were synthesized, which benefited from the magnetic property of its core and could be magnetically separated within 30 s. Moreover, the nonspecific DNA adsorption of the bare Fe_3O_4 NPs was inhibited by the PDA shell. SNA functionalization of the Fe_3O_4@PDA NPs was compared side-by-side with linear SH-DNA functionalization. A higher density of probe SNA can be loaded on the NPs in 30 min than of SH-DNA overnight. Fe_3O_4@PDA@SNA showed a ~ 4-fold higher DNA extraction capacity and 5-fold faster kinetics than Fe_3O_4@PDA@SH-DNA most likely due to the highly favorable upright conformation of the DNA strands in SNA. The conjugate showed a high extraction selectivity for the complementary DNA sequence. The extracted DNA can be effectively released by lowering the ionic strength. The probe was capable of effective DNA extraction in complex biological environments such as FBS and BSA. Furthermore, we showed that the same hybrid structure can be used for selective DNA detection. We believe that SNA-functionalization of nanomaterials can be a key method in bioanalytical chemistry due to the high stability of the conjugates, effective hybridization, and straightforward capture/release mechanisms. Moreover, this study has revealed an interesting application of PDA in producing hybrid nanomaterials for highly selective DNA extraction and detection.

Chapter 4

Adsorption of Linear and Spherical DNA Oligonucleotides onto Microplastics

The results presented in this chapter have been published as:

Mohamad Zandieh, Kshiti Patel, and Juewen Liu. "Adsorption of Linear and Spherical DNA Oligonucleotides onto Microplastics". *Langmuir* **2022**, 38, 5, 1915-1922.

4.1 Introduction

Plastic materials are extremely prevalent due to their low price, lightweight, versatility, and durability. Over 300 million tons of plastics are produced annually.[237] However, they do not degrade easily in the environment. Therefore, plastic wastes contaminate the soil, sea, fresh water, and food chains.[165, 238-239] When plastic materials are broken into tiny pieces (<1 mm) in the environment via mechanical force, chemical transformations, or microbiological degradation, microplastics are formed.[151] Due to a high surface-to-volume ratio of microplastics, a wide range of invasive marine microorganisms can adsorb onto microplastics and spread into the ecosystem.[155, 240-241] It is estimated that annually a minimum of 39,000–52,000 microplastic particles are consumed by each individual,[154] posing a serious threat to human health potentially leading to particle toxicity, disruption of the immune system, and cancer in the long-term.[242-243] The most extensively detected microplastics in freshwaters are composed of polyethylene (PE), polypropylene (PP), polystyrene (PS), polyvinyl chloride (PVC), and polyethylene terephthalate (PET).[244]

Studying the interactions between DNA and microplastics is particularly important for a few reasons.[33, 196, 245-247] On one hand, DNA is an important biopolymer, and biological DNA can be carried by microplastics in the environment. For example, extraction and sequencing of environmental DNA from marine microplastics have been investigated widely.[164, 248-250] Moreover, adsorption of DNA onto PP, PS, and polydimethylsiloxane (PDMS) have been reported.[171, 251-252] Investigation of the adsorption of DNA oligonucleotides onto materials and surfaces can provide useful information regarding their interaction mechanism. On the other hand, DNA oligonucleotides might serve as a probe to detect and study microplastics. DNA aptamers have been selected against various inorganic and polymeric surfaces. Selecting aptamers for microplastics can be important for

their extraction and detection. Before performing aptamer selections, it is important to understand nonspecific adsorption of DNA. If nonspecific adsorption is too strong, then it is difficult to obtain specific aptamers.[253] Besides single-stranded linear DNA, adsorption of spherical nucleic acids (SNA) may provide additional insights. SNA refers to a nanoparticle core (e.g., AuNP) functionalized with a high density of DNA oligonucleotides.[45, 48, 218, 254] Previous works showed that SNA can adsorb onto surfaces with much higher affinity than linear DNA of the same sequence due to polyvalent interactions amplifying weak individual interactions of a linear DNA.[50, 182, 197] The adsorption mechanism of SNA can also be different from linear DNA due to the confined conformation of the DNA.[226]

In this work, we investigated the interaction of linear and spherical DNA oligonucleotides with the most common microplastics, and we pay particular attention to the effect of metal ions that are abundant in the environment such as Na^+, Mg^{2+} and Ca^{2+}.[255] We observed that PET, PS/PVC, and PS showed the highest affinity for DNA adsorption due to their more favorable surface functional groups, and divalent metal ions can promote efficient DNA adsorption.

4.2 Materials and Methods

4.2.1 Chemicals

The 21-mer DNA (5′-AAA AAA AAA CCC AGG TTC TCT-3′) with different modifications (3′-FAM, or 5′-SH, or dual labeled 5′-SH and 3′-FAM) were purchased from Integrated DNA Technologies (IDT, Coralville, IA). Metal chloride salts, ethylenediaminetetraacetic acid (EDTA), Tween 80, sodium polyphosphate (25-mer), and potassium cyanide (KCN) were from Sigma-Aldrich. 4-(2-Hydroxyethyl) piperazine-1-ethanesulfonic acid (HEPES), urea, and adenosine were obtained from Mandel Scientific (Guelph, ON, Canada). Citrate-capped AuNPs (13 nm) were synthesized based on the literature,[227] and the concentration of stock AuNPs was calculated to be ~10 nM using the extinction coefficient of $2.7 \times 10^8 \ M^{-1} \ cm^{-1}$ at 520 nm. Milli-Q water was used for the preparation of all the buffers and solutions.

4.2.2 Instrumentation

The Raman spectra of solid plastic samples were collected using a spectrometer (DeltaNu, Advantage 785) with a 785 nm laser and a 10 s integration time. The morphology of the microplastics was visualized under a Nikon Eclipse Ti–S inverted microscope, and the transmission electron microscopy

(TEM) images were taken using a Phillips CM10 100 kV microscope. The ζ-potentials of microplastics were measured using a dynamic light scattering (DLS) instrument (Zetasizer Nano 90, Malvern). In a typical experiment, the microplastics (final concentration of ~50 μg/mL) were dispersed in 1 mL buffer (10 mM HEPES, pH 7.6), and the temperature was controlled at 25 °C.

4.2.3 Preparation of Microplastics

Six commonly used plastic objects were collected (Figure 1, insets) including a cylindrical plastic container (PE), a laboratory centrifuge tube (PP), a plastic fork or spoon (PS), a plastic sheet (PVC), a hand-sanitizer dispenser container (composite of PS/PVC), and a water bottle (PET). The composing material of the plastic objects was identified using Raman spectroscopy.[256-257] Then, the plastics were cut into small pieces and washed with ethanol in a sonication bath for 2 min to remove the organic residues on the surface. Finally, using a stainless steel kitchen grater, the plastics were shredded into microplastics via mechanical force and were dispersed in Milli-Q water at a concentration of 2 mg/mL. Due to the size of the microplastics, and depending on their density, they either settled down to the bottom or float on top of the aqueous suspensions. The samples were used for further studies within 2 days after the preparation to minimize the possible effect of aging.

4.2.4 Preparation of SNA

The freezing-directed method was used to prepare SNA.[44] In this method, a final concentration of 3 μM 5′-SH-DNA was mixed with 10 nM AuNPs and placed in a freezer (−20 °C) for 3 h. After thawing at room temperature, the SNAs were centrifuged (14,000 rpm, 15 min) at 15 °C and washed three times with water. To measure the density of attached DNA, a dual labeled 5′-SH and 3′-FAM-DNA was used to prepare the SNA. The AuNPs core was then dissolved by adding KCN (a final of 10 mM). Finally, using a fluorescence intensity vs DNA concentration standard curve, the number of DNA attached on each AuNPs was calculated.

4.2.5 Adsorption of Linear DNA

Typically, 10 nM FAM-DNA was incubated with ~50 μg/mL of microplastics in the presence of different metal ions in a buffer (10 mM HEPES, pH 7.6). To avoid precipitation of microplastic particles, the samples were gently agitated during the incubation. After 1 h, the samples were centrifuged (1,000 rpm, 2 min), and the fluorescence intensity of supernatants was measured to back-calculate the adsorbed DNA.

4.2.6 Adsorption of SNA

In a typical experiment, 1.58 nM SNA (total of ~200 nM DNA) was incubated with ~150 μg/mL of microplastics in the presence of different metal ions in a buffer (10 mM HEPES, pH 7.6). To avoid precipitation of microplastic particles, the samples were gently agitated during the reaction. After 4 h, the samples were centrifuged (1,000 rpm, 2 min), and the UV–vis absorbance of the supernatants were used to back-calculate the adsorbed SNA. The DNA and SNA concentration used was the minimum concentration at which a decent signal can be achieved. The concentration of microplastics also was optimized to ensure that the surface was in excess and was not a limiting factor to adsorb the DNA or SNA.

4.2.7 DNA Desorption Studies

To investigate the desorption of linear DNA, first, 10 nM FAM-DNA was adsorbed on PET in the presence of 200 mM Na^+, 2 mM Mg^{2+}, or 2 mM Ca^{2+} for 1 h. The preadsorption experiments for this section were designed in a way to ensure that 100% of the DNA or SNA were adsorbed prior to desorption studies. Then, 4 M urea, 10 mM EDTA, 5 mM adenosine, 0.2 mM polyphosphate (25-mer, total phosphate concentration: 5 mM), or 0.25% Tween 80 was mixed with the preadsorbed DNA in the same buffer for 1 h. For the SNA desorption studies, first, 1.58 nM SNA (total of ~200 nM DNA) was adsorbed on the microplastics in the presence of 4 mM Mg^{2+}, or 2 mM Ca^{2+} overnight. Then, 4 M urea, or 10 mM EDTA was mixed with the preadsorbed SNA in the same buffer for 1 h. Finally, the supernatants of the samples were collected after centrifugation (1,000 rpm, 2 min), and the desorbed DNA/SNA was quantified according to the fluorescence/absorbance enhancement.

4.3 Results and Discussion

4.3.1 Microplastics Preparation and Characterization

To best mimic microplastics in the environment, instead of using commercially available standard polymer microspheres, we prepared our microplastics samples via mechanical shredding of some commonly used plastic items such as water bottles and culinary utensils (insets of Figure 4.1). Using Raman spectroscopy, six types of plastic materials were identified and used for further studies including: PE, PP, PS, PVC, composite of PS/PVC, and PET (Figure 4.1). For example, the sample in Figure 4.1E had a strong peak at 1001 cm^{-1}, which is the characteristic peak of aromatic ring from its PS component.[258]
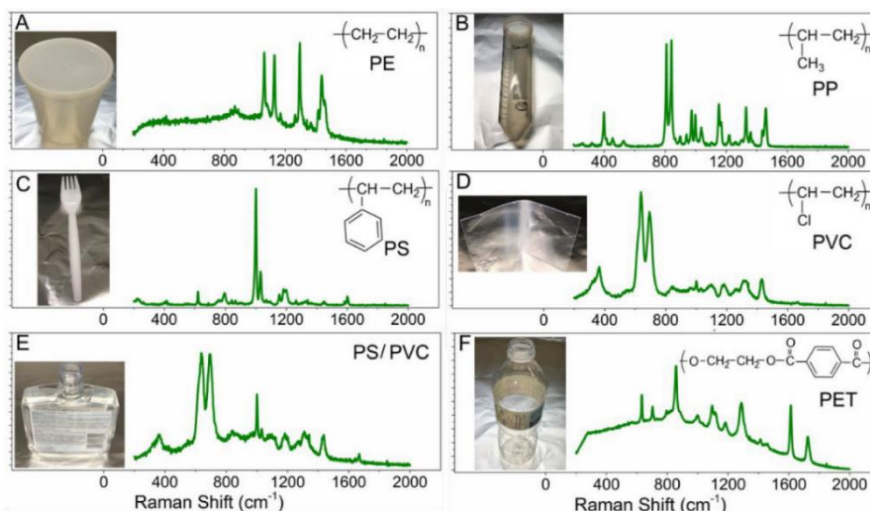
Figure 4.1 Photographs, Raman spectra and molecular structures of the plastic materials used in this work including (A) PE, (B) PP, (C) PS, (D) PVC, (E) composite of PS/PVC, and (F) PET.

After shredding the plastics (Figure 4.2), the obtained microplastics were observed under a microscope (Figure 4.3). The morphology of the microplastics was irregular including a combination of fragments, fibers, and foams.[259] Although the particle size distribution was broad for each sample, on average, PE and PP had the largest particles and PET had the smallest. This was likely due to the difference between the manufacturing and mechanical properties of the plastic materials. Nevertheless, all samples fulfilled the size requirement (<1 mm) to be defined as microplastics.[151]
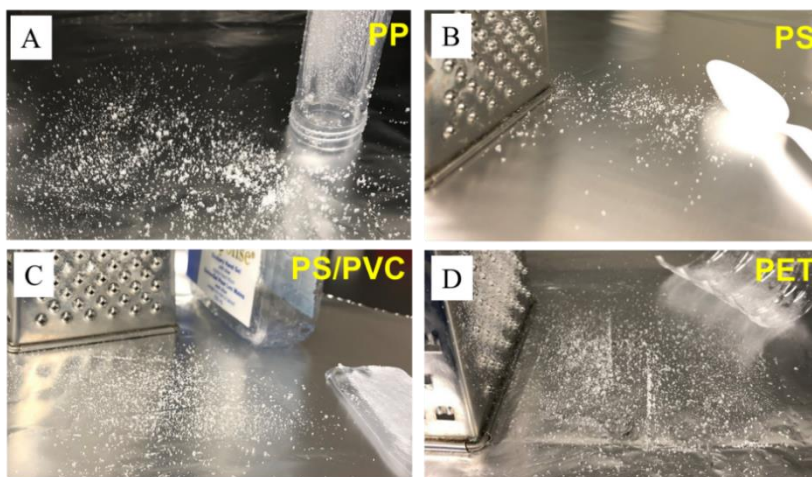
Figure 4.2 Photographs depicting microplastics of (A) PP, (B) PS, (C) PS/PVC, and (D) PET acquired by grating plastic objects with a stainless steel kitchen grater.
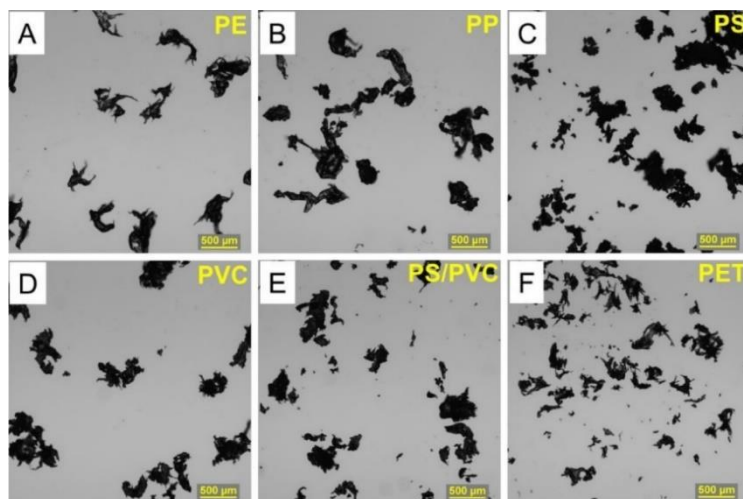
59

Figure 4.3 Micrographs of the microplastics acquired by shredding plastic materials composed of (A) PE, (B) PP, (C) PS, (D) PVC, (E) composite of PS/PVC, and (F) PET.

4.3.2 Adsorption of Linear DNA onto Microplastics

At pH 7.6, the ζ-potentials of the microplastics were all negative (Figure 4.4A), thereby repelling negatively charged DNA (Figure 4.4B). To screen the charge repulsion between the microplastics and DNA, different metal ions including Na^+, Mg^{2+}, or Ca^{2+} were added to the reaction buffer.[34, 260-261] Environmental waters typically contain high concentrations of these metal ions (e.g., ~450 mM Na^+, 50 mM Mg^{2+}, and 10 mM Ca^{2+} in seawater).[262]

First, adsorption of 10 nM of a carboxyfluorescein (FAM)-labeled 21-mer single-stranded DNA onto the microplastics was tested in the presence of 200 mM Na^+, 2 mM Mg^{2+}, or 2 mM Ca^{2+} (Figure 4.4C). None to negligible adsorption of the DNA occurred on PE, PP, PVC, and PS/PVC. On the other hand, the DNA was adsorbed onto PS and PET to different extents. Likely, the different chemical structure of the microplastics accounted for the different DNA adsorption efficiencies (compare the insets in Figure 4.1). The aromatic rings in PS and PET can provide π–π stacking with DNA nucleobases, cation–π interactions with the metal ions, and hydrogen bonding. Moreover, the carboxyl, hydroxyl and ester functional groups in PET could also enhance its interaction with DNA via hydrogen bonding, which could explain the higher efficiency of PET than PS. On the other hand, PE, PP, and PVC did not have aromatic structures and thus they showed weaker interactions with DNA. Moreover, comparing the metal ions, Mg^{2+} and Ca^{2+} were more efficient than Na^+ for

promoting the adsorption. With 2 mM Ca^{2+}, 28% and 87% of the DNA was adsorbed on PS and PET, respectively (Figure 4.4C).
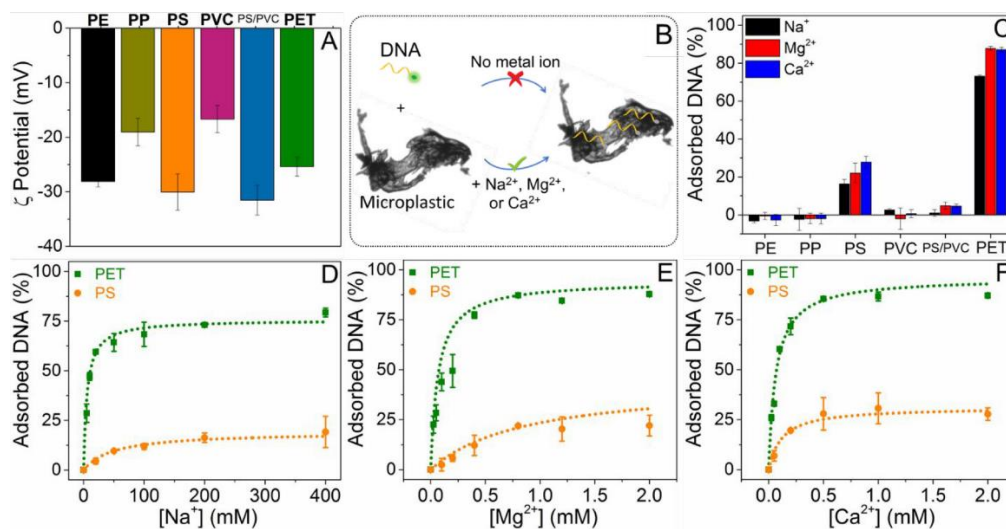

Figure 4.4 (A) ζ-Potentials of different microplastics in 10 mM HEPES buffer, pH 7.6. (B) A scheme illustrating the effect of metal ions for promoting DNA adsorption on the PS and PET microplastics. (C) Adsorption of 10 nM FAM-DNA onto 50 μg/mL of different microplastics in the presence of 200 mM Na^+, 2 mM Mg^{2+}, or 2 mM Ca^{2+}. Adsorption of 10 nM FAM-DNA on 50 μg/mL of the PET and PS microplastics in the presence of different concentrations of (D) Na^+, (E) Mg^{2+}, or (F) Ca^{2+}.

The effect of metal concentration on DNA adsorption on the PET and PS microplastics was then tested, and a higher adsorption efficiency onto PET was confirmed for all the metal ions (Figure 4.4D–F). The data fitted well with a one-site binding model, and thus the half-saturation concentration (K) were calculated. The efficiency of Mg^{2+} and Ca^{2+} to induce the DNA adsorption on PET was almost the same with a K of 66 μM (Figure 4.4E,F). However, a ~85-fold higher concentration of Na^+ was needed to reach the half-saturation (K of 5.7 mM). Similarly, the K of Na^+, Mg^{2+}, and Ca^{2+} for promoting DNA adsorption on PS was calculated to be 49 mM, 0.87 mM, and 0.12 mM, respectively. Mg^{2+} and Ca^{2+} can bridge the DNA adsorption, which may explain their higher efficiency than Na^+.[260, 262] Similar metal-dependent adsorption were also reported with other surfaces such as polydopamine and graphene oxide.[32, 197]

4.3.3 Adsorption of SNA onto Microplastics

After understanding the adsorption of linear DNA, we then tested the adsorption of SNA on the microplastics. The same DNA sequence bearing a 5′-SH was densely functionalized on 13 nm diameter AuNPs to form SNAs. The sequence of the DNA included a 9-adenine block, since it is a commonly used spacer for preparing SNA. On average 127 DNA strands were attached to each 13 nm AuNP, and the total DNA concentration was ∼200 nM for the adsorption experiments. Polyvalent binding of SNA can enhance individual weak interactions between DNA and nanomaterials, thereby leading to more stable adsorption.[50, 182, 197] This could provide us with more insights into the interactions between DNA and microplastics. Figure 4.5A is a TEM image depicting the adsorbed SNA onto a PET microplastic particle in the presence of 4 mM Mg^{2+}, where the AuNPs were densely adsorbed.
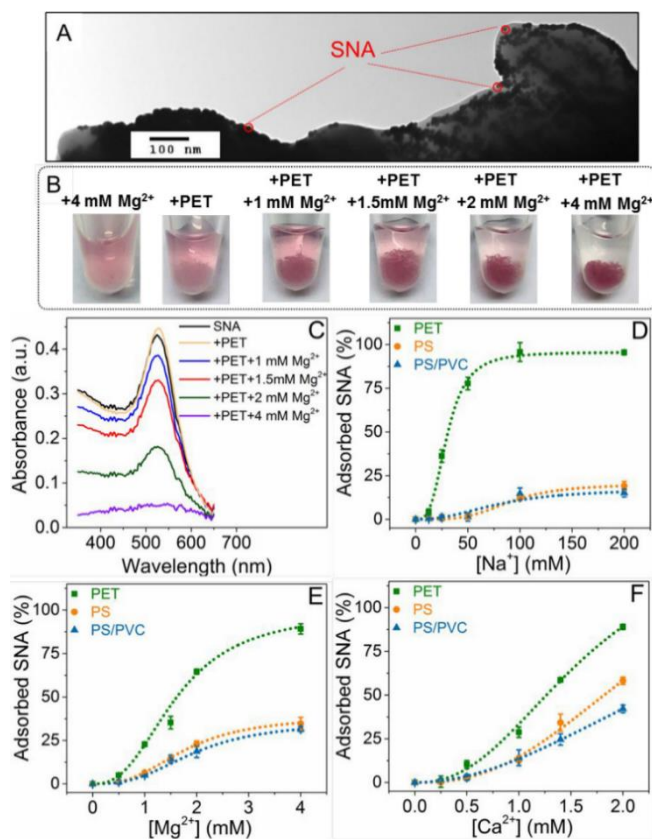

Figure 4.5 (A) A TEM micrograph depicting a high density of SNA adsorbed onto a PET microplastic in the presence of 4 mM Mg^{2+}. (B) Photographs illustrating the effect of Mg^{2+} concentration on the adsorption of 1.58 nM SNA (total of 200 nM DNA) onto ∼150 μg/mL of the PET microplastics. (C) UV−vis spectra of the

supernatants collected from the samples shown in panel (B). The adsorbed SNA was quantified according to the decrease of the absorbance. Adsorption of 1.58 nM SNA onto 150 μg/mL of the PET, PS, and PS/PVC microplastics in the presence of different concentrations of (D) Na$^+$, (E) Mg^{2+}, or (F) Ca^{2+}.

The adsorption of the SNA was quantified according to the decrease of the AuNP absorbance in the supernatants (Figure 4.5B,C). First, SNA adsorption onto the six types of microplastics were measured in the presence of 200 mM Na$^+$, 4 mM Mg^{2+}, or 2 mM Ca^{2+} (Figure 4.6A). Similar to the linear DNA, the SNA was not adsorbed onto PE, PP, or PVC, whereas PET and PS microplastics showed the highest SNA adsorption efficiency. Interestingly, the microplastics of composite of PS/PVC could also adsorb the SNA, although it did not adsorb the linear DNA (Figure 4.6A). This revealed the stronger polyvalent interactions enabled by the SNA. Note that the as-prepared citrate-capped AuNPs are aggregated by salt and thus we could not use salt to promote their adsorption (Figure 4.6B).
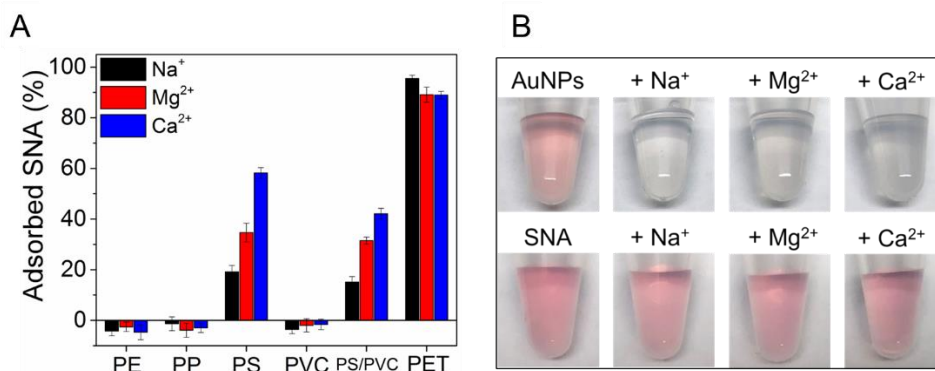

Figure 4.6 (A) Adsorption of 1.58 nM SNA (total of 200 nM DNA) onto 150 μg/mL of different microplastics in the presence of 200 mM Na$^+$, 4 mM Mg^{2+}, or 2 mM Ca^{2+}. (B) Effect of the presence of 200 mM Na$^+$, 4 mM Mg^{2+}, or 2 mM Ca^{2+} on bare AuNPs or SNA. Bare AuNPs were aggregated in the presence of different metal ions, while SNA was stable due to the protection provided by the high density of DNA.

We then studied the effect of metal concentration to induce SNA adsorption onto PET, PS, and PS/PVC. In this case, the shape of the binding curves was very different from the adsorption of the linear DNA in Figure 4.4. For SNA, sigmoidal binding curves were observed (Figure 4.5D–F), indicative of cooperative action of multiple metal ions for promoting SNA adsorption.[197] The data were fitted well with the Hill equation. From the apparent dissociation constant for different microplastics in the presence of the same metal ion, the SNA adsorption efficiency followed the order of PET, PS, and PS/PVC, which was the same order as for the adsorption of the linear DNA. The Hill

coefficients were obtained for different metal ions and microplastics. Overall, for the same microplastic, the Hill coefficients for Na^+ (PET (3.2), PS (3.7), PS/PVC (2.7)) were higher than for Mg^{2+} (PET (2.6), PS (2.8), PS/PVC (2.7)), and Ca^{2+}(PET (2.4), PS (2.2), PS/PVC (2.0)). This suggested that more Na^+ ions than Mg^{2+} or Ca^{2+} were needed to achieve the cooperative binding effect of the SNA adsorption, which can be explained by their different charges.

4.3.4 DNA Desorption Studies

The above studies investigated the efficiency of microplastics for DNA adsorption. The adsorption efficiency is influenced by not only the adsorption affinity but also the adsorption capacity. Therefore, to directly compare the adsorption affinity of microplastics, we also performed desorption studies by adding competing and denaturing agents to the pe-adsorbed DNA.

For the linear DNA, in the presence of 200 mM Na^+, 2 mM Mg^{2+}, or 2 mM Ca^{2+}, a high adsorption can be achieved only on PET (Figure 4.4C), allowing us to perform desorption studies only on PET. For all the three metal ions, ~35% of the linear DNA was desorbed from PET by 4 M urea (Figure 4.7A). In a control experiment, adding water instead of competing agents induced negligible DNA desorption. Since urea can disrupt hydrogen bonding, this revealed the significant role of hydrogen bonding for such adsorption. Then, 10 mM EDTA was separately added to probe the effect of polyvalent metal ions, since EDTA can strongly bind to Mg^{2+} and Ca^{2+} with logarithmic stability constant of 8.8 and 10.6, respectively.[205] In the presence of Na^+, the adsorbed DNA was undisturbed by EDTA (Figure 4.7A, black bar). Since EDTA can decrease the concentration of polyvalent metal ions to nanomolar region, this data showed that Na^+ alone can promote the DNA adsorption on PET. On the other hand, in the presence of Mg^{2+} and Ca^{2+}, 48% and 33% of the preadsorbed DNA strands were desorbed from PET after adding EDTA (Figure 4.7A, red and blue bar) showing the critical role of these divalent metal ions for the adsorption. Although EDTA has a higher stability constant for Ca^{2+}, less of the DNA was desorbed compared to the case of Mg^{2+}, suggesting that the DNA adsorption on PET was tighter in the presence of Ca^{2+} than Mg^{2+}. Therefore, the role of metal ions for DNA adsorption was confirmed.
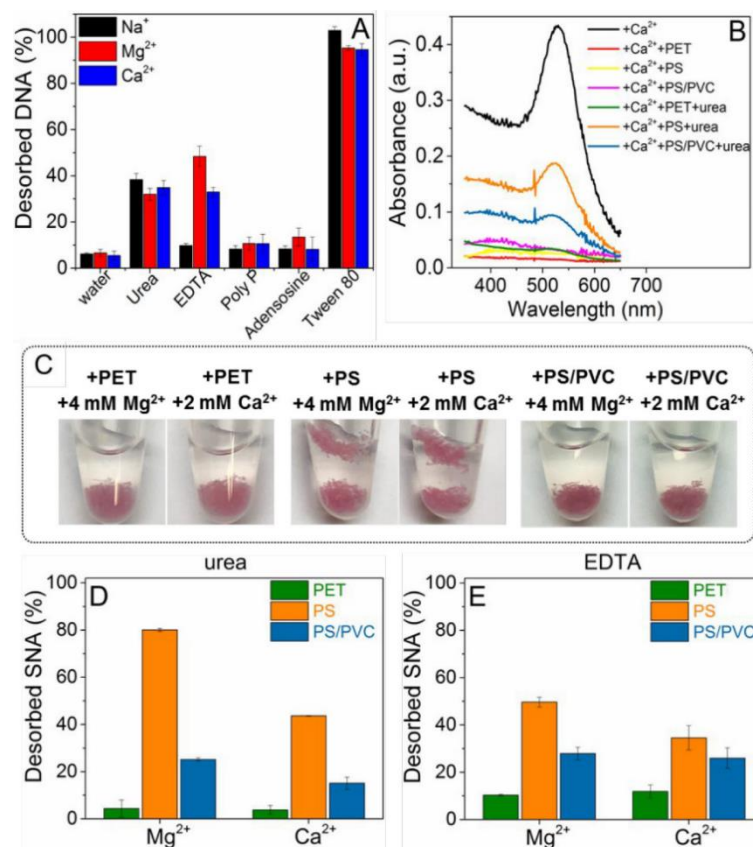
Figure 4.7 (A) The desorption of linear DNA from the PET microplastics in the presence of different metal ions (200 mM Na$^+$, 2 mM Mg^{2+}, or 2 mM Ca^{2+}) induced by 4 M urea, 10 mM EDTA, 5 mM polyphosphate, 5 mM adenosine, or 0.25% Tween 80. (B) Photographs depicting the complete adsorption of 1.58 nM SNA on the PET, PS, and PS/PVC microplastics in the presence of 4 mM Mg^{2+}, or 2 mM Ca^{2+} after overnight incubation. (C) UV–vis spectra of the supernatants collected from different samples demonstrating the urea-induced desorption of SNA from the PET, PS, and PS/PVC microplastics in the presence of 2 mM Ca^{2+}. The desorption of SNA from the PET, PS, and PS/PVC microplastics in the presence of different metal ions (200 mM Na$^+$, 4 mM Mg^{2+}, or 2 mM Ca^{2+}) included by (D) 4 M urea, or (E) 10 mM EDTA.

Typically, adding phosphate or adenosine can probe the binding via phosphate backbone or nucleobases of DNA.[206] When 5 mM phosphate or 5 mM adenosine was added, negligible desorption occurred (Figure 4.7A), suggesting that neither the DNA phosphate nor nucleobases dominated in the adsorption mechanism, but rather they both contributed to the adsorption. Finally, a surfactant (0.25% Tween 80), was added to the preadsorbed DNA, and the DNA was almost completely desorbed regardless of the type of metal ion present. This suggested that the surfactant likely interacted with PET via its hydrophobic tail and using van der Waals (VDW) force to displace the DNA. Beside the

65

mentioned interactions, microporous filling mechanisms may also contribute to the adsorption onto the microplastics,[263] where DNA might diffuse into the microplastics pores and be entrapped in there.

As mentioned above, linear DNA cannot be effectively adsorbed onto PS and PS/PVC unlike PET (Figure 4.4C). However, 200 nM SNA was thoroughly adsorbed in the presence of 4 mM Mg^{2+}, or 2 mM Ca^{2+} after overnight incubation (Figure 4.7B,C). This provided a chance of comparing the adsorption affinity of PET, PS, and PS/PVC via desorption studies. Four M urea and 10 mM EDTA were separately added to the preadsorbed SNA on the microplastics. For PET, almost no desorption occurred with urea, and negligible desorption occurred with EDTA (Figure 4.7D,E). This suggests an extraordinary stability of SNA adsorption on PET, which was enhanced compared to the linear DNA (compare to the urea- and EDTA-induced desorption in Figure 4.7A).[50, 197] Desorption from PET was in all cases lower than PS, and PS/PVC (Figure 4.7D,E) suggesting that PET had the highest affinity for DNA among these microplastics. For PS, urea desorbed 80% and 43% of the SNA in the presence of Mg^{2+} and Ca^{2+}, respectively (Figure 4.7D), confirming that a tighter adsorption can be achieved with Ca2+. For PS/PVC, the urea-induced adsorption was 25% and 15% in the presence of Mg^{2+} and Ca^{2+} (Figure 4.7D), which was interestingly lower than for PS. EDTA-induced desorption also confirmed a tighter binding with Ca^{2+} than Mg^{2+}, and a higher affinity of PS/PVC than PS (Figure 4.7E).

Overall, the desorption data indicated the order of DNA adsorption affinity as following: PET > PS/PVC > PS. The composite of PS/PVC, besides all the attraction forces provided by PS, probably can harness some extra forces provided by PVC such as halogen bonding. The chlorine atoms in PVC structure can act as electron acceptors while the oxygen, nitrogen and the aromatic nucleobase of DNA are electron rich sites that may function as electron donor to form halogen bonds.[264-265]

4.4 Conclusions

In summary, the interactions of DNA oligonucleotides with the most common microplastic materials were investigated including PE, PP, PS, PVC, PS/PVC, and PET. Adsorption of linear DNA and SNA onto the microplastics were tested in the presence of Na^+, Mg^{2+} or Ca^{2+} ions. The linear DNA adsorbed onto PET and PS more efficiently than the other microplastics, likely due to the aromatic functional groups present in the PET and PS structure. Desorption studies revealed that hydrogen bonding and metal-mediated interactions are the predominant forces between DNA and PET

microplastics. However, VDW force and hydrophobic interactions are also likely involved in the adsorption mechanism. Unlike linear DNA, stable adsorption of high concentrations of SNA were also achieved on PS and PS/PVC microplastics. Investigation of the SNA desorption from the microplastics suggested the order of adsorption affinity to be PET > PS/PVC > PS. Moreover, overall, Ca^{2+} and Mg^{2+} promoted a more efficient and tighter DNA adsorption than Na^+. This study has provided interesting insights to better comprehend the origins of interactions between microplastics and environmental DNA. In addition, it has supplied fundamental information which paves the way toward the future application of DNA aptamers in microplastic studies.

Chapter 5

Spherical DNA Adsorption to Study the Wettability of Microplastics

5.1 Introduction

Microplastics are submillimeter plastics particles that are either manufactured intentionally to be used in cosmetic and cleaning products (primary microplastics) or generated when plastic wastes are shredded via chemical, biological or mechanical transformation in the environment (secondary microplastics).[151] Due to a high surface-to-volume ratio, microplastics adsorb different pollutants in the environment such as heavy metal ions,[160] DNA,[174-175] and invasive living organisms.[240-241] This makes microplastics detrimental to ecosystems[155] and a threat to human and animal health.[242-243] Understanding the evolution of surface chemistry on microplastic particles in aqueous environments is a critical step for studying the adsorptive behavior and capacity of these pollutants such that risks can be identified and minimized.

Microplastics undergo gradual physical and chemical transformations in environmental water known as weathering.[266] Such changes are induced naturally when microplastics are dispersed in environmental waters over a long period of time. In addition, various methods have also been utilized to accelerate chemical and physical transformations in microplastics such as UV and gamma irradiation, oxidation and high temperature.[267-268] The most common changes are the generation of surface polar groups upon oxidation, production of micropores, and change in the surface roughness, all of which can change the surface properties of microplastics such as wettability. UV-treated microplastics can increase the adsorption of Cu^{2+},[269] and other heavy metal ions,[162] although the adsorption of some hydrophobic organic compounds was decreased.[270] The interaction of treated microplastics with the environment is also changed.[271]

Wetting is an important concept in colloidal science, which refers to the ability of a liquid to contact with a solid surface. Most fresh microplastics have hydrophobic surfaces, and when dispersed in water, they may gradually change to hydrophilic and thus enhance the wettability by water. Due to the irregular morphology of most microparticles, study of the wetting of microplastics has been quite limited. The wettability may change due to chemical transformations,[241] for which spectroscopic methods can be used to probe changes in the surface chemistry. However, if wettability changes are

only due to physical transformations, the quantification of the degree of wettability is more challenging. Upon wetting, the contact angle of the surface may change, which can in turn influence the flotation or sinking behavior of particles.[272-273] Lin et. al. used a camera to record the sinking ratio and velocity of polystyrene microplastics, which required extensive data analysis and was a rather complicated system.[272]

Certain DNA oligonucleotides have shown various applications in antisense delivery,[274] biosensing,[7] catalysis,[8] and nanomaterials assembly.[23] Spherical nucleic acid (SNA) is an interesting structure made of a high density of DNA or RNA oligonucleotides attached to a nanoparticle core such as a gold nanoparticle (AuNP).[44-46, 48, 218, 275] The very high extinction coefficient allows visual observation of AuNPs at a low particle concentration. We previously showed that SNA can strongly adsorb onto various materials surfaces, including a few microplastics, due to polyvalent DNA binding interactions.[50, 182, 197, 276]

In this work, we investigated the changes in the ability of common microplastics to adsorb SNA upon soaking in water. All the tested microplastics adsorbed greater amounts of SNA when they were soaked in water at room temperature over a few months than when the microplastics were freshly prepared. We show that the enhancement of SNA adsorption was due to the improved microplastics wettability rather than chemical transformations, and that enhanced wettability can be reproduced by gentle heating. This work establishes SNA adsorption as a powerful tool for analysis of wettability of microplastics.

5.2 Materials and Methods

5.2.1 Chemicals

The 21-mer DNA (5′-AAA AAA AAA CCC AGG TTC TCT) with a 3′-FAM label, or a 5′-SH label, or dual 5′-SH and 3′-FAM labels was purchased from Integrated DNA Technologies (IDT, Coralville, IA, USA). Sodium chloride, 4-(2-hydroxyethyl) piperazine-1-ethanesulfonic acid (HEPES), and urea were obtained from Mandel Scientific (Guelph, ON, Canada). Tween 80, potassium cyanide (KCN), H_2O_2 solution (30 wt%), and hydrochloric acid were from Sigma-Aldrich. Citrate-capped 13 nm AuNPs were synthesized *via* citrate reduction following a reported method.[227] Milli-Q water was used for preparing all the solutions.

5.2.2 Instrumentation

A Raman spectrometer (DeltaNu, Advantage 785) with a 785 nm laser and a 10 s integration time was utilized to acquire Raman spectra and identify the composing materials of the plastic items. The microscope images of the microplastics were collected using a Nikon Eclipse Ti−S inverted microscope, and transmission electron microscopy (TEM) images were taken using a Phillips CM10 100 kV microscope. UV−vis absorption spectroscopy was performed by a spectrometer (Agilent 8453A). Thermal gravimetric analysis (TGA) was performed using a TA instrument Q500 with a temperature ramp rate of 5°C/min.

5.2.3 Raman Spectroscopy

Raman spectroscopy of 3-month-soaked, heated and fresh microplastics was carried out using a Renishaw inVia Raman Microscope. A 633 nm laser (Renishaw HeNe laser, 17 mW) paired with an 1800 lines mm^{-1} diffraction grating and a 20X microscope objective to record spectra for each plastic sample between 0 and 4000 cm^{-1}. The data for each sample was acquired as a single spectrum, enabled by the Renishaw SynchroScan feature. The laser power was filtered to 50% intensity and spectra were acquired with 5 accumulations of 10 s each. The raw data files were processed using Renishaw WiRE 5.5 software by subtracting a polynomial baseline, removing any cosmic rays, and normalizing the intensity of the spectra between 0 and 1.

5.2.4 Preparation of the Fresh Microplastics

Multiple commonly used plastic items were collected including: a plastic container composed of polyethylene (PE), a centrifuge tube composed of polypropylene (PP), plastic spoons composed of polystyrene (PS), a plastic sheet composed of polyvinylchloride (PVC), a plastic dispenser composed of PS/PVC, and a plastic water bottle composed of polyethylene terephthalate (PET). The composing material of the plastics was verified by Raman spectroscopy,[256, 277] and they were then cut into smaller pieces and washed with ethanol. The plastic pieces were then shredded via mechanical force using a stainless-steel grater to acquire microplastics. The microplastics were collected and dried at room temperature overnight using a vacuum dryer. Prior to use for experiments, the microplastics were dispersed in water.

5.2.5 Preparation of the Wettable Microplastics.

Wettable microplastics were obtained by dispersing the fresh microplastics in water and storing them in a drawer at room temperature for 3 months. Accelerated wettability of PP microplastics was achieved by heating freshly dispersed PP microplastics in a water bath at various temperatures, typically for 0.5 h.

5.2.6 SNA Preparation

The freezing method was used to prepare SNA.[44] Typically, 3 μM of a 5′-SH modified 21-mer DNA was mixed with ~10 nM AuNPs (300:1 molar ratio) and the mixture was placed in a freezer (-20 °C) for 3 h. The sample was then thawed at room temperature and washed 3 times via centrifugation (14000 rpm, 15 min) at 15 °C. To quantify the density of the attached DNA, SNAs were prepared using the dual 5′-SH and 3′-FAM labeled DNA. The AuNPs core was dissolved by adding 10 mM KCN. Finally, the fluorescence intensity of the sample (excitation at 485 nm) was compared to a standard curve and the DNA concentration and average number of DNA attached to each AuNP was calculated.

5.2.7 DNA and SNA Adsorption

For the linear DNA adsorption, 10 nM 3′-FAM DNA was used, whereas for the SNA adsorption, 2 nM AuNP (total of ~250 nM DNA) was used. The concentrations were chosen to achieve a reliable signal with minimal standard deviations between multiple trials. The DNA samples were incubated with ~1 mg/mL of different microplastics in a buffer (200 mM NaCl, 20 mM HEPES, pH 7.6). The incubation times were long enough to achieve adsorption equilibrium: 1 h for the linear DNA, 4 h for SNA, and 0.5 h for SNA adsorption on heated samples. The samples were gently agitated during the incubation to prevent the precipitation of the microplastics particles. The samples were then centrifuged (1000 rpm, 2 min). The fluorescence intensity (for linear DNA) and UV-vis absorbance (for SNA) of the supernatants were measured to back calculate the adsorbed DNA/SNA.

5.2.8 SNA Desorption

First, 2 nM SNA (~250 nM DNA) was almost thoroughly adsorbed onto ~1 mg/mL of the PET microplastics in a buffer (200 mM NaCl, 20 mM HEPES, pH 7.6) over 4 h. Then, 4 M urea and/or 0.4% Tween 80 were added and incubated with the pre-adsorbed SNA. The samples were gently

agitated during the incubation to prevent the precipitation of the microplastics particles. After 1 h, the samples were centrifuged (1000 rpm, 2 min), and the SNA desorption was quantified based on the enhancement of absorbance at 520 nm of the supernatant.

5.3 Results and Discussion

5.3.1 Microplastics Preparation and Characterization

Six commonly used plastics objects such as a plastic spoon and a water bottle were collected. Raman spectroscopy was used to identify them to be made of PE, PP, PS, PVC, composite of PS/PVC, and PET (Figure 5.1). We prepared the microplastics samples via mechanical shredding of the plastic items. The size and morphology of the microplastics were then observed using an optical microscope (Figure 5.2). While the samples had a broad size and shape distribution, they all fulfilled the size requirement of microplastics (<1 mm).[151]
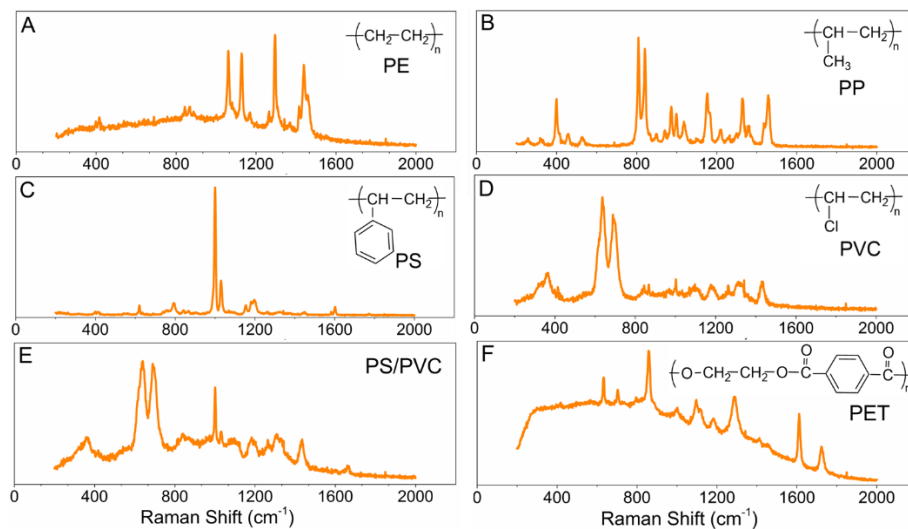
Figure 5.1 Raman spectra and molecular structures of the plastic materials used in this work including (A) PE, (B) PP, (C) PS, (D) PVC, (E) composite of PS/PVC, and (F) PET.

72
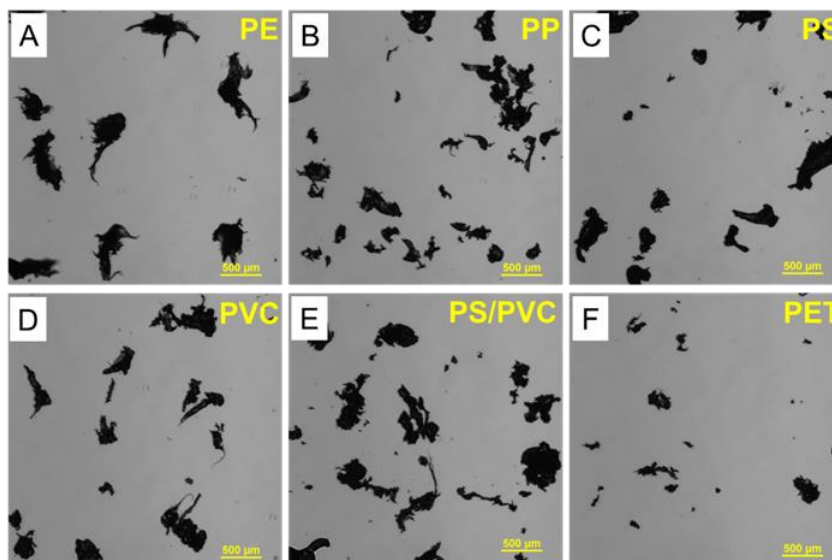
Figure 5.2 Micrographs of the microplastics acquired by shredding plastic materials composed of (A) PE, (B) PP, (C) PS, (D) PVC, (E) composite of PS/PVC, and (F) PET.

5.3.2 Soaked Microplastics More Efficiently Adsorbed SNA

The microplastics were freshly dispersed in water and compared with those soaked in water at room temperature for 3 months. First, adsorption of free oligonucleotides (called linear DNA) was studied in the presence of Na^+ as the most abundant metal ion in the environmental waters.[255] The linear DNA adsorption on the soaked microplastics was the same for the fresh and 3-month-soaked microplastics (Figure 5.3C). No adsorption was observed for PE, PP, PVC, or PS/PVC, while ~10% and ~65% of the DNA was adsorbed on PS and PET respectively. PS and PET have aromatic structures, which may stack with DNA bases to promote adsorption.

We then tested the adsorption of SNA consisting of the same DNA sequence with a 5'-SH label immobilized densely on a 13 nm AuNP core. On average, 125 DNA strands were attached to each AuNP, and the total DNA concentration was ~250 nM in this experiment. Since SNA enhances the overall interactions between DNA and materials via polyvalent binding,[50, 197] adsorption of SNA may provide better insights to the difference between the fresh and soaked microplastics. The absorbance at 520 nm of AuNPs in the supernatants was used to quantify the SNA adsorption (Figure 5.3A, B). Interestingly, SNA adsorption was remarkably enhanced on the soaked microplastics in all the cases (Figure 5.3B, D). In the presence of 200 mM NaCl, SNA adsorption increased on the soaked PE (36%), PP (70%), PS (50%), PVC (37%), and PS/PVC (52%) compared to the fresh microplastics

(Figure 5.3B, D). The SNA adsorption capacity on PET remained unchanged since the fresh PET microplastics already adsorbed ~90% SNA.
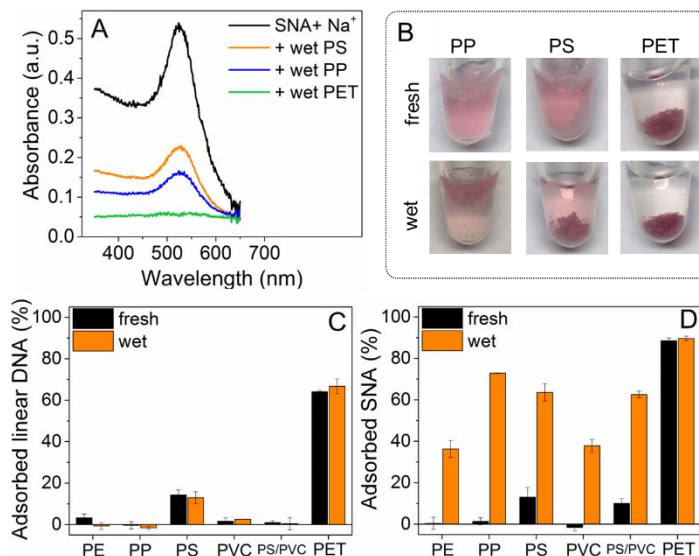
Figure 5.3 (A) UV–vis spectra of the supernatants and (B) photographs illustrating the adsorption of 2 nM SNA (total of 250 nM DNA) on freshly prepared and 3-month-soaked microplastics. The adsorbed SNA was quantified according to the decrease of the absorbance. Adsorption of (C) 10 nM FAM-DNA, and (D) 2 nM SNA onto 1 mg/mL of different fresh and soaked microplastics in the presence of 200 mM NaCl.

5.3.3 The Origin of Change

Among the six tested microplastics, PP showed the most dramatic change upon soaking in water (Figure 5.3D). Therefore, it was chosen for investigating the reason of the enhanced SNA adsorption. We first dried the PP microplastics that were soaked for 3 months, and then redispersed it in water right before the SNA adsorption experiment. Interestingly, the SNA adsorption efficiency of this dried sample was zero and similar to the fresh PP microplastics (Figure 5.4A, green and black curves). This observation suggested that the enhancement of SNA adsorption was reversible and likely due to physical processes at the microplastics surface instead of irreversible chemical transformations.

Due to its lower density than water, PP naturally floats at the surface of water. Figure 5.4B illustrates the floating behavior of 20 mg PP microplastics dispersed in 1 mL water. Fresh PP microplastics were located at the top of the water surface shying away from water, thereby the majority of them were barely floating. On the other hand, the 3-month-soaked microplastics nicely floated and partially

sank close to the surface of water suggesting an enhanced wettability. Drying and redispersing the microplastics decreased the wettability again similar to the fresh microplastics (Figure 5.4B).

Raman spectroscopy was used to investigate for any possible changes in functional groups in samples after soaking. Comparing the Raman spectra of the fresh and soaked PP samples, no apparent change was observed in the carbonyl (~1600-1800 cm^{-1}) and hydroxyl regions (~3400-3600 cm^{-1}) confirming that only physical changes occurred leading to the increased wettability (Figure 5.4C). Oxidation of microplastics can generate surface carbonyl and hydroxyl groups,[278] which can also enhance adsorption on microplastics.[162, 175, 261] Studies of oxidation of microplastics typically use a remarkably harsher artificial conditions such as heating time of 1-90 days and temperatures of 70-120°C.[279-280] For example, when PP microplastics were oxidized at 70°C in the presence of an oxidizing agent (K$_2$S$_2$O$_8$), after 5 days, the carbonyl peak started to appear in the IR signal.[281] Thus, it was not surprising that our fast and mild wetting conditions did not induce a change in the chemistry of the microplastics surface.

We also performed TGA analysis on the fresh and 3-month-soaked PP microplastics to investigate the water evaporation behavior. As shown in Figure 5.4D, water evaporated from the fresh PP samples with a sharper slope, and the temperature at which water fully evaporated was 90°C. In contrast, the soaked PP depleted water at 98°C. Therefore, the soaked microplastics showed a higher resistance to water evaporation, which could be attributable to the presence of more surface areas with stronger affinity to interaction with water (e.g. water trapped in pores). After ruling out chemical changes, we reasoned that a portion of water was able to access pores with smaller features and those water molecules are more difficult to evaporate due to a higher Laplace pressure.

Therefore, the data in Figure 5.4 suggested that the enhancement of SNA adsorption on the soaked microplastics was reversible and due to an increase in the microplastics wettability. We reason that when they are freshly dispersed in water, air is trapped at their micro- and nanopores at the surface making it resistant to wetting and disallowing SNA to come close to the surface. Over time, these micro- and nanobubbles would break leading to wetting of the surfaces with nanoscale features to facilitate the adsorption of SNA with a larger contact area. The adsorption of normal linear DNA is too weak for plastics like PP and wetting to increase the contact surface area could not help the adsorption of linear DNA.
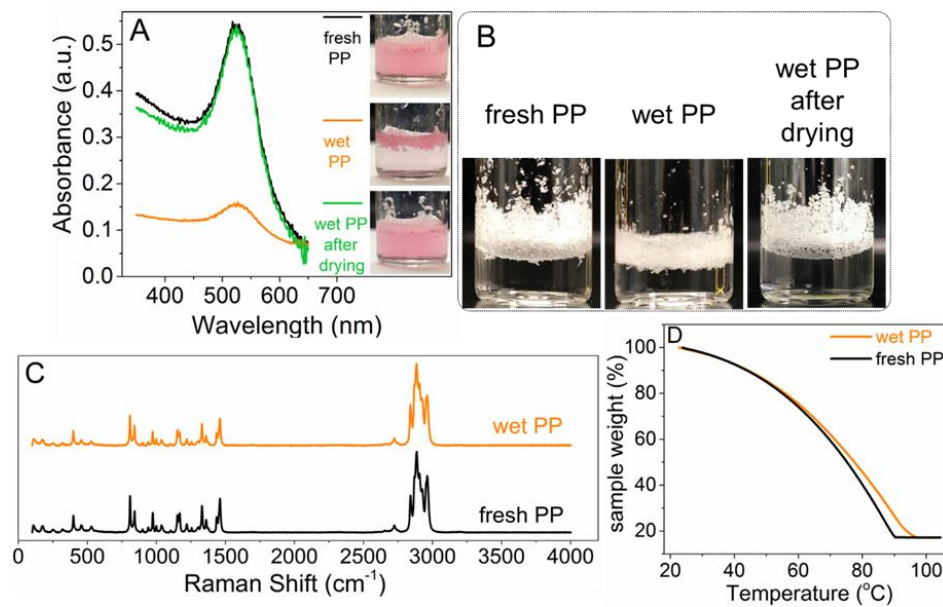
Figure 5.4 (A) UV–vis spectra of the supernatants and photographs illustrating the adsorption of 2 nM SNA (total of 250 nM DNA) on the freshly prepared PP, wettable PP, and wettable PP after drying and redispersing in water. (B) Photographs illustrating the floating behavior of the freshly prepared PP, wettable PP, and wettable PP after drying and redispersing in water. The wettable PP microplastics showed a more hydrophilic behavior which correlated with its higher SNA adsorption efficiency. (C) The identical Raman spectra of the freshly prepared PP and soaked PP suggesting a lack of measurable chemical changes. (D) TGA of 5 mg of the PP microplastics containing 25 μL of water (total of 30 mg sample). Upon heating, the water portion was evaporated resulting in a mass loss and dry PP samples were acquired in the end.

5.3.4 Closer Investigation of the Wet PET

Since the SNA adsorption capacity on the fresh and soaked PET was the same (Figure 5.3D), we further tested the kinetics of SNA adsorption on PET. The kinetic data fitted well with the pseudo-second-order (PSO) adsorption kinetics model with correlation coefficients (R^2) of greater than 0.98 for both fresh and soaked PET (Figure 5.5A). The SNA adsorption on microplastics was described by the PSO model, since the SNA (the adsorbate) concentration was relatively low in this experiment and decreased dramatically during the adsorption.[202] As shown in Figure 5.5A, the adsorption approached to a plateau for both microplastics after 2 h, and it reached to a saturation of ~90% after 4 h. This data agreed with the observation in Figure 5.3D. However, based on the kinetic traces, the half-saturation time ($t_{1/2}$) was 45 min and 11 min for fresh and soaked PET, respectively. Therefore, for PET, the effect of wetting was apparent in its faster adsorption kinetics.

76

Urea (4 M) was used as a hydrogen bonding disrupter to induce the desorption. Zero to negligible desorption occurred from either of the fresh and wet microplastics (Figure 5.5B). It appeared that the strong polyvalent interaction of SNA with both microplastics provided the same adsorption stability against urea. Further, a surfactant (0.4% Tween 80) was separately added to the pre-adsorbed SNA. Surfactants may use their hydrophobic tail and van der Waals (VDW) force to adsorb onto the microplastics and displace the SNA. Interestingly, 76% and 40% of the SNA desorbed from fresh and the soaked PET, respectively (Figure 3B). This data revealed a range of adsorption affinities for SNA, and more SNA were adsorbed with a higher affinity onto the soaked PET than the fresh PET. Moreover, hydrophobic interactions were likely significant for the adsorption on PET. We then added urea and Tween 80 together to reinforce the effect of competing and disrupting agents. SNA was thoroughly desorbed from the fresh PET, while 63% desorption occurred from the soaked PET (Figure 5.5B), confirming a portion of strongly adsorbed SNA on the soaked PET.
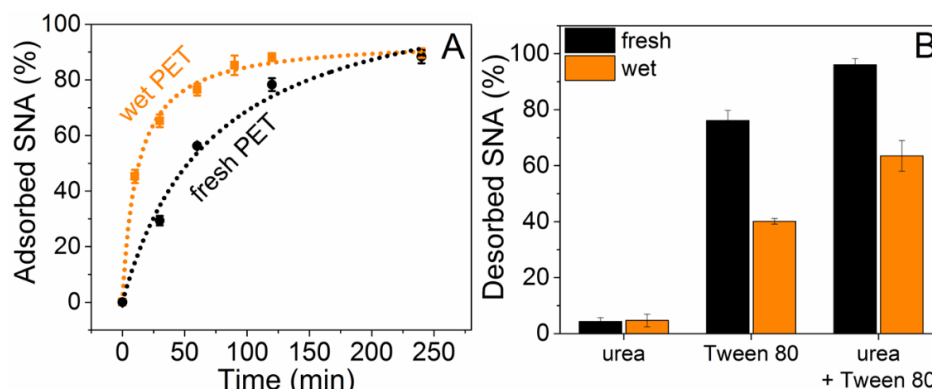
Figure 5.5 (A) Kinetics of adsorption of 2 nM SNA on the freshly prepared PET and wettable PET in the presence of 200 mM Na^+. (B) The desorption of SNA from the freshly prepared PET and wettable PET induced by 4 M urea, 0.4% Tween 80, or 4 M urea plus 0.4% Tween 80.

5.3.5 Effect of Heating on SNA Adsorption

Heating is one of the dominant processes in the environment,[267] and we then tested the SNA adsorption on PP microplastics that were heated at various temperatures (37, 50, 60, 70, and 85°C) for 0.5 h. The PP samples heated at 37 and 50°C adsorbed SNA slightly more than the fresh PP (Figure 5.6A). When the heating temperature was increased to 60°C and 70°C, the adsorption enhancement was more noticeable and ~25% of the SNA were adsorbed onto the PP microplastics. Eventually, heating the PP microplastics at 85°C remarkably increased its SNA adsorption efficiency to 80%

(Figure 5.6A). The floating behavior of PP microplastics after heating at different temperatures confirmed that their wettability correlated to the SNA adsorption enhancement (Figure 5.6B).

We then heated the PP microplastics at 85°C for different durations. In the presence of 200 mM NaCl, adsorption efficiency of 0.5 h and 3 h heated PP was 80% and 96%, respectively (Figure 5.6A). This suggested that heating at higher temperatures or for longer times can enhance the SNA adsorption efficiency. Figure 5.6C is a TEM image of SNAs adsorbed onto the edge of a PP microplastic particle that were heated at 85°C. The AuNPs were not evenly distributed but seem to be concentrated in a few regions, which could be the regions with more roughness and small porosity.

To investigate the origin of change of these heated samples, we performed Raman spectroscopy on the most harshly-heated PP sample (at 85°C for 3h). The oxygen related regions were still unchanged compared to the fresh PP microplastics (Figure 5.6D). Therefore, similar to the 3-months-soaked PP microplastics, these heated samples also did not change chemically. Heating only accelerated the wetting of the surface compared to that at room temperature.
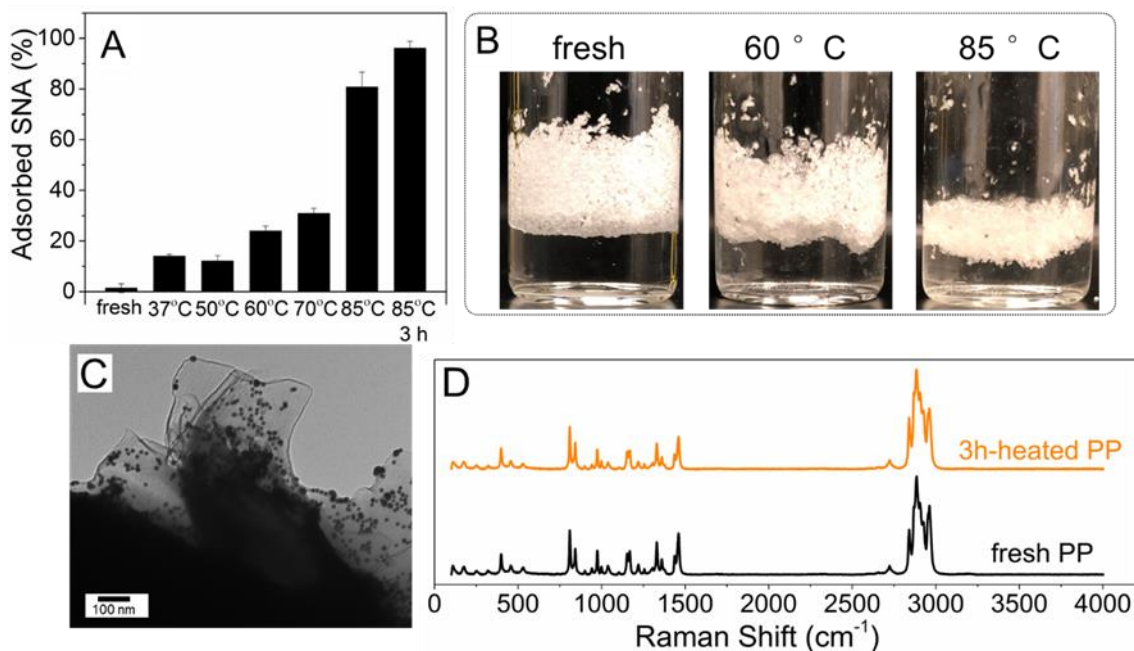
Figure 5.6 (A) Adsorption 2 nM SNA in the presence of 200 mM Na$^+$ on the freshly prepared PP and the wettable PP prepared by heating at various temperatures for 0.5 h. (B) Photographs illustrating the floating behavior of the freshly prepared PP, and wettable PP prepared by heating at two different temperatures for 0.5 h. The wettable PP microplastics at higher temperatures showed a more hydrophilic behavior which correlated

with their higher SNA adsorption efficiency. (C) A TEM micrograph depicting the SNA adsorbed onto a wettable PP microplastic prepared by heating at 85 °C for 0.5h. (D) Raman spectra of the freshly prepared PP and the 3h-heated PP which were identical suggesting that no chemical change (e.g. oxidation) occurred upon the heating of PP microplastics.

5.3.6 Mechanism of SNA adsorption on Wettable Microplastics

Based on the above results, we reason that microplastics have areas with more roughness with nanoscale porosity comparable with the size of SNAs. These surface pores can provide more contact with SNA, but they easily entrap air (Figure 5.7A). Therefore, for fresh microplastics, SNA contact with the surface is zero or minimal leading to no adsorption (e.g. PP) or a loose adsorption (e.g. PET). Soaking allows wetting of rough surfaces and SNA can efficiently contact such nanoscale pores (Figure 5.7B), resulting in a higher adsorption capacity (e.g. PP) and a tighter adsorption via polyvalent binding (e.g. PET).

The feature of roughness is still too large for a linear DNA and that is why soaking cannot enhance the adsorption of linear DNA (Figure 5.7C, D). Such an understanding can also be potentially applicable to the adsorption of other nanoscale objects and biological agents.
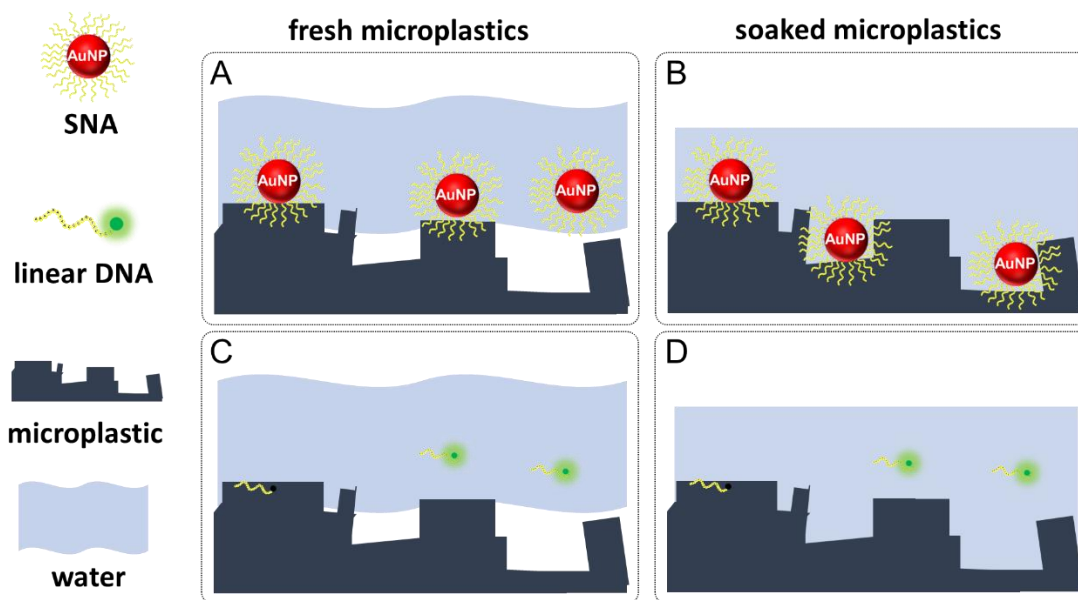
Figure 5.7. Schemes illustrating the difference between the SNA/linear DNA adsorption mechanism onto (A/C) fresh microplastics, and (B/D) wettable microplastics. Soaking enhances the access of SNA to more surface

nanoscale pores thereby enhancing both capacity and affinity of adsorption, whereas the roughness features are too large for linear DNA and soaking does not affect its adsorption.

5.4 Conclusions

When dispersed in water, microplastics continuously go through chemical and/or physical transformations. While harsh conditions are necessary to induce chemical transformations such as oxidation, physical changes may occur at milder conditions. Herein, we observed that the interaction of microplastics with SNA was highly influenced when microplastics were soaked in water at room temperature for 3 months or when they were heated on a scale of a few hours. When these microplastics were dried, they behaved similar to the fresh microplastics for SNA adsorption suggesting a reversible physical change, which was also supported using Raman spectroscopy. Based on the better retention of water on the long-term-soaked microplastics, the effect of soaking was likely related to the access of nanoscale porosity. It was concluded that the surface of the soaked microplastics had more of their porosity wetted by water, allowing SNA to access those nanoscale features to establish stronger adsorption due to increased contact areas. Based on the observations in this work, different adsorption studies should more carefully take into account the time- or temperature-dependent change of microplastics.

.

Chapter 6
Conclusions and Future Work

6.1 Conclusions

Interfacing DNA with nanomaterials has been useful in many biomedical applications including biosensing. In this thesis, I aimed to study the metal-mediated adsorption of DNA on two important polymeric materials: PDA and microplastics. On one hand, I aimed to solve some shortcomings of the previous work on PDA-DNA conjugates to develop the current methods for DNA extraction and sensing. On the other hand, I explored the fundamentals of DNA adsorption on microplastics to provide useful insights for the potential future research in the field of microplastics detection.

In Chapter 2, I involved polyvalent metal ions during the synthesis of PDA to produce metal-doped PDA NPs. The metal-doped PDA NPs showed a higher DNA adsorption capacity as well as a tighter DNA binding compared to the previously common strategy of using metal-adsorbed PDA NPs. The metal-doped PDA NPs showed a higher selectivity for detection of target DNA compared to metal-adsorbed PDA NPs. They also showed a remarkable DNA extraction efficiency in serum and were highly resistant to nonspecific protein and phosphate displacement. Therefore, metal-doped PDA NPs were found to be promising for sensing in real biological samples.

In Chapter 3, I first did some fundamental investigation to compare SNA adsorption versus linear DNA adsorption on PDA NPs. I showed that the metal ions have a cooperative effect on promotion of SNA adsorption. Moreover, the SNA adsorption showed an extraordinary stability comparable to covalent attachment. Therefore, I designed a hybrid material to be used for extraction and detection of DNA. This consisted of a Fe_3O_4 core (to provide magnetic separation), a PDA shell (to achieve specific DNA extraction) and a SNA decoration (to achieve efficient hybridization of target DNA). Using this conjugate, highly robust and selective extraction and detection of DNA was achieved.

In Chapter 4, I conducted a systematic study to fundamentally investigate the metal-mediated adsorption of linear DNA and SNA on microplastics. The effect of the most abundant metal ions Na^+, Mg^{2+}, and Ca^{2+} was studied for DNA adsorption onto the most common microplastics materials including PE, PP, PVC, PS, and PET. Among the microplastics, PET and PS showed the highest DNA adsorption efficiency likely due to the interactions provided by their aromatic rings. I also

performed desorption studies, and metal-mediated interactions and hydrogen bonding were found to be crucial for DNA adsorption on microplastics.

Finally, in Chapter 5, I utilized DNA to study "wetting", an important property of microplastics which can highly affect its adsorption behavior. It was observed that water-soaked microplastics can adsorb SNA more efficiently while no change was noticeable for adsorption of linear DNA. Raman spectroscopy analysis suggested that no chemical change occurred to the microplastics upon soaking in water. This and the irreversible nature of the change suggested that the soaked microplastics can adsorb SNA more efficiently due to the better wettability of surface roughness features which was also observable in floating behavior of the microplastics. Therefore, I proposed SNA adsorption as a simple method for studying and quantification of the wettability of microplastics.

6.2 Original Contributions

Based on the above work, the original contributions I have made can be summarized as follows:

1. Metal-doped PDA NPs adsorb DNA more tightly which can improve the selectivity and robustness of the PDA-DNA sensors.

2. PDA-SNA conjugates can be used for DNA extraction and detection with extraordinary selectivity, since PDA has zero non-specific adsorption of DNA in the presence of Na^+.

3. PET and PS microplastics can nonspecifically adsorb DNA oligonucleotides, and metal-mediated interactions and hydrogen bonding are vital for such adsorption.

4. SNA adsorption enhances on more wettable microplastics. Therefore, SNA can be used to probe the wettability of microplastics.

6.3 Future Work

This thesis has provided some new insights about DNA adsorption on PDA and have presented PDA-DNA biosensors with a higher selectivity and robustness. Moreover, it has answered some fundamental questions about interfacing DNA and microplastics. Following, some potential future work ideas are proposed.

With regard to metal-doped PDA NPs, some applications were shown in the past such as in magnetic resonance imaging (MRI) and thermochemotherapy (TCT).[77-78] In this thesis, we applied them for designing DNA biosensors. Yet, the excellent metal-coordination property of PDA and the

82

wide range of functionality of metal ions envision a higher research potential on these NPs. For instance, very recently, Fe-doped PDA NPs have been used to provide catalytic peroxidase-like activity.[282]

In addition, in this thesis we only proved the remarkable stability and selectivity of PDA-SNA conjugate in buffers and serum. Therefore, such conjugate has the potential be used in different biomedical applications in order to achieve an efficient DNA delivery into cells or *in-vivo*.

With regard to microplastics, we presented a very fundamental study in this thesis and many future directions need to be explored. The nonspecific DNA adsorption efficiency of microplastics can be very insightful prior to selection of DNA aptamers for microplastics. Since PET and PS showed non-specific adsorption under the mentioned buffer conditions, aptamer selection is likely to be challenging for these microplastics. On the other hand, PE, PP and PVC had minimal interactions with ssDNA, therefore there is a higher potential to select aptamers for them.

Finally, the microplastics wetting conditions used in this thesis were rather mild, but it showed a remarkable effect on SNA adsorption. Therefore, future adsorption studies on microplastics need to account for time-dependent change of microplastics in water more carefully.

Letters of Copyright Permission

For article used in Chapter 1

For article used in Chapter 2

For the first article used in Chapter 3

For the second article used in Chapter 3

For article used in Chapter 4

Adsorption of Linear and Spherical DNA Oligonucleotides onto Microplastics

ACS Publications
Most Trusted. Most Cited. Most Read.

Author: Mohamad Zandieh, Kshiti Patel, Juewen Liu

Publication: Langmuir

Publisher: American Chemical Society

Date: Feb 1, 2022

Copyright © 2022, American Chemical Society

References

1.   Jones, M. R.; Seeman, N. C.; Mirkin, C. A., Programmable Materials and the Nature of the DNA Bond. *Science* **2015,** *347* (6224).

2.   Zhou, W.; Saran, R.; Liu, J., Metal Sensing by DNA. *Chemical Reviews* **2017,** *117* (12), 8272-8325.

3.   Li, L.; Xing, H.; Zhang, J.; Lu, Y., Functional DNA Molecules Enable Selective and Stimuli-Responsive Nanoparticles for Biomedical Applications. *Accounts of Chemical Research* **2019,** *52* (9), 2415-2426.

4.   Hu, Q.; Li, H.; Wang, L.; Gu, H.; Fan, C., DNA Nanotechnology-Enabled Drug Delivery Systems. *Chemical Reviews* **2018,** *119* (10), 6459-6506.

5.   Kahn, J. S.; Hu, Y.; Willner, I., Stimuli-Responsive DNA-Based Hydrogels: From Basic Principles to Applications. *Accounts of Chemical Research* **2017,** *50* (4), 680-690.

6.   Qing, Z.; Xu, J.; Hu, J.; Zheng, J.; He, L.; Zou, Z.; Yang, S.; Tan, W.; Yang, R., In Situ Amplification-Based Imaging of Rna in Living Cells. *Angewandte Chemie* **2019,** *131* (34), 11698-11709.

7.   Dunn, M. R.; Jimenez, R. M.; Chaput, J. C., Analysis of Aptamer Discovery and Technology. *Nature Reviews Chemistry* **2017,** *1* (10), 1-16.

8.   Lake, R. J.; Yang, Z.; Zhang, J.; Lu, Y., Dnazymes as Activity-Based Sensors for Metal Ions: Recent Applications, Demonstrated Advantages, Current Challenges, and Future Directions. *Accounts of Chemical Research* **2019,** *52* (12), 3275-3286.

9.   Dey, S.; Fan, C.; Gothelf, K. V.; Li, J.; Lin, C.; Liu, L.; Liu, N.; Nijenhuis, M. A.; Saccà, B.; Simmel, F. C., DNA Origami. *Nature Reviews Methods Primers* **2021,** *1* (1), 1-24.

10.   Rothemund, P. W., Folding DNA to Create Nanoscale Shapes and Patterns. *Nature* **2006,** *440* (7082), 297-302.

11.   Kool, E. T., Hydrogen Bonding, Base Stacking, and Steric Effects in DNA Replication. *Annual review of biophysics and biomolecular structure* **2001,** *30* (1), 1-22.

12.   Agboola, O.; Achile, F.; Fayomi, S. O.; Sanni, S. E.; Abatan, O.; Sadiku, E. R.; Popoola, P.; Mubiayi, M. P.; Akinlabi, E. T.; Makhatha, M. E.; Adedoyin, T.; Ekere, I., Adsorptive Performance Mechanism of the DNA of Calf Thymus Gland (CTGDNA) on 3CR12 Stainless Steel as Corrosion Inhibitor in Acidic Medium. *Journal of Bio- and Tribo-Corrosion* **2019,** *5* (3), 52.

13.   Sun, H.; Zhu, X.; Lu, P. Y.; Rosato, R. R.; Tan, W.; Zu, Y., Oligonucleotide Aptamers: New Tools for Targeted Cancer Therapy. *Molecular Therapy - Nucleic Acids* **2014,** *3*, e182.

14.   Bock, L. C.; Griffin, L. C.; Latham, J. A.; Vermaas, E. H.; Toole, J. J., Selection of Single-Stranded DNA Molecules That Bind and Inhibit Human Thrombin. *Nature* **1992,** *355* (6360), 564-566.

15.   Famulok, M.; Hartig, J. S.; Mayer, G., Functional Aptamers and Aptazymes in Biotechnology, Diagnostics, and Therapy. *Chemical Reviews* **2007,** *107* (9), 3715-3743.

16.   Yu, H.; Alkhamis, O.; Canoura, J.; Liu, Y.; Xiao, Y., Advances and Challenges in Small-Molecule DNA Aptamer Isolation, Characterization, and Sensor Development. *Angewandte Chemie International Edition* **2021,** *60* (31), 16800-16823.

17.   Sefah, K.; Shangguan, D.; Xiong, X.; O'donoghue, M. B.; Tan, W., Development of DNA Aptamers Using Cell-Selex. *Nature Protocols* **2010,** *5* (6), 1169-1185.

18.   Liu, J.; Cao, Z.; Lu, Y., Functional Nucleic Acid Sensors. *Chemical Reviews* **2009,** *109* (5), 1948-1998.

19.   Kruger, K.; Grabowski, P. J.; Zaug, A. J.; Sands, J.; Gottschling, D. E.; Cech, T. R., Self-Splicing Rna: Autoexcision and Autocyclization of the Ribosomal RNA Intervening Sequence of Tetrahymena. *cell* **1982,** *31* (1), 147-157.

20.   Breaker, R. R.; Joyce, G. F., A DNA Enzyme That Cleaves RNA. *Chemistry & Biology* **1994,** *1* (4), 223-229.

21.   Lu, Y.; Liu, J., Functional DNA Nanotechnology: Emerging Applications of Dnazymes and Aptamers. *Current Opinion in Biotechnology* **2006,** *17* (6), 580-588.

22.   Saccà, B.; Niemeyer, C. M., DNA Origami: The Art of Folding DNA. *Angewandte Chemie International Edition* **2012,** *51* (1), 58-66.

23.   Li, M.; Wang, C.; Di, Z.; Li, H.; Zhang, J.; Xue, W.; Zhao, M.; Zhang, K.; Zhao, Y.; Li, L., Engineering Multifunctional DNA Hybrid Nanospheres through Coordination-Driven Self-Assembly. *Angewandte Chemie International Edition* **2019,** *58* (5), 1350-1354.

24.   Sigel, H., Interactions of Metal Ions with Nucleotides and Nucleic Acids and Their Constituents. *Chemical Society Reviews* **1993,** *22* (4), 255-267.

25.   Navarro, J. A.; Lippert, B., Molecular Architecture with Metal Ions, Nucleobases and Other Heterocycles. *Coordination Chemistry Reviews* **1999,** *185*, 653-667.

26.   Sigel, R. K.; Sigel, H., A Stability Concept for Metal Ion Coordination to Single-Stranded Nucleic Acids and Affinities of Individual Sites. *Accounts of Chemical Research* **2010,** *43* (7), 974-984.

27.   Verma, S.; Mishra, A. K.; Kumar, J., The Many Facets of Adenine: Coordination, Crystal Patterns, and Catalysis. *Accounts of Chemical Research* **2010,** *43* (1), 79-91.

28.   Turel, I.; Kljun, J., Interactions of Metal Ions with DNA, Its Constituents and Derivatives, Which May Be Relevant for Anticancer Research. *Current Topics in Medicinal Chemistry* **2011,** *11* (21), 2661-2687.

29.   Zhou, Y.; Tang, L.; Zeng, G.; Zhang, C.; Zhang, Y.; Xie, X., Current Progress in Biosensors for Heavy Metal Ions Based on DNAzymes/DNA Molecules Functionalized Nanostructures: A Review. *Sensors and Actuators B: Chemical* **2016,** *223*, 280-294.

30.   Lu, C.; Xu, Y.; Huang, P.-J. J.; Zandieh, M.; Wang, Y.; Zheng, J.; Liu, J., Protection of DNA by Metal Ions at 95 °C: From Lower Critical Solution Temperature (LCST) Behavior to Coordination-Driven Self-Assembly. *Nanoscale* **2022**.

31.   Wu, M.; Kempaiah, R.; Huang, P.-J. J.; Maheshwari, V.; Liu, J., Adsorption and Desorption of DNA on Graphene Oxide Studied by Fluorescently Labeled Oligonucleotides. *Langmuir* **2011,** *27* (6), 2731-2738.

32.   Meng, Y.; Liu, P.; Zhou, W.; Ding, J.; Liu, J., Bioorthogonal DNA Adsorption on Polydopamine Nanoparticles Mediated by Metal Coordination for Highly Robust Sensing in Serum and Living Cells. *ACS Nano* **2018,** *12* (9), 9070-9080.

33.   Lu, C.; Liu, Y.; Ying, Y.; Liu, J., Comparison of MoS_2, WS_2, and Graphene Oxide for DNA Adsorption and Sensing. *Langmuir* **2017,** *33* (2), 630-637.

34.   Kushalkar, M. P.; Liu, B.; Liu, J., Promoting DNA Adsorption by Acids and Polyvalent Cations: Beyond Charge Screening. *Langmuir* **2020,** *36* (38), 11183-11195.

35.   Hurst, S. J.; Lytton-Jean, A. K.; Mirkin, C. A., Maximizing DNA Loading on a Range of Gold Nanoparticle Sizes. *Analytical chemistry* **2006,** *78* (24), 8313-8318.

36.   Li, H.; Rothberg, L., Colorimetric Detection of DNA Sequences Based on Electrostatic Interactions with Unmodified Gold Nanoparticles. *Proceedings of the National Academy of Sciences* **2004,** *101* (39), 14036-14039.

37.   Seferos, D. S.; Giljohann, D. A.; Hill, H. D.; Prigodich, A. E.; Mirkin, C. A., Nano-Flares: Probes for Transfection and MRNA Detection in Living Cells. *Journal of the American Chemical Society* **2007,** *129* (50), 15477-15479.

38.   Giljohann, D. A.; Seferos, D. S.; Patel, P. C.; Millstone, J. E.; Rosi, N. L.; Mirkin, C. A., Oligonucleotide Loading Determines Cellular Uptake of DNA-Modified Gold Nanoparticles. *Nano Letters* **2007,** *7* (12), 3818-3821.

39.   Jin, R.; Wu, G.; Li, Z.; Mirkin, C. A.; Schatz, G. C., What Controls the Melting Properties of DNA-Linked Gold Nanoparticle Assemblies? *Journal of the American Chemical Society* **2003,** *125* (6), 1643-1654.

40.   Lytton-Jean, A. K.; Mirkin, C. A., A Thermodynamic Investigation into the Binding Properties of DNA Functionalized Gold Nanoparticle Probes and Molecular Fluorophore Probes. *Journal of the American Chemical Society* **2005,** *127* (37), 12754-12755.

41.   Jones, M. R.; Macfarlane, R. J.; Lee, B.; Zhang, J.; Young, K. L.; Senesi, A. J.; Mirkin, C. A., DNA-Nanoparticle Superlattices Formed from Anisotropic Building Blocks. *Nature materials* **2010,** *9* (11), 913-917.

42.   Storhoff, J. J.; Elghanian, R.; Mucic, R. C.; Mirkin, C. A.; Letsinger, R. L., One-Pot Colorimetric Differentiation of Polynucleotides with Single Base Imperfections Using Gold Nanoparticle Probes. *Journal of the American Chemical Society* **1998,** *120* (9), 1959-1964.

43.   Zhang, X.; Servos, M. R.; Liu, J., Instantaneous and Quantitative Functionalization of Gold Nanoparticles with Thiolated DNA Using a pH-Assisted and Surfactant-Free Route. *Journal of the American Chemical Society* **2012,** *134* (17), 7266-7269.

44.   Liu, B.; Liu, J., Freezing Directed Construction of Bio/Nano Interfaces: Reagentless Conjugation, Denser Spherical Nucleic Acids, and Better Nanoflares. *Journal of the American Chemical Society* **2017,** *139* (28), 9471-9474.

45.   Hao, Y.; Li, Y.; Song, L.; Deng, Z., Flash Synthesis of Spherical Nucleic Acids with Record DNA Density. *Journal of the American Chemical Society* **2021**.

46.   Huang, M.; Xiong, E.; Wang, Y.; Hu, M.; Yue, H.; Tian, T.; Zhu, D.; Liu, H.; Zhou, X., Fast Microwave Heating-Based One-Step Synthesis of DNA and Rna Modified Gold Nanoparticles. *Nature Communications* **2022,** *13* (1), 1-14.

47.   Ye, Y.; Hao, Y.; Ye, M.; Song, X.; Deng, Z., Evaporative Drying: A General and Readily Scalable Route to Spherical Nucleic Acids with Quantitative, Fully Tunable, and Record-High DNA Loading. *Small* **2022**, 2202458.

48.   Liu, B.; Liu, J., Interface-Driven Hybrid Materials Based on DNA-Functionalized Gold Nanoparticles. *Matter* **2019,** *1* (4), 825-847.

49.   Liu, B.; Liu, J., Methods for Preparing DNA-Functionalized Gold Nanoparticles, a Key Reagent of Bioanalytical Chemistry. *Analytical Methods* **2017,** *9* (18), 2633-2643.

50.   Liu, B.; Huang, Z.; Liu, J., Polyvalent Spherical Nucleic Acids for Universal Display of Functional DNA with Ultrahigh Stability. *Angewandte Chemie* **2018,** *130* (30), 9583-9586.

51.   Saha, K.; Agasti, S. S.; Kim, C.; Li, X.; Rotello, V. M., Gold Nanoparticles in Chemical and Biological Sensing. *Chemical Reviews* **2012,** *112* (5), 2739-2779.

52.   Yu, W.; Sisi, L.; Haiyan, Y.; Jie, L., Progress in the Functional Modification of Graphene/Graphene Oxide: A Review. *RSC Advances* **2020,** *10* (26), 15328-15345.

53.   Lin, H.; Chen, Y.; Shi, J., Insights into 2D MXenes for Versatile Biomedical Applications: Current Advances and Challenges Ahead. *Advanced Science* **2018,** *5* (10), 1800518.

54.   Liu, J., Adsorption of DNA onto Gold Nanoparticles and Graphene Oxide: Surface Science and Applications. *Physical Chemistry Chemical Physics* **2012,** *14* (30), 10485-10496.

55.   Yang, T.; Luo, Z.; Tian, Y.; Qian, C.; Duan, Y., Design Strategies of AuNPs-Based Nucleic Acid Colorimetric Biosensors. *TrAC Trends in Analytical Chemistry* **2020,** *124*, 115795.

56.   Liu, J.; Li, Y.; Li, Y.; Li, J.; Deng, Z., Noncovalent DNA Decorations of Graphene Oxide and Reduced Graphene Oxide toward Water-Soluble Metal–Carbon Hybrid Nanostructures Via Self-Assembly. *Journal of Materials Chemistry* **2010,** *20* (5), 900-906.

57.   Liu, B.; Liu, J., DNA Adsorption by Magnetic Iron Oxide Nanoparticles and Its Application for Arsenate Detection. *Chemical Communications* **2014,** *50* (62), 8568-8570.

58.   Lee, H.; Dellatore, S. M.; Miller, W. M.; Messersmith, P. B., Mussel-Inspired Surface Chemistry for Multifunctional Coatings. *Science* **2007,** *318* (5849), 426-430.

59.   Jastrzebska, M. M.; Isotalo, H.; Paloheimo, J.; Stubb, H., Electrical Conductivity of Synthetic Dopa-Melanin Polymer for Different Hydration States and Temperatures. *Journal of Biomaterials Science, Polymer Edition* **1996,** *7* (7), 577-586.

60.   Wang, X.; Sheng, J.; Yang, M., Melanin-Based Nanoparticles in Biomedical Applications: From Molecular Imaging to Treatment of Diseases. *Chinese Chemical Letters* **2019,** *30* (3), 533-540.

61.   Liebscher, J. r.; Mrówczyński, R.; Scheidt, H. A.; Filip, C.; Hădade, N. D.; Turcu, R.; Bende, A.; Beck, S., Structure of Polydopamine: A Never-Ending Story? *Langmuir* **2013,** *29* (33), 10539-10548.

62.   Faure, E.; Falentin-Daudré, C.; Jérôme, C.; Lyskawa, J.; Fournier, D.; Woisel, P.; Detrembleur, C., Catechols as Versatile Platforms in Polymer Chemistry. *Progress in Polymer Science* **2013,** *38* (1), 236-270.

63.   Dreyer, D. R.; Miller, D. J.; Freeman, B. D.; Paul, D. R.; Bielawski, C. W., Elucidating the Structure of Poly (Dopamine). *Langmuir* **2012,** *28* (15), 6428-6435.

64.   Liebscher, J., Chemistry of Polydopamine–Scope, Variation, and Limitation. *European Journal of Organic Chemistry* **2019,** *2019* (31-32), 4976-4994.

65.   Klosterman, L.; Bettinger, C. J., Calcium-Mediated Control of Polydopamine Film Oxidation and Iron Chelation. *International journal of molecular sciences* **2017,** *18* (1), 14.

66.   Della Vecchia, N. F.; Avolio, R.; Alfè, M.; Errico, M. E.; Napolitano, A.; d'Ischia, M., Building-Block Diversity in Polydopamine Underpins a Multifunctional Eumelanin-Type Platform Tunable through a Quinone Control Point. *Advanced Functional Materials* **2013,** *23* (10), 1331-1340.

67.   Hong, L.; Simon, J. D., Current Understanding of the Binding Sites, Capacity, Affinity, and Biological Significance of Metals in Melanin. ACS Publications: 2007.

68.   Liu, Y.; Ai, K.; Liu, J.; Deng, M.; He, Y.; Lu, L., Dopamine-Melanin Colloidal Nanospheres: An Efficient near-Infrared Photothermal Therapeutic Agent for in vivo Cancer Therapy. *Advanced Materials* **2013,** *25* (9), 1353-1359.

69.   Ju, K.-Y.; Lee, Y.; Lee, S.; Park, S. B.; Lee, J.-K., Bioinspired Polymerization of Dopamine to Generate Melanin-Like Nanoparticles Having an Excellent Free-Radical-Scavenging Property. *Biomacromolecules* **2011,** *12* (3), 625-632.

70.   Wei, Q.; Zhang, F.; Li, J.; Li, B.; Zhao, C., Oxidant-Induced Dopamine Polymerization for Multifunctional Coatings. *Polymer Chemistry* **2010,** *1* (9), 1430-1433.

71.   Wang, Z.; Xu, C.; Lu, Y.; Wei, G.; Ye, G.; Sun, T.; Chen, J., Microplasma Electrochemistry Controlled Rapid Preparation of Fluorescent Polydopamine Nanoparticles and Their Application in Uranium Detection. *Chemical Engineering Journal* **2018,** *344*, 480-486.

72.   Bridelli, M. G., Self-Assembly of Melanin Studied by Laser Light Scattering. *Biophysical chemistry* **1998,** *73* (3), 227-239.

73.   Ponzio, F.; Ball, V., Persistence of Dopamine and Small Oxidation Products Thereof in Oxygenated Dopamine Solutions and in "Polydopamine" Films. *Colloids and Surfaces A: Physicochemical and Engineering Aspects* **2014,** *443*, 540-543.

74.   Li, Y.; Xie, Y.; Wang, Z.; Zang, N.; Carniato, F.; Huang, Y.; Andolina, C. M.; Parent, L. R.; Ditri, T. B.; Walter, E. D., Structure and Function of Iron-Loaded Synthetic Melanin. *ACS Nano* **2016,** *10* (11), 10186-10194.

75.   Wang, Z.; Carniato, F.; Xie, Y.; Huang, Y.; Li, Y.; He, S.; Zang, N.; Rinehart, J. D.; Botta, M.; Gianneschi, N. C., High Relaxivity Gadolinium-Polydopamine Nanoparticles. *Small* **2017,** *13* (43), 1701830.

76.   Miao, Z.-H.; Wang, H.; Yang, H.; Li, Z.-L.; Zhen, L.; Xu, C.-Y., Intrinsically Mn^{2+}-Chelated Polydopamine Nanoparticles for Simultaneous Magnetic Resonance Imaging and Photothermal Ablation of Cancer Cells. *ACS Applied Materials & Interfaces* **2015,** *7* (31), 16946-16952.

77.   Wang, Z.; Xie, Y.; Li, Y.; Huang, Y.; Parent, L. R.; Ditri, T.; Zang, N.; Rinehart, J. D.; Gianneschi, N. C., Tunable, Metal-Loaded Polydopamine Nanoparticles Analyzed by Magnetometry. *Chemistry of Materials* **2017,** *29* (19), 8195-8201.

78.   Ge, R.; Lin, M.; Li, X.; Liu, S.; Wang, W.; Li, S.; Zhang, X.; Liu, Y.; Liu, L.; Shi, F., Cu^{2+}-Loaded Polydopamine Nanoparticles for Magnetic Resonance Imaging-Guided pH-and Near-Infrared-Light-Stimulated Thermochemotherapy. *ACS Applied Materials & Interfaces* **2017,** *9* (23), 19706-19716.

79.   Arzillo, M.; Mangiapia, G.; Pezzella, A.; Heenan, R. K.; Radulescu, A.; Paduano, L.; d'Ischia, M., Eumelanin Buildup on the Nanoscale: Aggregate Growth/Assembly and Visible Absorption Development in Biomimetic 5, 6-Dihydroxyindole Polymerization. *Biomacromolecules* **2012,** *13* (8), 2379-2390.

80.   Mateescu, M.; Metz-Boutigue, M.-H.; Bertani, P.; Ball, V., Polyelectrolytes to Produce Nanosized Polydopamine. *Journal of Colloid and Interface Science* **2016,** *469*, 184-190.

81.   Yu, X.; Fan, H.; Wang, L.; Jin, Z., Formation of Polydopamine Nanofibers with the Aid of Folic Acid. *Angewandte Chemie International Edition* **2014,** *53* (46), 12600-12604.

82.   Fan, H.; Yu, X.; Liu, Y.; Shi, Z.; Liu, H.; Nie, Z.; Wu, D.; Jin, Z., Folic Acid–Polydopamine Nanofibers Show Enhanced Ordered-Stacking Via Π–Π Interactions. *Soft Matter* **2015,** *11* (23), 4621-4629.

83.   Xuan, S.; Wang, Y.-X. J.; Yu, J. C.; Cham-Fai Leung, K., Tuning the Grain Size and Particle Size of Superparamagnetic Fe_3O_4 Microparticles. *Chemistry of Materials* **2009,** *21* (21), 5079-5087.

84.   Liu, Y.; Jin, H.; Zhu, S.; Liu, Y.; Long, M.; Zhou, Y.; Yan, D., A Facile Method for Fabricating TiO_2@ Mesoporous Carbon and Three-Layered Nanocomposites. *Nanotechnology* **2012,** *23* (32), 325602.

85.   Yoon, T. H.; Park, Y. J., Polydopamine-Assisted Carbon Nanotubes/Co_3O_4 Composites for Rechargeable Li-Air Batteries. *Journal of Power Sources* **2013,** *244*, 344-353.

86.   Zhang, M.; He, X.; Chen, L.; Zhang, Y., Preparation of IDA-Cu Functionalized Core–Satellite Fe_3O_4/Polydopamine/Au Magnetic Nanocomposites and Their Application for Depletion of Abundant Protein in Bovine Blood. *Journal of Materials Chemistry* **2010,** *20* (47), 10696-10704.

87.   Mrówczyński, R.; Turcu, R.; Leostean, C.; Scheidt, H. A.; Liebscher, J., New Versatile Polydopamine Coated Functionalized Magnetic Nanoparticles. *Materials Chemistry and Physics* **2013,** *138* (1), 295-302.

88.   Liu, M.; Jiang, W.; Chen, Q.; Wang, S.; Mao, Y.; Gong, X.; Cham-Fai Leung, K.; Tian, J.; Wang, H.; Xuan, S., A Facile One-Step Method to Synthesize SiO_2@Polydopamine Core–Shell Nanospheres for Shear Thickening Fluid. *RSC Advances* **2016,** *6* (35), 29279-29287.

89.   Wang, C.; Zhou, J.; Wang, P.; He, W.; Duan, H., Robust Nanoparticle–DNA Conjugates Based on Mussel-Inspired Polydopamine Coating for Cell Imaging and Tailored Self-Assembly. *Bioconjugate Chemistry* **2016,** *27* (3), 815-823.

90.   Choi, C. K. K.; Li, J.; Wei, K.; Xu, Y. J.; Ho, L. W. C.; Zhu, M.; To, K. K.; Choi, C. H. J.; Bian, L., A Gold@ Polydopamine Core–Shell Nanoprobe for Long-Term Intracellular Detection of Micrornas in Differentiating Stem Cells. *Journal of the American Chemical Society* **2015,** *137* (23), 7337-7346.

91.   Zhou, J.; Duan, B.; Fang, Z.; Song, J.; Wang, C.; Messersmith, P. B.; Duan, H., Interfacial Assembly of Mussel-Inspired Au@Ag@ Polydopamine Core–Shell Nanoparticles for Recyclable Nanocatalysts. *Advanced Materials* **2014,** *26* (5), 701-705.

92.   Ball, V., Polydopamine Nanomaterials: Recent Advances in Synthesis Methods and Applications. *Frontiers in Bioengineering and Biotechnology* **2018,** *6*, 109.

93.   Sun, D. T.; Peng, L.; Reeder, W. S.; Moosavi, S. M.; Tiana, D.; Britt, D. K.; Oveisi, E.; Queen, W. L., Rapid, Selective Heavy Metal Removal from Water by a Metal–Organic Framework/Polydopamine Composite. *ACS Central Science* **2018,** *4* (3), 349-356.

94.   Cao, N.; Lyu, Q.; Li, J.; Wang, Y.; Yang, B.; Szunerits, S.; Boukherroub, R., Facile Synthesis of Fluorinated Polydopamine/Chitosan/Reduced Graphene Oxide Composite Aerogel for Efficient Oil/Water Separation. *Chemical Engineering Journal* **2017,** *326*, 17-28.

95.   Zhang, L.; Wu, J.; Wang, Y.; Long, Y.; Zhao, N.; Xu, J., Combination of Bioinspiration: A General Route to Superhydrophobic Particles. *Journal of the American Chemical Society* **2012,** *134* (24), 9879-9881.

96.   Zhao, S.; Golestani, M.; Penesyan, A.; Deng, B.; Zheng, C.; Strezov, V., Antibiotic Enhanced Dopamine Polymerization for Engineering Antifouling and Antimicrobial Membranes. *Chinese Chemical Letters* **2020,** *31* (3), 851-854.

97.   Jiang, B.; He, Y.; Li, B.; Zhao, S.; Wang, S.; He, Y. B.; Lin, Z., Polymer-Templated Formation of Polydopamine-Coated SnO_2 Nanocrystals: Anodes for Cyclable Lithium-Ion Batteries. *Angewandte Chemie International Edition* **2017,** *56* (7), 1869-1872.

98.   Sun, T.; Li, Z. j.; Wang, H. g.; Bao, D.; Meng, F. l.; Zhang, X. b., A Biodegradable Polydopamine-Derived Electrode Material for High-Capacity and Long-Life Lithium-Ion and Sodium-Ion Batteries. *Angewandte Chemie International Edition* **2016,** *55* (36), 10662-10666.

99.   Mao, Z.; Han, Y.; Liu, S.; Zhang, X.; Zhang, P.; Lu, X.; Tong, Y., Lithium Ferrites@ Polydopamine Core–Shell Nanoparticles as a New Robust Negative Electrode for Advanced Asymmetric Supercapacitors. *Particle & Particle Systems Characterization* **2018,** *35* (7), 1800128.

100.   Duan, X.; Huang, Z.; Liu, C.; Yang, J.; Tan, L.; Chen, Y., A Bendable Nickel Oxide Interfacial Layer Via Polydopamine Crosslinking for Flexible Perovskite Solar Cells. *Chemical Communications* **2019,** *55* (25), 3666-3669.

101.   Zeng, T.; Niu, H.-y.; Ma, Y.-r.; Li, W.-h.; Cai, Y.-q., In Situ Growth of Gold Nanoparticles onto Polydopamine-Encapsulated Magnetic Microspheres for Catalytic Reduction of Nitrobenzene. *Applied Catalysis B: Environmental* **2013,** *134*, 26-33.

102.   Luo, J.; Zhang, N.; Liu, R.; Liu, X., In Situ Green Synthesis of Au Nanoparticles onto Polydopamine-Functionalized Graphene for Catalytic Reduction of Nitrophenol. *RSC Advances* **2014,** *4* (110), 64816-64824.

103.   Sureshkumar, M.; Siswanto, D. Y.; Lee, C.-K., Magnetic Antimicrobial Nanocomposite Based on Bacterial Cellulose and Silver Nanoparticles. *Journal of Materials Chemistry* **2010,** *20* (33), 6948-6955.

104.   Bian, S.-W.; Liu, S.; Chang, L., Synthesis of Magnetically Recyclable Fe_3O_4@ Polydopamine–Pt Composites and Their Application in Hydrogenation Reactions. *Journal of Materials Science* **2016,** *51* (7), 3643-3649.

105.   Li, H.; Xi, J.; Donaghue, A. G.; Keum, J.; Zhao, Y.; An, K.; McKenzie, E. R.; Ren, F., Synthesis and Catalytic Performance of Polydopamine Supported Metal Nanoparticles. *Scientific Reports* **2020,** *10* (1), 1-7.

106.   Xu, L. Q.; Yang, W. J.; Neoh, K.-G.; Kang, E.-T.; Fu, G. D., Dopamine-Induced Reduction and Functionalization of Graphene Oxide Nanosheets. *Macromolecules* **2010,** *43* (20), 8336-8339.

107.   Luo, F.; Wu, K.; Shi, J.; Du, X.; Li, X.; Yang, L.; Lu, M., Green Reduction of Graphene Oxide by Polydopamine to a Construct Flexible Film: Superior Flame Retardancy and High Thermal Conductivity. *Journal of Materials Chemistry A* **2017,** *5* (35), 18542-18550.

108.   Yang, S. H.; Kang, S. M.; Lee, K.-B.; Chung, T. D.; Lee, H.; Choi, I. S., Mussel-Inspired Encapsulation and Functionalization of Individual Yeast Cells. *Journal of the American Chemical Society* **2011,** *133* (9), 2795-2797.

109.   Kang, K.; Choi, I. S.; Nam, Y., A Biofunctionalization Scheme for Neural Interfaces Using Polydopamine Polymer. *Biomaterials* **2011,** *32* (27), 6374-6380.

110.   Yu, B.; Wang, D. A.; Ye, Q.; Zhou, F.; Liu, W., Robust Polydopamine Nano/Microcapsules and Their Loading and Release Behavior. *Chemical Communications* **2009,** (44), 6789-6791.

111.   Jia, X.; Sheng, W.-b.; Li, W.; Tong, Y.-b.; Liu, Z.-y.; Zhou, F., Adhesive Polydopamine Coated Avermectin Microcapsules for Prolonging Foliar Pesticide Retention. *ACS applied materials & interfaces* **2014,** *6* (22), 19552-19558.

112.   Hong, S.; Kim, K. Y.; Wook, H. J.; Park, S. Y.; Lee, K. D.; Lee, D. Y.; Lee, H., Attenuation of the in vivo Toxicity of Biomaterials by Polydopamine Surface Modification. *Nanomedicine* **2011,** *6* (5), 793-801.

113.   Lin, M.; Huang, H.; Liu, Y.; Liang, C.; Fei, S.; Chen, X.; Ni, C., High Loading of Uniformly Dispersed Pt Nanoparticles on Polydopamine Coated Carbon Nanotubes and Its Application in Simultaneous Determination of Dopamine and Uric Acid. *Nanotechnology* **2013,** *24* (6), 065501.

114.   Lin, M.; Liu, Y.; Chen, X.; Fei, S.; Ni, C.; Fang, Y.; Liu, C.; Cai, Q., Poly (Dopamine) Coated Gold Nanocluster Functionalized Electrochemical Immunosensor for Brominated Flame Retardants Using

Multienzyme-Labeling Carbon Hollow Nanochains as Signal Amplifiers. *Biosensors and Bioelectronics* **2013,** *45*, 82-88.

115.   Wang, Y.; Liu, L.; Li, M.; Xu, S.; Gao, F., Multifunctional Carbon Nanotubes for Direct Electrochemistry of Glucose Oxidase and Glucose Bioassay. *Biosensors and Bioelectronics* **2011,** *30* (1), 107-111.

116.   Guan, H.; Wang, L.; Zhang, J.; Xing, Y.; Cai, K., Selective Enrichment of Polydopamine in Mesoporous Nanocarriers for Nuclear-Targeted Drug Delivery. *Particle & Particle Systems Characterization* **2018,** *35* (6), 1800011.

117.   Liu, B.; Han, X.; Liu, J., Iron Oxide Nanozyme Catalyzed Synthesis of Fluorescent Polydopamine for Light-up Zn^{2+} Detection. *Nanoscale* **2016,** *8* (28), 13620-13626.

118.   LaVoie, M. J.; Ostaszewski, B. L.; Weihofen, A.; Schlossmacher, M. G.; Selkoe, D. J., Dopamine Covalently Modifies and Functionally Inactivates Parkin. *Nature Medicine* **2005,** *11* (11), 1214-1221.

119.   Yang, J.; Saggiomo, V.; Velders, A. H.; Stuart, M. A. C.; Kamperman, M., Reaction Pathways in Catechol/Primary Amine Mixtures: A Window on Crosslinking Chemistry. *PloS One* **2016,** *11* (12).

120.   Sedó, J.; Saiz-Poseu, J.; Busqué, F.; Ruiz-Molina, D., Catechol-Based Biomimetic Functional Materials. *Advanced Materials* **2013,** *25* (5), 653-701.

121.   Yu, B.; Liu, J.; Liu, S.; Zhou, F., Pdop Layer Exhibiting Zwitterionicity: A Simple Electrochemical Interface for Governing Ion Permeability. *Chemical Communications* **2010,** *46* (32), 5900-5902.

122.   Ball, V., Impedance Spectroscopy and Zeta Potential Titration of Dopa-Melanin Films Produced by Oxidation of Dopamine. *Colloids and Surfaces A: Physicochemical and Engineering Aspects* **2010,** *363* (1-3), 92-97.

123.   Liu, Q.; Yu, B.; Ye, W.; Zhou, F., Highly Selective Uptake and Release of Charged Molecules by Ph-Responsive Polydopamine Microcapsules. *Macromolecular bioscience* **2011,** *11* (9), 1227-1234.

124.   Wang, Y.; Ma, X.; Ding, C.; Jia, L., Ph-Responsive Deoxyribonucleic Acid Capture/Release by Polydopamine Functionalized Magnetic Nanoparticles. *Analytica Chimica Acta* **2015,** *862*, 33-40.

125.   Holten-Andersen, N.; Harrington, M. J.; Birkedal, H.; Lee, B. P.; Messersmith, P. B.; Lee, K. Y. C.; Waite, J. H., pH-Induced Metal-Ligand Cross-Links Inspired by Mussel Yield Self-Healing Polymer Networks with near-Covalent Elastic Moduli. *Proceedings of the National Academy of Sciences* **2011,** *108* (7), 2651-2655.

126.   Zeng, H.; Hwang, D. S.; Israelachvili, J. N.; Waite, J. H., Strong Reversible Fe^{3+}-Mediated Bridging between Dopa-Containing Protein Films in Water. *Proceedings of the National Academy of Sciences* **2010,** *107* (29), 12850-12853.

127.   Liu, Q.; Pu, Z.; Asiri, A. M.; Al-Youbi, A. O.; Sun, X., Polydopamine Nanospheres: A Biopolymer-Based Fluorescent Sensing Platform for DNA Detection. *Sensors and Actuators B: Chemical* **2014,** *191*, 567-571.

128.   Qiang, W.; Li, W.; Li, X.; Chen, X.; Xu, D., Bioinspired Polydopamine Nanospheres: A Superquencher for Fluorescence Sensing of Biomolecules. *Chemical Science* **2014,** *5* (8), 3018-3024.

129.   Xie, Y.; Lin, X.; Huang, Y.; Pan, R.; Zhu, Z.; Zhou, L.; Yang, C. J., Highly Sensitive and Selective Detection of Mirna: DNAse I-Assisted Target Recycling Using DNA Probes Protected by Polydopamine Nanospheres. *Chemical Communications* **2015,** *51* (11), 2156-2158.

130.   Qiang, W.; Wang, X.; Li, W.; Chen, X.; Li, H.; Xu, D., A Fluorescent Biosensing Platform Based on the Polydopamine Nanospheres Intergrating with Exonuclease Iii-Assisted Target Recycling Amplification. *Biosensors and Bioelectronics* **2015,** *71*, 143-149.

131.   Lin, L.-S.; Cong, Z.-X.; Cao, J.-B.; Ke, K.-M.; Peng, Q.-L.; Gao, J.; Yang, H.-H.; Liu, G.; Chen, X., Multifunctional Fe_3O_4@ Polydopamine Core–Shell Nanocomposites for Intracellular mRNA Detection and Imaging-Guided Photothermal Therapy. *ACS nano* **2014,** *8* (4), 3876-3883.

132.   Li, N.; Hao, X.; Kang, B. H.; Xu, Z.; Shi, Y.; Li, N. B.; Luo, H. Q., Enzyme-Free Fluorescent Biosensor for the Detection of DNA Based on Core–Shell Fe_3O_4 Polydopamine Nanoparticles and Hybridization Chain Reaction Amplification. *Biosensors and Bioelectronics* **2016,** *77*, 525-529.

133.   Fan, D.; Wang, E.; Dong, S., Exploiting Polydopamine Nanospheres to DNA Computing: A Simple, Enzyme-Free and G-Quadruplex-Free DNA Parity Generator/Checker for Error Detection During Data Transmission. *ACS Applied Materials & Interfaces* **2017,** *9* (2), 1322-1330.

134.   Fan, D.; Zhu, X.; Zhai, Q.; Wang, E.; Dong, S., Polydopamine Nanotubes as an Effective Fluorescent Quencher for Highly Sensitive and Selective Detection of Biomolecules Assisted with Exonuclease III Amplification. *Analytical Chemistry* **2016,** *88* (18), 9158-9165.

135.   He, D.; He, X.; Yang, X.; Li, H.-W., A Smart ZnO@ Polydopamine-Nucleic Acid Nanosystem for Ultrasensitive Live Cell Mrna Imaging by the Target-Triggered Intracellular Self-Assembly of Active DNAzyme Nanostructures. *Chemical Science* **2017,** *8* (4), 2832-2840.

136.   Cen, Y.; Deng, W.-J.; Yu, R.-Q.; Chu, X., Sensitive Fluorescence Sensing of T4 Polynucleotide Kinase Activity and Inhibition Based on DNA/Polydopamine Nanospheres Platform. *Talanta* **2018,** *180*, 271-276.

137.   Lee, J.; Yim, Y.; Kim, S.; Choi, M.-H.; Choi, B.-S.; Lee, Y.; Min, D.-H., In-Depth Investigation of the Interaction between DNA and Nano-Sized Graphene Oxide. *Carbon* **2016,** *97*, 92-98.

138.   Lopez, A.; Liu, J., Covalent and Noncovalent Functionalization of Graphene Oxide with DNA for Smart Sensing. *Advanced Intelligent Systems* **2020,** *2* (11), 2000123.

139.   Šafařík, I.; Ptáčková, L.; Šafaříková, M., Large-Scale Separation of Magnetic Bioaffinity Adsorbents. *Biotechnology Letters* **2001,** *23* (23), 1953-1956.

140.   Franzreb, M.; Siemann-Herzberg, M.; Hobley, T. J.; Thomas, O. R., Protein Purification Using Magnetic Adsorbent Particles. *Applied Microbiology and Biotechnology* **2006,** *70* (5), 505-516.

141.   Zhong, Z.; Yao, X.; Gao, X.; Jia, L., Polydopamine-Immobilized Polypropylene Microfuge Tube as a pH-Responsive Platform for Capture/Release of DNA from Foodborne Pathogens. *Analytical biochemistry* **2017,** *534*, 14-18.

142.   Wood, J. B.; Szyndler, M. W.; Halpern, A. R.; Cho, K.; Corn, R. M., Fabrication of DNA Microarrays on Polydopamine-Modified Gold Thin Films for SPR Imaging Measurements. *Langmuir* **2013,** *29* (34), 10868-10873.

143.   Zhang, Y.; Geng, X.; Ai, J.; Gao, Q.; Qi, H.; Zhang, C., Signal Amplification Detection of DNA Using a Sensor Fabricated by One-Step Covalent Immobilization of Amino-Terminated Probe DNA onto the Polydopamine-Modified Screen-Printed Carbon Electrode. *Sensors and Actuators B: Chemical* **2015,** *221*, 1535-1541.

144.   Fan, D.; Wu, C.; Wang, K.; Gu, X.; Liu, Y.; Wang, E., A Polydopamine Nanosphere Based Highly Sensitive and Selective Aptamer Cytosensor with Enzyme Amplification. *Chemical Communications* **2016,** *52* (2), 406-409.

145.   Wang, Y.; Li, Z.; Hu, D.; Lin, C.-T.; Li, J.; Lin, Y., Aptamer/Graphene Oxide Nanocomplex for in Situ Molecular Probing in Living Cells. *Journal of the American Chemical Society* **2010,** *132* (27), 9274-9276.

146.   Ma, L.; Lei, Z.; Liu, F.; Wang, Z., Cy5 Labeled Single-Stranded DNA-Polydopamine Nanoparticle Conjugate-Based FRET Assay for Reactive Oxygen Species Detection. *Sensing and Bio-Sensing Research* **2015,** *3*, 92-97.

147.   Feng, J.; Xu, Z.; Liu, F.; Zhao, Y.; Yu, W.; Pan, M.; Wang, F.; Liu, X., Versatile Catalytic Deoxyribozyme Vehicles for Multimodal Imaging-Guided Efficient Gene Regulation and Photothermal Therapy. *ACS nano* **2018,** *12* (12), 12888-12901.

148.   Tokura, Y.; Harvey, S.; Chen, C.; Wu, Y.; Ng, D. Y.; Weil, T., Fabrication of Defined Polydopamine Nanostructures by DNA Origami-Templated Polymerization. *Angewandte Chemie International Edition* **2018,** *57* (6), 1587-1591.

149.   Winterwerber, P.; Harvey, S.; Ng, D. Y.; Weil, T., Photocontrolled Dopamine Polymerization on DNA Origami with Nanometer Resolution. *Angewandte Chemie International Edition* **2020,** *59* (15), 6144-6149.

150.   Geyer, R., Production, Use, and Fate of Synthetic Polymers. In *Plastic Waste and Recycling*, Elsevier: 2020; pp 13-32.

151.   Ivleva, N. P., Chemical Analysis of Microplastics and Nanoplastics: Challenges, Advanced Methods, and Perspectives. *Chemical Reviews* **2021**.

152.   Ju, S.; Shin, G.; Lee, M.; Koo, J. M.; Jeon, H.; Ok, Y. S.; Hwang, D. S.; Hwang, S. Y.; Oh, D. X.; Park, J., Biodegradable Chito-Beads Replacing Non-Biodegradable Microplastics for Cosmetics. *Green Chemistry* **2021,** *23* (18), 6953-6965.

153.   Wright, S. L.; Kelly, F. J., Plastic and Human Health: A Micro Issue? *Environmental science & technology* **2017,** *51* (12), 6634-6647.

154.   Cox, K. D.; Covernton, G. A.; Davies, H. L.; Dower, J. F.; Juanes, F.; Dudas, S. E., Human Consumption of Microplastics. *Environmental Science & Technology* **2019,** *53* (12), 7068-7074.

155.   Rech, S.; Borrell, Y.; García-Vazquez, E., Marine Litter as a Vector for Non-Native Species: What We Need to Know. *Marine Pollution Bulletin* **2016,** *113* (1-2), 40-43.

156.   Huang, J.; Peng, S.; Mao, X.; Li, F.; Guo, S.; Shi, L.; Shi, Y.; Yu, H.; Zeng, G.-m., Source Apportionment and Spatial and Quantitative Ecological Risk Assessment of Heavy Metals in Soils from a Typical Chinese Agricultural County. *Process Safety and Environmental Protection* **2019,** *126*, 339-347.

157.   Tang, S.; Lin, L.; Wang, X.; Yu, A.; Sun, X., Interfacial Interactions between Collected Nylon Microplastics and Three Divalent Metal Ions (Cu(II), Ni(II), Zn(II)) in Aqueous Solutions. *Journal of Hazardous Materials* **2021,** *403*, 123548.

158.   Guo, X.; Shu, Y.; Kim, G.-H.; Palmer, M.; Choi, H.; Kim, D. W., Pseudorandom Orbiting Stroke for Freeform Optics Postprocessing. *Optical Engineering* **2019,** *58* (9), 092608.

159.   Ashton, K.; Holmes, L.; Turner, A., Association of Metals with Plastic Production Pellets in the Marine Environment. *Marine Pollution Bulletin* **2010,** *60* (11), 2050-2055.

160.   Liu, S.; Huang, J.; Zhang, W.; Shi, L.; Yi, K.; Yu, H.; Zhang, C.; Li, S.; Li, J., Microplastics as a Vehicle of Heavy Metals in Aquatic Environments: A Review of Adsorption Factors, Mechanisms, and Biological Effects. *Journal of Environmental Management* **2022,** *302*, 113995.

161.   Li, J.; Zhang, K.; Zhang, H., Adsorption of Antibiotics on Microplastics. *Environmental Pollution* **2018,** *237*, 460-467.

162.   Mao, R.; Lang, M.; Yu, X.; Wu, R.; Yang, X.; Guo, X., Aging Mechanism of Microplastics with UV Irradiation and Its Effects on the Adsorption of Heavy Metals. *Journal of Hazardous Materials* **2020,** *393*, 122515.

163.   Han, X.; Vogt, R. D.; Zhou, J.; Zheng, B.; Yu, X.; Feng, J.; Lu, X., Increased Cu (II) Adsorption onto Uv-Aged Polyethylene, Polypropylene, and Polyethylene Terephthalate Microplastic Particles in Seawater. *Plastic Pollution in the Bay Areas* **2022**.

164.   Debeljak, P.; Pinto, M.; Proietti, M.; Reisser, J.; Ferrari, F. F.; Abbas, B.; Van Loosdrecht, M. C.; Slat, B.; Herndl, G. J., Extracting DNA from Ocean Microplastics: A Method Comparison Study. *Analytical methods* **2017,** *9* (9), 1521-1526.

165.   Prokić, M. D.; Radovanović, T. B.; Gavrić, J. P.; Faggio, C., Ecotoxicological Effects of Microplastics: Examination of Biomarkers, Current State and Future Perspectives. *TrAC Trends in Analytical Chemistry* **2019,** *111*, 37-46.

166.   Tu, C.; Zhou, Q.; Zhang, C.; Liu, Y.; Luo, Y., Biofilms of Microplastics. *Microplastics in Terrestrial Environments* **2020**, 299-317.

167.   Ribeiro, F.; Garcia, A. R.; Pereira, B. P.; Fonseca, M.; Mestre, N. C.; Fonseca, T. G.; Ilharco, L. M.; Bebianno, M. J., Microplastics Effects in Scrobicularia Plana. *Marine Pollution Bulletin* **2017,** *122* (1), 379-391.

168.   Pittura, L.; Avio, C. G.; Giuliani, M. E.; d'Errico, G.; Keiter, S. H.; Cormier, B.; Gorbi, S.; Regoli, F., Microplastics as Vehicles of Environmental Pahs to Marine Organisms: Combined Chemical and Physical Hazards to the Mediterranean Mussels, Mytilus Galloprovincialis. *Frontiers in Marine Science* **2018,** *5*, 103.

169.   Chen, H.; Yang, Y.; Wang, C.; Hua, X.; Li, H.; Xie, D.; Xiang, M.; Yu, Y., Reproductive Toxicity of UV-Photodegraded Polystyrene Microplastics Induced by DNA Damage-Dependent Cell Apoptosis in Caenorhabditis Elegans. *Science of the Total Environment* **2022,** *811*, 152350.

170.   Zhao, Y.; Xu, J.; Jiang, X., DNA Cleavage and Chemical Transformation of Nano-Plastics Mediated by Surface Ligand and Size. *Chemical Communications* **2021,** *57* (76), 9740-9743.
171.   Gaillard, C.; Strauss, F., Avoiding Adsorption of DNA to Polypropylene Tubes and Denaturation of Short DNA Fragments. *Technical Tips Online* **1998,** *3* (1), 63-65.
172.   Gaillard, C.; Strauss, F., Eliminating DNA Loss and Denaturation During Storage in Plastic Microtubes. *American Clinical Laboratory* **2001,** *20* (2), 52-54.
173.   Li, Y.; Wang, Z.; Ou, L. M.; Yu, H.-Z., DNA Detection on Plastic: Surface Activation Protocol to Convert Polycarbonate Substrates to Biochip Platforms. *Analytical chemistry* **2007,** *79* (2), 426-433.
174.   Dong, H.; Chen, Y.; Wang, J.; Zhang, Y.; Zhang, P.; Li, X.; Zou, J.; Zhou, A., Interactions of Microplastics and Antibiotic Resistance Genes and Their Effects on the Aquaculture Environments. *Journal of Hazardous Materials* **2021,** *403*, 123961.
175.   Yuan, Q.; Sun, R.; Yu, P.; Cheng, Y.; Wu, W.; Bao, J.; Alvarez, P. J., UV-Aging of Microplastics Increases Proximal ARG Donor-Recipient Adsorption and Leaching of Chemicals That Synergistically Enhance Antibiotic Resistance Propagation. *Journal of Hazardous Materials* **2022,** *427*, 127895.
176.   Liu, B.; Liu, J., Sensors and Biosensors Based on Metal Oxide Nanomaterials. *TrAC Trends in Analytical Chemistry* **2019,** *121*, 115690.
177.   Moon, W. J.; Liu, J., Interfacing Catalytic DNA with Nanomaterials. *Advanced Materials Interfaces* **2020,** *7* (21), 2001017.
178.   Ebrahimi, S. B.; Samanta, D.; Mirkin, C. A., DNA-Based Nanostructures for Live-Cell Analysis. *Journal of the American Chemical Society* **2020,** *142* (26), 11343-11356.
179.   Chen, L.; Liu, B.; Xu, Z.; Liu, J., NiO Nanoparticles for Exceptionally Stable DNA Adsorption and Its Extraction from Biological Fluids. *Langmuir* **2018,** *34* (31), 9314-9321.
180.   Pan, X.; Cheng, S.; Su, T.; Zuo, G.; Zhang, C.; Wu, L.; Jiao, Y.; Dong, W., Poly (2-Hydroxypropylene Imines) Functionalized Magnetic Polydopamine Nanoparticles for High-Efficiency DNA Isolation. *Applied Surface Science* **2019,** *498*, 143888.
181.   Fan, Q.; Guan, Y.; Zhang, Z.; Xu, G.; Yang, Y.; Guo, C., A New Method of Synthesis Well-Dispersion and Dense $Fe_3O_4@ SiO_2$ Magnetic Nanoparticles for DNA Extraction. *Chemical Physics Letters* **2019,** *715*, 7-13.
182.   Zandieh, M.; Liu, J., Spherical Nucleic Acid Mediated Functionalization of Polydopamine-Coated Nanoparticles for Selective DNA Extraction and Detection. *Bioconjugate Chemistry* **2021,** *32* (4), 801-809.
183.   Di Santo, R.; Digiacomo, L.; Palchetti, S.; Palmieri, V.; Perini, G.; Pozzi, D.; Papi, M.; Caracciolo, G., Microfluidic Manufacturing of Surface-Functionalized Graphene Oxide Nanoflakes for Gene Delivery. *Nanoscale* **2019,** *11* (6), 2733-2741.
184.   Demirer, G. S.; Zhang, H.; Matos, J. L.; Goh, N. S.; Cunningham, F. J.; Sung, Y.; Chang, R.; Aditham, A. J.; Chio, L.; Cho, M.-J., High Aspect Ratio Nanomaterials Enable Delivery of Functional Genetic Material without DNA Integration in Mature Plants. *Nature Nanotechnology* **2019,** *14* (5), 456-464.
185.   Wu, R.; Wang, H.; Hai, L.; Wang, T.; Hou, M.; He, D.; He, X.; Wang, K., A Photosensitizer-Loaded Zinc Oxide-Polydopamine Core-Shell Nanotherapeutic Agent for Photodynamic and Photothermal Synergistic Therapy of Cancer Cells. *Chinese Chemical Letters* **2020,** *31* (1), 189-192.
186.   Ding, T.; Xing, Y.; Wang, Z.; Guan, H.; Wang, L.; Zhang, J.; Cai, K., Structural Complementarity from DNA for Directing Two-Dimensional Polydopamine Nanomaterials with Biomedical Applications. *Nanoscale Horizons* **2019,** *4* (3), 652-657.
187.   Liu, X.; Zhang, F.; Jing, X.; Pan, M.; Liu, P.; Li, W.; Zhu, B.; Li, J.; Chen, H.; Wang, L., Complex Silica Composite Nanomaterials Templated with DNA Origami. *Nature* **2018,** *559* (7715), 593-598.
188.   Shang, Y.; Li, N.; Liu, S.; Wang, L.; Wang, Z. G.; Zhang, Z.; Ding, B., Site-Specific Synthesis of Silica Nanostructures on DNA Origami Templates. *Advanced Materials* **2020,** *32* (21), 2000294.

189.   Kan, Y.; Tan, Q.; Wu, G.; Si, W.; Chen, Y., Study of DNA Adsorption on Mica Surfaces Using a Surface Force Apparatus. *Scientific reports* **2015,** *5* (1), 1-6.
190.   Huang, Z.; Liu, B.; Liu, J., Mn^{2+}-Assisted DNA Oligonucleotide Adsorption on Ti_2C MXene Nanosheets. *Langmuir* **2019,** *35* (30), 9858-9866.
191.   Wang, Z.; Huang, Z.; Han, J.; Xie, G.; Liu, J., Polyvalent Metal Ion Promoted Adsorption of DNA Oligonucleotides by Montmorillonite. *Langmuir* **2021,** *37* (3), 1037-1044.
192.   Ryu, J. H.; Messersmith, P. B.; Lee, H., Polydopamine Surface Chemistry: A Decade of Discovery. *ACS Applied Materials & Interfaces* **2018,** *10* (9), 7523-7540.
193.   Li, Y.; Cao, Y., The Molecular Mechanisms Underlying Mussel Adhesion. *Nanoscale Advances* **2019,** *1* (11), 4246-4257.
194.   Lee, H. A.; Ma, Y.; Zhou, F.; Hong, S.; Lee, H., Material-Independent Surface Chemistry Beyond Polydopamine Coating. *Accounts of Chemical Research* **2019,** *52* (3), 704-713.
195.   Zandieh, M.; Hagar, B. M.; Liu, J., Interfacing DNA and Polydopamine Nanoparticles and Its Applications. *Particle & Particle Systems Characterization* **2020,** *37* (11), 2000208.
196.   Zandieh, M.; Liu, J., Transition Metal-Mediated DNA Adsorption on Polydopamine Nanoparticles. *Langmuir* **2020,** *36* (12), 3260-3267.
197.   Zandieh, M.; Liu, J., Cooperative Metal Ion-Mediated Adsorption of Spherical Nucleic Acids with a Large Hysteresis. *Langmuir* **2020,** *36* (47), 14324-14332.
198.   Li, X.; Gao, P.; Tan, J.; Xiong, K.; Maitz, M. F.; Pan, C.; Wu, H.; Chen, Y.; Yang, Z.; Huang, N., Assembly of Metal–Phenolic/Catecholamine Networks for Synergistically Anti-Inflammatory, Antimicrobial, and Anticoagulant Coatings. *ACS applied Materials & Interfaces* **2018,** *10* (47), 40844-40853.
199.   He, Y.; Lopez, A.; Zhang, Z.; Chen, D.; Yang, R.; Liu, J., Nucleotide and DNA Coordinated Lanthanides: From Fundamentals to Applications. *Coordination Chemistry Reviews* **2019,** *387*, 235-248.
200.   Soroka, K.; Vithanage, R. S.; Phillips, D. A.; Walker, B.; Dasgupta, P. K., Fluorescence Properties of Metal Complexes of 8-Hydroxyquinoline-5-Sulfonic Acid and Chromatographic Applications. *Analytical Chemistry* **1987,** *59* (4), 629-636.
201.   Ma, L.; Liu, B.; Huang, P.-J. J.; Zhang, X.; Liu, J., DNA Adsorption by ZnO Nanoparticles near Its Solubility Limit: Implications for DNA Fluorescence Quenching and Dnazyme Activity Assays. *Langmuir* **2016,** *32* (22), 5672-5680.
202.   Azizian, S., Kinetic Models of Sorption: A Theoretical Analysis. *Journal of Colloid and Interface Science* **2004,** *276* (1), 47-52.
203.   Xiao, Y.; Azaiez, J.; Hill, J. M., Erroneous Application of Pseudo-Second-Order Adsorption Kinetics Model: Ignored Assumptions and Spurious Correlations. *Industrial & Engineering Chemistry Research* **2018,** *57* (7), 2705-2709.
204.   Habibiyan, A.; Ramezanzadeh, B.; Mahdavian, M.; Bahlakeh, G.; Kasaeian, M., Rational Assembly of Mussel-Inspired Polydopamine (PDA)-Zn (II) Complex Nanospheres on Graphene Oxide Framework Tailored for Robust Self-Healing Anti-Corrosion Coatings Application. *Chemical Engineering Journal* **2020,** *391*, 123630.
205.   Anderegg, G., *Critical Survey of Stability Constants of Edta Complexes: Critical Evaluation of Equilibrium Constants in Solution: Stability Constants of Metal Complexes*. Elsevier: 2013.
206.   Liu, B.; Ma, L.; Huang, Z.; Hu, H.; Wu, P.; Liu, J., Janus DNA Orthogonal Adsorption of Graphene Oxide and Metal Oxide Nanoparticles Enabling Stable Sensing in Serum. *Materials Horizons* **2018,** *5* (1), 65-69.
207.   Praetorius, F.; Kick, B.; Behler, K. L.; Honemann, M. N.; Weuster-Botz, D.; Dietz, H., Biotechnological Mass Production of DNA Origami. *Nature* **2017,** *552* (7683), 84-87.
208.   Krieg, E.; Shih, W. M., Selective Nascent Polymer Catch-and-Release Enables Scalable Isolation of Multi-Kilobase Single-Stranded DNA. *Angewandte Chemie International Edition* **2018,** *57* (3), 714-718.

209.   Krieg, E.; Gupta, K.; Dahl, A.; Lesche, M.; Boye, S.; Lederer, A.; Shih, W. M., A Smart Polymer for Sequence-Selective Binding, Pulldown, and Release of DNA Targets. *Communications Biology* **2020,** *3* (1), 1-9.

210.   Wang, S.-K.; Stiles, A. R.; Guo, C.; Liu, C.-Z., Harvesting Microalgae by Magnetic Separation: A Review. *Algal Research* **2015,** *9*, 178-185.

211.   Jung, S. H.; Hahn, Y. K.; Oh, S.; Kwon, S.; Um, E.; Choi, S.; Kang, J. H., Advection Flows-Enhanced Magnetic Separation for High-Throughput Bacteria Separation from Undiluted Whole Blood. *Small* **2018,** *14* (34), 1801731.

212.   Fatima, H.; Kim, K.-S., Magnetic Nanoparticles for Bioseparation. *Korean Journal of Chemical Engineering* **2017,** *34* (3), 589-599.

213.   Wang, J.; Ali, Z.; Si, J.; Wang, N.; He, N.; Li, Z., Simultaneous Extraction of DNA and RNA from Hepatocellular Carcinoma (Hep G2) Based on Silica-Coated Magnetic Nanoparticles. *Journal of Nanoscience and Nanotechnology* **2017,** *17* (1), 802-806.

214.   Bai, Y.; Roncancio, D.; Suo, Y.; Shao, Y.; Zhang, D.; Zhou, C., A Method Based on Amino-Modified Magnetic Nanoparticles to Extract DNA for Pcr-Based Analysis. *Colloids and Surfaces B: Biointerfaces* **2019,** *179*, 87-93.

215.   Ali, T. H.; Mandal, A. M.; Heidelberg, T.; Hussen, R. S. D.; Goh, E. W., Ionic Magnetic Core–Shell Nanoparticles for DNA Extraction. *RSC Advances* **2020,** *10* (64), 38818-38830.

216.   Pan, X.; Cheng, S.; Su, T.; Zuo, G.; Zhao, W.; Qi, X.; Wei, W.; Dong, W., Fenton-Like Catalyst Fe_3O_4@Polydopamine-MnO_2 for Enhancing Removal of Methylene Blue in Wastewater. *Colloids and Surfaces B: Biointerfaces* **2019,** *181*, 226-233.

217.   Pan, X.; Cheng, S.; Zhang, C.; Jiao, Y.; Lin, X.; Dong, W.; Qi, X., Mussel-Inspired Magnetic Pullulan Hydrogels for Enhancing Catalytic Degradation of Antibiotics from Biomedical Wastewater. *Chemical Engineering Journal* **2021,** *409*, 128203.

218.   Cutler, J. I.; Auyeung, E.; Mirkin, C. A., Spherical Nucleic Acids. *Journal of the American Chemical Society* **2012,** *134* (3), 1376-1391.

219.   Choi, C. H. J.; Hao, L.; Narayan, S. P.; Auyeung, E.; Mirkin, C. A., Mechanism for the Endocytosis of Spherical Nucleic Acid Nanoparticle Conjugates. *Proceedings of the National Academy of Sciences* **2013,** *110* (19), 7625-7630.

220.   Yeo, D. C.; Wiraja, C.; Paller, A. S.; Mirkin, C. A.; Xu, C., Abnormal Scar Identification with Spherical-Nucleic-Acid Technology. *Nature Biomedical Engineering* **2018,** *2* (4), 227-238.

221.   Hu, X.; Ke, G.; Liu, L.; Fu, X.; Kong, G.; Xiong, M.; Chen, M.; Zhang, X.-B., Valency-Controlled Molecular Spherical Nucleic Acids with Tunable Biosensing Performances. *Analytical chemistry* **2019,** *91* (17), 11374-11379.

222.   Yao, G.; Li, J.; Li, Q.; Chen, X.; Liu, X.; Wang, F.; Qu, Z.; Ge, Z.; Narayanan, R. P.; Williams, D., Programming Nanoparticle Valence Bonds with Single-Stranded DNA Encoders. *Nature Materials* **2020,** *19* (7), 781-788.

223.   Li, B.-R.; Tang, H.; Yu, R.-Q.; Jiang, J.-H., Single-Nanoparticle Icpms DNA Assay Based on Hybridization-Chain-Reaction-Mediated Spherical Nucleic Acid Assembly. *Analytical Chemistry* **2020,** *92* (3), 2379-2382.

224.   Zhu, C.; Wang, M.; Dong, J.; Zhou, C.; Wang, Q., Modular Assembly of Plasmonic Nanoparticles Assisted by DNA Origami. *Langmuir* **2018,** *34* (49), 14963-14968.

225.   Ma, W.; Sun, M.; Fu, P.; Li, S.; Xu, L.; Kuang, H.; Xu, C., A Chiral-Nanoassemblies-Enabled Strategy for Simultaneously Profiling Surface Glycoprotein and Microrna in Living Cells. *Advanced Materials* **2017,** *29* (42), 1703410.

226.   Fong, L.-K.; Wang, Z.; Schatz, G. C.; Luijten, E.; Mirkin, C. A., The Role of Structural Enthalpy in Spherical Nucleic Acid Hybridization. *Journal of the American Chemical Society* **2018,** *140* (20), 6226-6230.

227.   Liu, J.; Lu, Y., Preparation of Aptamer-Linked Gold Nanoparticle Purple Aggregates for Colorimetric Sensing of Analytes. *Nature Protocols* **2006,** *1* (1), 246-252.

228.   Deng, H.; Li, X.; Peng, Q.; Wang, X.; Chen, J.; Li, Y., Monodisperse Magnetic Single-Crystal Ferrite Microspheres. *Angewandte Chemie* **2005,** *117* (18), 2842-2845.

229.   Demers, L. M.; Mirkin, C. A.; Mucic, R. C.; Reynolds, R. A.; Letsinger, R. L.; Elghanian, R.; Viswanadham, G., A Fluorescence-Based Method for Determining the Surface Coverage and Hybridization Efficiency of Thiol-Capped Oligonucleotides Bound to Gold Thin Films and Nanoparticles. *Analytical chemistry* **2000,** *72* (22), 5535-5541.

230.   Martell, A. E.; Smith, R. M., *Critical Stability Constants*. Springer: 1974; Vol. 1.

231.   Lynge, M. E.; van der Westen, R.; Postma, A.; Städler, B., Polydopamine—a Nature-Inspired Polymer Coating for Biomedical Science. *Nanoscale* **2011,** *3* (12), 4916-4928.

232.   Bazylewski, P.; Divigalpitiya, R.; Fanchini, G., In Situ Raman Spectroscopy Distinguishes between Reversible and Irreversible Thiol Modifications in L-Cysteine. *RSC Advances* **2017,** *7* (5), 2964-2970.

233.   Horák, D.; Španová, A.; Tvrdíková, J.; Rittich, B., Streptavidin-Modified Magnetic Poly (2-Hydroxyethyl Methacrylate-Co-Glycidyl Methacrylate) Microspheres for Selective Isolation of Bacterial DNA. *European polymer journal* **2011,** *47* (5), 1090-1096.

234.   Verbruggen, B.; Leirs, K.; Puers, R.; Lammertyn, J., Selective DNA Extraction with Microparticles in Segmented Flow. *Microfluidics and Nanofluidics* **2015,** *18* (2), 293-303.

235.   Wang, J.; Guo, X., Adsorption Kinetic Models: Physical Meanings, Applications, and Solving Methods. *Journal of Hazardous Materials* **2020,** *390*, 122156.

236.   Bai, M.; Chen, F.; Cao, X.; Zhao, Y.; Xue, J.; Yu, X.; Fan, C.; Zhao, Y., Intracellular Entropy-Driven Multi-Bit DNA Computing for Tumor Progression Discrimination. *Angewandte Chemie* **2020,** *132* (32), 13369-13374.

237.   Geyer, R.; Jambeck, J. R.; Law, K. L., Production, Use, and Fate of All Plastics Ever Made. *Science Advances* **2017,** *3* (7), e1700782.

238.   Chae, Y.; An, Y.-J., Current Research Trends on Plastic Pollution and Ecological Impacts on the Soil Ecosystem: A Review. *Environmental Pollution* **2018,** *240*, 387-395.

239.   Reid, A. J.; Carlson, A. K.; Creed, I. F.; Eliason, E. J.; Gell, P. A.; Johnson, P. T.; Kidd, K. A.; MacCormack, T. J.; Olden, J. D.; Ormerod, S. J., Emerging Threats and Persistent Conservation Challenges for Freshwater Biodiversity. *Biological Reviews* **2019,** *94* (3), 849-873.

240.   De Oliveira, T. T. S.; Andreu, I.; Machado, M. C.; Vimbela, G.; Tripathi, A.; Bose, A., Interaction of Cyanobacteria with Nanometer and Micron Sized Polystyrene Particles in Marine and Fresh Water. *Langmuir* **2020,** *36* (14), 3963-3969.

241.   Al Harraq, A.; Bharti, B., Microplastics through the Lens of Colloid Science. *ACS Environmental Au* **2021**.

242.   Sharma, S.; Chatterjee, S., Microplastic Pollution, a Threat to Marine Ecosystem and Human Health: A Short Review. *Environmental Science and Pollution Research* **2017,** *24* (27), 21530-21547.

243.   Prata, J. C.; da Costa, J. P.; Lopes, I.; Duarte, A. C.; Rocha-Santos, T., Environmental Exposure to Microplastics: An Overview on Possible Human Health Effects. *Science of the total environment* **2020,** *702*, 134455.

244.   Koelmans, A. A.; Nor, N. H. M.; Hermsen, E.; Kooi, M.; Mintenig, S. M.; De France, J., Microplastics in Freshwaters and Drinking Water: Critical Review and Assessment of Data Quality. *Water Research* **2019,** *155*, 410-422.

245.   Liu, B.; Salgado, S.; Maheshwari, V.; Liu, J., DNA Adsorbed on Graphene and Graphene Oxide: Fundamental Interactions, Desorption and Applications. *Current Opinion in Colloid & Interface Science* **2016,** *26*, 41-49.

246.   Liu, B.; Zhao, Y.; Jia, Y.; Liu, J., Heating Drives DNA to Hydrophobic Regions While Freezing Drives DNA to Hydrophilic Regions of Graphene Oxide for Highly Robust Biosensors. *Journal of the American Chemical Society* **2020,** *142* (34), 14702-14709.

247.   Zandieh, M.; Liu, J., Metal-Doped Polydopamine Nanoparticles for Highly Robust and Efficient DNA Adsorption and Sensing. *Langmuir* **2021,** *37* (30), 8953-8960.

248.   McCormick, A.; Hoellein, T. J.; Mason, S. A.; Schluep, J.; Kelly, J. J., Microplastic Is an Abundant and Distinct Microbial Habitat in an Urban River. *Environmental Science & Technology* **2014,** *48* (20), 11863-11871.

249.   Jiang, P.; Zhao, S.; Zhu, L.; Li, D., Microplastic-Associated Bacterial Assemblages in the Intertidal Zone of the Yangtze Estuary. *Science of the Total Environment* **2018,** *624*, 48-54.

250.   Ibabe, A.; Rayon, F.; Martinez, J. L.; Garcia-Vazquez, E., Environmental DNA from Plastic and Textile Marine Litter Detects Exotic and Nuisance Species Nearby Ports. *PloS One* **2020,** *15* (6), e0228811.

251.   Klein, D.; Gurevich, L.; Janssen, J.; Kouwenhoven, L.; Carbeck, J.; Sohn, L., Ordered Stretching of Single Molecules of Deoxyribose Nucleic Acid between Microfabricated Polystyrene Lines. *Applied Physics Letters* **2001,** *78* (16), 2396-2398.

252.   Benke, A.; Mertig, M.; Pompe, W., pH-and Salt-Dependent Molecular Combing of DNA: Experiments and Phenomenological Model. *Nanotechnology* **2010,** *22* (3), 035304.

253.   Zhou, Y.; Huang, Z.; Yang, R.; Liu, J., Selection and Screening of DNA Aptamers for Inorganic Nanomaterials. *Chemistry–A European Journal* **2018,** *24* (11), 2525-2532.

254.   Banga, R. J.; Chernyak, N.; Narayan, S. P.; Nguyen, S. T.; Mirkin, C. A., Liposomal Spherical Nucleic Acids. *Journal of the American Chemical Society* **2014,** *136* (28), 9866-9869.

255.   Bretti, C.; Cardiano, P.; Irto, A.; Lando, G.; Milea, D.; Sammartano, S., Interaction of N-Acetyl-L-Cysteine with Na^+, Ca^{2+}, Mg^{2+} and Zn^{2+}. Thermodynamic Aspects, Chemical Speciation and Sequestering Ability in Natural Fluids. *Journal of Molecular Liquids* **2020,** *319*, 114164.

256.   Araujo, C. F.; Nolasco, M. M.; Ribeiro, A. M.; Ribeiro-Claro, P. J., Identification of Microplastics Using Raman Spectroscopy: Latest Developments and Future Prospects. *Water Research* **2018,** *142*, 426-440.

257.   Sobhani, Z.; Al Amin, M.; Naidu, R.; Megharaj, M.; Fang, C., Identification and Visualisation of Microplastics by Raman Mapping. *Analytica chimica acta* **2019,** *1077*, 191-199.

258.   Gillibert, R.; Balakrishnan, G.; Deshoules, Q.; Tardivel, M.; Magazzù, A.; Donato, M. G.; Maragò, O. M.; Lamy de La Chapelle, M.; Colas, F.; Lagarde, F., Raman Tweezers for Small Microplastics and Nanoplastics Identification in Seawater. *Environmental Science & Technology* **2019,** *53* (15), 9003-9013.

259.   de Ruijter, V. N.; Redondo-Hasselerharm, P. E.; Gouin, T.; Koelmans, A. A., Quality Criteria for Microplastic Effect Studies in the Context of Risk Assessment: A Critical Review. *Environmental Science & Technology* **2020,** *54* (19), 11692-11705.

260.   Xiong, Y.; Zhao, J.; Li, L.; Wang, Y.; Dai, X.; Yu, F.; Ma, J., Interfacial Interaction between Micro/Nanoplastics and Typical PPCPs and Nanoplastics Removal Via Electrosorption from an Aqueous Solution. *Water Research* **2020,** *184*, 116100.

261.   Wu, X.; Liu, P.; Huang, H.; Gao, S., Adsorption of Triclosan onto Different Aged Polypropylene Microplastics: Critical Effect of Cations. *Science of the Total Environment* **2020,** *717*, 137033.

262.   Besson, P.; Degboe, J.; Berge, B.; Chavagnac, V.; Fabre, S.; Berger, G., Calcium, Na, K and Mg Concentrations in Seawater by Inductively Coupled Plasma-Atomic Emission Spectrometry: Applications to Iapso Seawater Reference Material, Hydrothermal Fluids and Synthetic Seawater Solutions. *Geostandards and Geoanalytical Research* **2014,** *38* (3), 355-362.

263.   Wang, Y.; Yang, Y.; Liu, X.; Zhao, J.; Liu, R.; Xing, B., Interaction of Microplastics with Antibiotics in Aquatic Environment: Distribution, Adsorption, and Toxicity. *Environmental Science & Technology* **2021**.

264.   Parisini, E.; Metrangolo, P.; Pilati, T.; Resnati, G.; Terraneo, G., Halogen Bonding in Halocarbon–Protein Complexes: A Structural Survey. *Chemical Society Reviews* **2011,** *40* (5), 2267-2278.

265.   Jimmy Huang, P.-J.; Moon, W. J.; Liu, J., Instantaneous Iodine-Assisted Dnazyme Cleavage of Phosphorothioate RNA. *Biochemistry* **2018,** *58* (5), 422-429.

266.   Büks, F.; Kaupenjohann, M., The Impact of Microplastic Weathering on Interactions with the Soil Environment: A Review. *SOIL Discussions* **2021**, 1-22.

267.   Liu, P.; Shi, Y.; Wu, X.; Wang, H.; Huang, H.; Guo, X.; Gao, S., Review of the Artificially-Accelerated Aging Technology and Ecological Risk of Microplastics. *Science of the total environment* **2021,** *768*, 144969.

268.   Liu, P.; Qian, L.; Wang, H.; Zhan, X.; Lu, K.; Gu, C.; Gao, S., New Insights into the Aging Behavior of Microplastics Accelerated by Advanced Oxidation Processes. *Environmental science & technology* **2019,** *53* (7), 3579-3588.

269.   Han, X.; Vogt, R. D.; Zhou, J.; Zheng, B.; Yu, X.; Feng, J.; Lu, X., Increased Cu (II) Adsorption onto UV-Aged Polyethylene, Polypropylene, and Polyethylene Terephthalate Microplastic Particles in Seawater. *Frontiers in Marine Science* **2021,** *8*.

270.   Hüffer, T.; Weniger, A.-K.; Hofmann, T., Sorption of Organic Compounds by Aged Polystyrene Microplastic Particles. *Environmental Pollution* **2018,** *236*, 218-225.

271.   Vockenberg, T.; Wichard, T.; Ueberschaar, N.; Franke, M.; Stelter, M.; Braeutigam, P., The Sorption Behaviour of Amine Micropollutants on Polyethylene Microplastics–Impact of Aging and Interactions with Green Seaweed. *Environmental Science: Processes & Impacts* **2020,** *22* (8), 1678-1687.

272.   Lin, J.; Wu, X.; Liu, Y.; Fu, J.; Chen, Y.; Ou, H., Sinking Behavior of Polystyrene Microplastics after Disinfection. *Chemical Engineering Journal* **2022,** *427*, 130908.

273.   Chen, Y.; Liu, R.; Wu, X.; Liu, Y.; Fu, J.; Ou, H., Surface Characteristic and Sinking Behavior Modifications of Microplastics During Potassium Permanganate Pre-Oxidation. *Journal of Hazardous Materials* **2022,** *422*, 126855.

274.   Shen, X.; Corey, D. R., Chemistry, Mechanism and Clinical Status of Antisense Oligonucleotides and Duplex Rnas. *Nucleic Acids Research* **2018,** *46* (4), 1584-1600.

275.   Tseng, W.-B.; Hsieh, M.-M.; Chen, C.-H.; Chiu, T.-C.; Tseng, W.-L., Functionalized Gold Nanoparticles for Sensing of Pesticides: A Review. *Journal of Food & Drug Analysis* **2020,** *28* (4).

276.   Zandieh, M.; Patel, K.; Liu, J., Adsorption of Linear and Spherical DNA Oligonucleotides onto Microplastics. *Langmuir* **2022**.

277.   Adarsh, U.; Kartha, V.; Santhosh, C.; Unnikrishnan, V., Spectroscopy: A Promising Tool for Plastic Waste Management. *TrAC Trends in Analytical Chemistry* **2022**, 116534.

278.   Liu, P.; Lu, K.; Li, J.; Wu, X.; Qian, L.; Wang, M.; Gao, S., Effect of Aging on Adsorption Behavior of Polystyrene Microplastics for Pharmaceuticals: Adsorption Mechanism and Role of Aging Intermediates. *Journal of Hazardous Materials* **2020,** *384*, 121193.

279.   Karlsson, T. M.; Hassellöv, M.; Jakubowicz, I., Influence of Thermooxidative Degradation on the in Situ Fate of Polyethylene in Temperate Coastal Waters. *Marine Pollution Bulletin* **2018,** *135*, 187-194.

280.   Ding, L.; Mao, R.; Ma, S.; Guo, X.; Zhu, L., High Temperature Depended on the Ageing Mechanism of Microplastics under Different Environmental Conditions and Its Effect on the Distribution of Organic Pollutants. *Water Research* **2020,** *174*, 115634.

281.   Kong, F.; Xu, X.; Xue, Y.; Gao, Y.; Zhang, L.; Wang, L.; Jiang, S.; Zhang, Q., Investigation of the Adsorption of Sulfamethoxazole by Degradable Microplastics Artificially Aged by Chemical Oxidation. *Archives of Environmental Contamination and Toxicology* **2021,** *81* (1), 155-165.

282.   Zhang, Y.; Gao, X.; Ye, Y.; Shen, Y., Fe-Doped Polydopamine Nanoparticles with Peroxidase-Mimicking Activity for the Detection of Hypoxanthine Related to Meat Freshness. *Analyst* **2022,** *147* (5), 956-964.